



Cooperative Research Centre for  
Landscape Environments  
and Mineral Exploration



OPEN FILE  
REPORT  
SERIES

# **GOLD DISTRIBUTION, REGOLITH AND GROUNDWATER CHARACTERISTICS AT THE MT JOEL PROSPECT, WESTERN AUSTRALIA**

*C.G. Porto, N.B. Sergeev and D.J. Gray*

**CRC LEME OPEN FILE REPORT 218**

**February 2007**

CRCLEME

(CRC LEME Restricted Report 96R / E&M Report 553R, April 1999)

CRC LEME is an unincorporated joint venture between CSIRO-Exploration & Mining, and Land & Water, The Australian National University, Curtin University of Technology, University of Adelaide, Geoscience Australia, Primary Industries and Resources SA, NSW Department of Primary Industries and Minerals Council of Australia, established and supported under the Australian Government's Cooperative Research Centres Program.





# **GOLD DISTRIBUTION, REGOLITH AND GROUNDWATER CHARACTERISTICS AT THE MT JOEL PROSPECT, WESTERN AUSTRALIA**

*C.G. Porto, N.B. Sergeev and D.J. Gray*

**CRC LEME OPEN FILE REPORT 218**

April 2007

(CRC LEME Restricted Report 96R / E&M Report 553R, April 1999)

© CRC LEME 2007

---

CRC LEME is an unincorporated joint venture between CSIRO-Exploration & Mining, and Land & Water, The Australian National University, Curtin University of Technology, University of Adelaide, Geoscience Australia, Primary Industries and Resources SA, NSW Department of Primary Industries and Minerals Council of Australia.

*Headquarters:* CRC LEME c/o CSIRO Exploration and Mining, PO Box 1130, Bentley WA 6102, Australia

## PREFACE

The principal objective of CRC LEME-AMIRA Project 504, *Supergene mobilization of gold and other elements in the Yilgarn Craton*, is to determine the mechanisms of supergene/secondary depletion, enrichment and dispersion of Au and other elements, so as to improve selection of drilling targets and further optimize interpretation of geochemical data. This report documents the investigations undertaken at Mt Joel.

The Mt Joel prospect is situated in the northern part of the Yilgarn Craton, NW of Bronzewing. It is an area where the occurrence of substantial supergene mobilization of Au is uncertain. Mt Joel consists of a number of mineralized targets in an area of relatively homogeneous geology, with highly variable regolith; in particular, the alluvial cover varies in thickness from less than one metre to greater than 80 m. For these reasons, this area provides a valuable study site for enhancing our knowledge of regional differences affecting the mobility of Au. Developing methods for the recognition and understanding of any such mobilization of Au, and potential pathfinder elements, is of major importance. This report details methods for estimating the degree of mobilization and understanding the processes by which it occurs. Detailed work is focussed on two areas of the deposit, which show contrasting regolith characteristics with respect to the thickness of alluvial cover.

D.J. Gray  
Project Leader  
April 1999

## EXECUTIVE SUMMARY

Supergene gold mobility has been investigated at the Mount Joel prospect 20 km NE of the Bronzewing Au mine in the Yandal greenstone belt, Western Australia. Gold mineralization has been delineated along an 8 km long trend, primarily hosted in variably sheared and hydrothermally altered metabasalts. Gold occurs in a sulphide-poor, quartz stockwork vein system associated with slightly anomalous concentrations of As, Sb and W. The area is generally flat and with a regolith cover of up to 100 m, including a variable thickness of alluvial cover.

In the 2400 and 3000 mN areas the saprolite is about 60 m thick and its upper portion is strongly leached, resulting in a Au- and Si-depleted zone which is kaolinite rich. Alluvial cover less than 10 m thick overlies the saprolite. The cover and the top few metres of the saprolite are silicified. In comparison, in the 0 and 800 mN areas, saprolite is commonly less than 30 m thick, more ferruginized and does not contain a leached zone. It is overlain by nearly 10 m of lateritic residuum, pisolitic at the top, and up to 80 m of palaeochannel sediments.

The patterns of Au distribution in the 2400 and 3000 mN areas remain essentially unchanged from fresh rock to lower saprolite. However, supergene Au has been identified in several samples in these zones, implying that Au mobility was restricted and did not result in lateral dispersion or enrichment blankets. Above 30 m depth, the saprolite is leached and Au strongly depleted. At the top of the saprolite, Au is enriched and homogenized, but lateral dispersion is not pronounced. In the 0 and 800 mN areas, Au redistribution immediately above the weathering front is more pronounced than in the 2400 and 3000 mN areas, with no Au depletion in the saprolite. Instead, Au is enriched and dispersed in the lateritic zone, especially the pisolitic layer.

For all Mt Joel samples analysed, the proportion of iodide-soluble Au is greatest at the top of the saprolite in the 2400 and 3000 mN areas. This suggests that Au is recently reprecipitated in this horizon. In comparison, Au in the lateritic zone in the 0 and 800 mN areas is less iodide-soluble. In this zone, Au dispersion is probably enhanced by mechanical transport of the Au-enriched lateritic material during burial by palaeochannel sediments.

The pristine nature of the supergene Au grains shows that chemical reworking is minimal. This is in agreement with the results of groundwater geochemistry, which suggest that present day mobility of metals, including Au, should be minimal. The potential use of transported material as an indicator of mineralization underneath is therefore low. However, near the weathering front, the distribution of salinity, Eh and pH are more heterogeneous and may be locally conducive to Au mobilization.

There is no evidence to suggest that trace elements other than Au should be used for exploration in these areas, with the possible exception of W, which remains anomalous in the Au depleted zones but with very limited areal extension. Exploration drilling should target sampling at the top of the residuum where Au is most enriched and dispersed. However, because the nature of the enrichment and dispersion differs between the lateritic residuum and top of saprolite, interpretation should be conducted separately for different regolith stratigraphies, as distinguished between the 2400/3000 and 0/800 mN areas. PIMA proved to be an invaluable tool for discriminating between residual and transported regolith materials.

## TABLE OF CONTENTS

1	INTRODUCTION .....	1
1.1	Characteristics of the area .....	1
1.2	Objectives.....	1
2	ANALYTICAL PROCEDURES.....	2
2.1	Multi-element geochemical analysis .....	2
2.2	Partial extractions for gold .....	2
2.3	Mineralogical investigations .....	2
2.3.1	X-ray diffraction analysis .....	2
2.3.2	Semi-quantitative analysis .....	2
2.3.3	PIMA analysis .....	3
2.4	3D gridding and visualisation (MVS) .....	3
2.5	Gold grain separation and analysis.....	4
2.6	Groundwater sampling and analysis.....	4
3	REGOLITH STRATIGRAPHY .....	7
3.1	Regolith stratigraphy, as defined by Great Central Mines logging.....	7
3.2	Regolith stratigraphy defined by CRC LEME logging.....	11
3.3	Nomenclature used in this report.....	15
4	REGOLITH MINERALOGY .....	17
4.1	3000 mN area .....	17
4.2	800 mN area.....	24
5	PIMA SURVEY.....	26
5.1	Introduction .....	26
5.2	Results .....	26
6	REGOLITH GEOCHEMISTRY .....	34
6.1	Sample distribution and data treatment .....	34
6.2	Major oxides: Si, Fe, Al.....	34
6.3	Alkaline earth elements: Mg, Ca, Ba, Sr.....	37
6.4	Alkali metals: Na, K, Rb, Cs.....	37
6.5	Elements associated with gold mineralization: Au, As, Sb, W.....	38
6.6	Base metals: Cu, Pb, Zn, Ni, Co.....	38
6.7	Other Transition metals: Cr, Sc, Ti, V .....	39
6.8	Immobile elements: Zr, Hf, Th, Nb.....	39
6.9	Rare earth elements: La, Ce, Sm, Eu, Lu, Yb, Y.....	40
6.10	Other elements: P, Cl, Br, Ga, Mn.....	40
6.11	Summary of geochemical trends in the 3000 mN area.....	41
6.12	Summary of geochemical trends in the 800 mN area.....	41
7	HYDROGEOCHEMISTRY.....	42
7.1	Introduction .....	42
7.2	Compilation of results and comparison with other sites.....	42
7.3	Acidity and oxidation potential .....	43
7.4	Salinity effects and major element hydrogeochemistry .....	43
7.5	Minor element hydrogeochemistry .....	46
7.6	Gold chemistry.....	47
7.7	Mapping of the shallow groundwater data.....	48
7.8	Mapping of the deep groundwater data.....	49

7.9	Summary.....	50
8	DISTRIBUTION OF GOLD.....	51
8.1	Sample distribution.....	51
8.2	Visualization of gold distribution.....	51
8.3	Statistical analysis.....	52
8.3.1	Sample distribution.....	52
8.3.2	Results for 3000 and 2400 mN areas.....	53
8.3.3	Results for 800 and 0 mN areas.....	57
8.4	Normalization of Au to immobile elements.....	60
9	GOLD DISPERSION STUDIES.....	64
9.1	Gold selective extraction analysis.....	64
9.2	Lateral gold dispersion in the 3000 mN area.....	66
9.2.1	Gold distribution in the 3000 mN section.....	66
9.2.2	Grain size and selective extraction analyses.....	67
9.3	Lateral gold dispersion in the 800 mN area.....	70
10	CHARACTERISTICS OF PARTICULATE GOLD.....	75
10.1	Mineral composition of heavy concentrates.....	75
10.2	Characteristics of gold grains.....	76
10.2.1	Size.....	76
10.2.2	Morphology.....	77
10.2.3	Composition.....	78
10.3	Gold grains in the primary mineralization.....	78
10.4	Gold grains in the saprock.....	79
10.5	Gold grains in the lower saprolite.....	80
10.6	Gold grains in the saprolite.....	82
10.7	Gold grains in the top of saprolite, ferruginous saprolite and nodular laterite.....	83
10.8	Gold selective extractions in the bulk samples.....	83
10.8.1	Size distribution of Au grains versus shape distribution of Au grains.....	84
10.8.2	Size distribution of Au grains versus the results of selective extractions.....	85
10.8.3	Shape distribution of Au grains versus the results of selective extractions.....	87
10.9	Interpretation.....	88
11	DISCUSSION AND CONCLUSIONS.....	90
11.1	Regolith evolution.....	90
11.2	Gold distribution.....	90
11.3	Gold dissolution and role of the present groundwater:.....	93
11.4	Exploration significance.....	93
	ACKNOWLEDGEMENTS.....	92
	REFERENCES.....	93

## **LIST OF APPENDICES**

Scanning electron microscope photographs of gold grains

Appendix 1: Geochemical profiles for drill holes RC453, RC670/730, RC731 and RC218/326

Appendix 2: Geochemical data for section 3000N

Appendix 3: Box and whisker plots of element concentration in the regolith

Appendix 4: Element/ion concentrations for groundwaters

Appendix 5: Saturation indices for groundwaters

Appendix 6: Element/ion distribution maps – shallow groundwaters

Appendix 7: Element/ion distribution maps – deep groundwaters

Appendix 8: Histograms and cumulative frequency curves of gold in regolith zones

Appendix 9: Contents of enclosed CD

## LIST OF FIGURES

Figure 1:	Groundwater sample positions and deep sample depths, showing averaged Au grade and 20 and 50 m alluvium contours. ....	5
Figure 2:	Average depths of weathering front, BOCO and unconformity in the 3000 and 800 mN areas. ....	7
Figure 3:	Depth of the base of weathering (mRL). ....	8
Figure 4:	Depth of the base of complete oxidation (BOCO) (mRL). ....	9
Figure 5:	Depth of unconformity (mRL). ....	10
Figure 6:	Thickness and elevation of the oxide zone for the Mt Joel study area. ....	11
Figure 7:	Regolith stratigraphy: Section 2920 mN. ....	12
Figure 8:	Log of drill hole RC453. ....	13
Figure 9:	Log of drill hole RC670/730. ....	13
Figure 10:	Regolith stratigraphy of section 3000 mN. ....	13
Figure 11:	Regolith stratigraphy: Section 800 mN. ....	14
Figure 12:	Log of drill holes RC218/326. ....	15
Figure 13:	Mineralogical composition by XRD and XRF of drill hole RC453. ....	18
Figure 14:	Mineralogical composition by XRD and XRF of drill hole RC670/730. ....	20
Figure 15:	Mineralogical composition by XRD and XRF of drill hole RC731. ....	23
Figure 16:	Mineralogical composition by XRD and XRF of drill hole RC218/326. ....	25
Figure 17:	Example deconvolutions for H <sub>2</sub> O rich (RC453, 2 m) and H <sub>2</sub> O poor (RC453, 70 m) samples: ....	27
Figure 18:	Wavelength of the 1390 nm kaolinite peak in drill hole RC453. ....	27
Figure 19:	Wavelength of the 1390 nm kaolinite peak in drill hole RC218/326. ....	28
Figure 20:	Area of water peak at 1460 nm and 1910 nm in drill hole RC453. ....	29
Figure 21:	Area of water peak at 1460 nm and 1910 nm in drill hole RC218/326. ....	29
Figure 22:	Area of water peak at 1910 nm in drill hole RC670/730. ....	30
Figure 23:	Area of water peak at 1910 nm in drill hole RC731. ....	30
Figure 24:	Area of water peak at 1910 nm in traverse 3000 mN. ....	30
Figure 25:	Ratio of reflected intensities in drill hole RC453. ....	31
Figure 26:	Ratio of reflected intensities in drill hole RC670/730. ....	31
Figure 27:	Ratio of reflected intensities in drill hole RC731. ....	32
Figure 28:	Ratio of reflected intensities in drill hole RC218/326. ....	32
Figure 29:	Ratio of reflected intensities in traverse 3000 mN. ....	33
Figure 30:	Cluster analysis from 39 fresh rock samples - 3000 mN area, using single linkage, Pearson correlation coefficients. ....	35
Figure 31:	Cluster analysis from 40 saprock samples, 3000 mN area, using single linkage, Pearson correlation coefficients. ....	35
Figure 32:	Cluster analysis from 35 lower saprolite samples, 3000 mN area, using single linkage, Pearson correlation coefficients. ....	35
Figure 33:	Cluster analysis from 24 leached zone samples, 3000 mN area, using single linkage, Pearson correlation coefficients. ....	36
Figure 34:	Cluster analysis from 18 top of saprolite samples, 3000 mN area, using single linkage, Pearson correlation coefficients. ....	36

Figure 35:	Cluster analysis from 14 alluvium samples, 3000 mN area, using single linkage, Pearson correlation coefficients.....	36
Figure 36:	Eh vs pH for groundwaters from Mt Joel and other sites. ....	44
Figure 37:	pH vs TDS for groundwaters from Mt Joel and other sites. ....	44
Figure 38:	Salinity vs depth for Mt Joel groundwaters.....	49
Figure 39:	Gold distribution in the 3000 mN area. ....	52
Figure 40:	Gold distribution in the 800 mN area. ....	53
Figure 41:	Geometric mean of Au grades relative to unconformity (3000 and 2400 mN areas). ....	54
Figure 42:	Arithmetic mean of Au grades relative to unconformity (3000 and 2400 mN areas). ....	54
Figure 43:	Geometric mean of Au grades relative to the BOCO surface (3000 and 2400 mN areas). ....	55
Figure 44:	Arithmetic mean of Au grades relative to the BOCO surface (3000 and 2400 mN areas). ....	55
Figure 45:	Geometric mean of Au grades relative to base of weathering (3000 and 2400 mN areas). ....	56
Figure 46:	Arithmetic mean of Au grades relative to base of weathering (3000 and 2400 mN areas). ....	56
Figure 47:	Geometric mean of Au grades relative to the unconformity (800 and 0 mN areas). ....	57
Figure 48:	Arithmetic mean of Au grades relative to the unconformity (800 and 0 mN areas). ....	57
Figure 49:	Geometric mean of Au grades relative to the BOCO surface (800 and 0 mN areas). ....	59
Figure 50:	Arithmetic mean of Au grades relative to the BOCO surface (800 and 0 mN areas). ....	59
Figure 51:	Geometric mean of Au grades relative to the weathering front (800 and 0 mN areas). ....	60
Figure 52:	Arithmetic mean of Au grades relative to the weathering front (800 and 0 mN areas). ....	60
Figure 53:	Normalization of Au ratios to immobile element ratios (3000 and 2400 mN areas).....	62
Figure 54:	Normalization of Au ratios to immobile element ratios (800 and 0 mN areas). ....	63
Figure 55:	Distribution of Au and W in the traverse 3000 mN. ....	66
Figure 56:	Gold distribution in different size fractions from drill holes in the 3000 mN area .....	68
Figure 57:	Au distribution in size fractions of pisolitic laterite samples from the 800 mN traverse.....	72
Figure 58:	Au distribution in size fractions of nodular laterite samples from the 800 mN traverse.....	79
Figure 60:	Size distribution of gold grains in the saprock (%). ....	80
Figure 61:	Size distribution of gold grains in the lower saprolite (%). ....	81
Figure 62:	Size distribution of gold grains in the upper saprolite (%). ....	82

Figure 63:	Size distribution of gold grains in the siliceous saprolite, ferruginous saprolite and nodular laterite (%). .....	83
Figure 64:	Plot of eigenvalues for size vs shape distribution.....	85
Figure 65:	3D plot of factor loadings for size vs shape distribution. ....	85
Figure 66:	Plot of eigenvalues for size distribution vs. selective extraction.....	86
Figure 67:	3D plot of factor loadings for size distribution vs. selective extraction. ....	86
Figure 68:	Plot of eigenvalues for shape distribution vs selective extraction.....	87
Figure 69:	3D plot of factor loadings for shape distribution vs selective extraction. ....	87
Figure 70:	Percentage of the supergene Au crystals in the regolith, 3000mN area. ....	89
Figure 71:	Diagrammatic model for proposed regolith evolution at Mt Joel.....	91
Figure 72:	3D plot showing the weathering zones .....	92
Figure 73:	3D plot showing the weathering zones .....	92

## LIST OF TABLES

Table 1:	Summary of the regolith stratigraphy terms used in this report, with approximate equivalencies between logging systems. ....	16
Table 2:	Mineralogical composition by XRD of drill hole RC453.....	19
Table 3:	Mineralogical composition by XRD of drill hole RC670/730. ....	21
Table 4:	Mineralogical composition by XRD of drill hole RC731.....	22
Table 5:	Mineralogical composition by XRD of drill hole RC218/326. ....	24
Table 6:	SI values for the Mt Joel groundwaters, for a number of relevant solid phases.....	45
Table 7:	Median minor element compositions of groundwaters. ....	47
Table 8:	Statistics of Au grades relative to the unconformity surface (3000 and 2400 mN areas). ....	54
Table 9:	Statistics of Au grades relative to the BOCO surface (3000 and 2400 mN areas). ....	55
Table 10:	Statistics of Au grades relative to the base of weathering (3000 and 2400 mN areas). ....	56
Table 11:	Statistics of Au grades from whole 3000 and 2400 mN areas. ....	57
Table 12:	Statistics of Au grades relative to the unconformity surface (800 and 0 mN areas). ....	58
Table 13:	Statistics of Au grades relative to the BOCO surface (800 and 0 mN areas). ....	58
Table 14:	Statistics of Au grades relative to the base of weathering (800 and 0 mN areas). ....	59
Table 15:	Statistics of Au grades from whole 800 and 0 mN areas. ....	60
Table 16:	Mean values of immobile elements in the 3000 mN and 800 mN areas. ....	61
Table 17:	Selective Au extraction of samples from drill hole RC453. ....	64
Table 18:	Selective Au extraction of samples from drill hole RC670. ....	65
Table 19:	Selective Au extraction of samples from drill hole RC218/326.....	65
Table 20:	Concentrations of Au, As, Sb, W, Fe and K in size fractions from top of saprolite samples in the 3000 mN area. ....	67
Table 21:	Selective Au extraction in grain size fractions of samples from the 3000 and 800 mN area.....	69
Table 22:	Concentrations of Au, As, Sb, W, Fe and K in grain size fractions from drill hole samples of pisolitic laterite from the 800 mN traverse. ....	71
Table 23:	Concentrations of Au, As, Sb, W, Fe and K in grain size fractions from drill hole samples of nodular laterite from the 800 mN traverse. ....	73
Table 24:	Mineral composition of heavy concentrates from bulk samples, Mt Joel.....	75
Table 25:	Size distribution of gold grains collected from bulk samples from Mt Joel.....	76
Table 26:	Size distribution (% of total) of gold grains collected from bulk samples from Mt Joel. ....	76
Table 27:	Shape distribution (in % of total) of gold grains collected from bulk samples from Mt Joel. ....	78
Table 28:	Electron microprobe analyses of Au from the primary mineralization (ppm).....	79
Table 29:	Electron microprobe analyses of the residual Au from the regolith (ppm). ....	81
Table 30:	Electron microprobe analyses of the supergene Au from the regolith (ppm).....	81
Table 31:	Selective Au extraction of Mt Joel bulk samples.....	84
Table 32:	Significant eigenvalues - size distribution versus shape distribution of Au grains.....	84

Table 33:	Factor loadings - size distribution versus shape distribution of Au grains.....	85
Table 34:	Significant eigenvalues - size distribution of Au grains vs selective extraction results.....	86
Table 35:	Factor loadings - size distribution of Au grains vs selective extraction results. ....	86
Table 36:	Significant eigenvalues - shape distribution of Au grains vs selective extraction results.....	87
Table 37:	Factor loadings - shape distribution of Au grains vs selective extraction results.....	88

# 1 INTRODUCTION

## 1.1 Characteristics of the area

The Mount Joel gold prospect belongs to Great Central Mines Ltd (GCM). It is located 20 km NE of the Bronzewing gold mine in the Yandal Greenstone Belt, about 400 km north of Kalgoorlie, latitude 27° 16' and longitude 121° 13'. The Yandal Greenstone Belt is located in the extreme NE portion of the Yilgarn Craton. The belt is approximately 200 km long but mostly covered by thick regolith which was probably one of the main reasons why its full mineral potential was not realized until the early '90s (Phillips et al., 1998). The Yandal belt is an approximately 2 700 Ma sequence dominated by mafic and ultramafic volcanics and intrusions varying from lower greenschist facies in the north to amphibolite facies in the south, where Mt. Joel is located. The Au deposits in the Yandal belt are shear hosted in quartz veins and surrounded by broad carbonate alteration with proximal K-mica and Fe-sulphides. Later brittle structures are thought to have played a central role in localizing Au.

The mineralized trend at Mount Joel runs for about 8 km in a nearly N-S direction. Gold occurs in a quartz vein system hosted in metabasalts and amphibolites. Most of the Au is free, sometimes visible, but the vein system is generally sulphide-poor. The amphibolite grade mineral assemblage at Mt. Joel overprints the tectonic fabric, implying that Au mineralization occurred before peak metamorphism and that the alteration envelop is metamorphosed (Phillips et al., 1998).

Several mineralized zones were detected at Mount Joel and are under evaluation. Nearly 1000 reverse circulation holes have been drilled in these zones in a 40 x 40 m grid pattern, locally closed to 20 x 20 m. The whole area is generally flat and deeply weathered. The regolith can be more than 80 m thick and transported overburden is present, varying in thickness from a few metres in the centre and north of the study area to greater than 80 m in the south, where the residual profile is overlain by palaeochannel sediments.

## 1.2 Objectives

The principal objective of AMIRA Project 504 is to determine the main controls of Au mobilization in different areas of the Yilgarn Craton. This report focuses on the work conducted at the Mount Joel gold prospect, which aims to:

- i. Characterize the regolith stratigraphy and determine the geochemistry and mineralogy of the different materials in order to establish a framework to interpret the observed patterns of Au distribution in the regolith.
- ii. Assess the ability of PIMA to characterize regolith materials, particularly for discriminating between transported and residual materials.
- iii. Characterize the groundwater geochemistry to assist in the interpretation of geochemical data and dispersion mechanisms of Au and to assess its use as an exploration tool.
- iv. Characterize the spatial distribution of Au in the regolith (including 3-dimensional distribution of Au related to stratigraphy) and obtain statistical parameters of the Au distribution using a Au database (provided by GCM) based on exploration drilling.
- v. Obtain morphological and chemical parameters of particulate Au and determine mode of Au occurrence using partial extraction techniques and grain size analysis to aid in the interpretation of the mechanisms of Au dispersion.
- vi. Discuss the exploration significance and make recommendations on Au exploration procedures for this terrain type.

## 2 ANALYTICAL PROCEDURES

### 2.1 Multi-element geochemical analysis

Regolith samples were dried at 45°C and a 200 g split was pulverized to <75 µm in a hard carbon steel ring mill (Robertson et al., 1996a). A 30 g aliquot was sent to Becquerel Laboratories for neutron activation analysis (INAA) (detection limit in ppm given in brackets) for: Ag (5), As (1), Au (0.005), Ba (100), Br (1), Ce (2), Co (1), Cr (5), Cs (1), Eu (0.5), Fe (500), Hf (0.5), Ir (0.02), K (2000), La (0.5), Lu (0.5), Na (100), Mo (5), Rb (20), Sb (0.2), Sc (0.1), Se (5), Sm (0.2), Ta (1), Te (5), Th (0.5), U (2), W (2) and Yb (0.5).

X-ray fluorescence (XRF) analysis (detection limit in brackets, % for oxides and ppm for elements) was conducted on fused powders for: Al<sub>2</sub>O<sub>3</sub> (0.01), CaO (0.001), MgO (0.01), MnO (0.002), P<sub>2</sub>O<sub>5</sub> (0.002), SiO<sub>2</sub> (0.01) and TiO<sub>2</sub> (0.003) plus Cl (20), Cu (10), Ga (3), Ni (10), Nb (4), Pb (5), S (10), Sr (5), V (5), Y (5), Zn (5) and Zr (5) in the CSIRO laboratories, Floreat Park. All results for Ag, Ir, Mo, Se, Ta, Te and U were below detection and therefore are not reported.

### 2.2 Partial extractions for gold

Three types of partial extractions were used to test the solubility of Au on selected samples (Gray and Lintern, 1993). The extractant solutions were as follows:

- i. Deionized water: dissolves the most soluble Au.
- ii. Iodide: a 0.1M KI solution is adjusted to pH 7.4 with HCl whilst CO<sub>2</sub> is bubbled through. This extraction dissolves more Au than water alone.
- iii. Cyanide: 0.03M KCN solution saturated with CaO dissolves all but the most refractory Au (which may include larger pieces of Au and Au encapsulated within resistant material such as quartz).

Each extraction was performed on pulverized and unpulverized materials of the same sample. A 25 g portion of sample material was mixed with 50 mL of extractant in a screw-cap polyethylene plastic bottle with a plastic mesh sachet containing 1g of activated carbon, and then gently agitated for one week. At this stage the carbon sachet was removed, washed in deionized water, and analysed for Au by INAA with a detection limit of 1 ppb, thus providing a detection limit of 0.04 ppb for a 25g subsample. The deionized water and iodide extractions were performed on separate subsamples, whereas the cyanide extraction was sequential to the iodide extraction.

### 2.3 Mineralogical investigations

#### 2.3.1 X-ray diffraction analysis

X-ray diffractometry analysis was conducted in pulped samples by CuKα radiation using Phillips PW1050 diffractometer fitted with a graphite-crystal diffracted beam monochromator. Each sample was scanned over a range 3-65° 2θ at a speed of 1°/min and data were collected at 0.02° 2θ intervals. The data were plotted in charts and also made available in digital form for measurement of peak areas in X-ray counts and the width at half height (WHH) of the kaolinite peak at 12.38° 2θ.

#### 2.3.2 Semi-quantitative analysis

Semi-quantitative normative analysis has been performed based on results of whole rock geochemistry by XRF. For that, the weight percent K<sub>2</sub>O has been fully assigned to muscovite or feldspar depending on the indications of the XRD traces. The remaining Al<sub>2</sub>O<sub>3</sub> was then assigned to kaolinite, and after that, the remaining SiO<sub>2</sub> was assigned to free silica (quartz or amorphous silica). This procedure could not be applied to samples with more complex mineralogy, such as those from the lowermost and uppermost parts of the profile.

Results of the XRD analyses were also treated semi-quantitatively by measuring the X-ray counts of the XRD peaks selected to identify mica ( $8.76^\circ 2\theta$ ); kaolinite ( $12.38^\circ 2\theta$ ) and quartz ( $26.66^\circ 2\theta$ ). The peak areas were then corrected for the average mass attenuation coefficient of each sample (this coefficient was calculated according to the major oxide composition of the samples assuming these are sufficiently fine grained and homogeneously distributed; Brindley, 1980). The corrected peak areas were then rationed to an arbitrary number and plotted with the results obtained from whole rock geochemistry for comparison. In the case of quartz, the peak area was further corrected according to a quartz standard, which was analysed under the same conditions. With this procedure, the approximate percentage of quartz in the sample could be estimated.

Other minerals identified by XRD include goethite, hematite, feldspars, chlorite, smectite, vermiculites and carbonates. Their relative amounts were estimated according to visual estimation of the size of the characteristic XRD peaks.

### **2.3.3 PIMA analysis**

PIMA-II (Portable Infrared Mineral Analyser) spectrometer was used to measure the diffuse reflectance spectra at 1300 to 2500 nm (shortwave infrared). Processing and enhancement of the spectral data involved the use of the hull quotient technique for removing “background” albedo effects, and lorentzian deconvolution of spectra using the commercial software package, ORIGIN (Gray and Cudahy, 1996).

## **2.4 3D gridding and visualisation (MVS)**

The regolith stratigraphy and geochemistry of the various Mt Joel Au prospects, with geochemical and logging information provided by GCM, were studied using the 3D visualisation program MVS (Mining Visualisation System, © C Tech Development Corporation). With the exception of the 1600 mN area, logging appeared to be highly consistent, enabling reasonably precise delineation of the:

- i. natural surface;
- ii. base of alluvium (BOA);
- iii. base of complete oxidation (BOCO); and
- iv. base of weathering.

The materials between the base of alluvium and BOCO include all residual regolith, down to approximately the base of saprolite.

Regolith horizons were gridded, “point” anomalies removed by filtering the input data, and the data re-gridded. The authors are aware of the potential to bias the data; however, it was considered necessary to give coherent weathering horizons. Pre-processing of the data included logarithmic transform (base 10) of Au concentrations before gridding. Although this can affect the gridded magnitude of the main mineralization pattern, this is used to enhance detail of the subtle supergene redistributions.

The grid size used was X:Y:Z - 6.5 m:6.5 m:2.5 m. A 95% confidence filter was done on the final result to remove all node points with poor calculated accuracy. The stratigraphy was gridded using the KRIG\_3D\_GEOLOGY module (within MVS), using Convex hull (which confines the krigging domain to a region defined by the sample locations), the maximum number of samples points set to 80, convex hull boundary offset to 0.05, and other settings at default. The geochemical data were then gridded in relation to the surfaces using the KRIG\_3D module, with maximum number of data points (within the specified reach) considered for the parameter estimation at a model node set to 180, horizontal/vertical anisotropy set at 2.5, rectilinear offset parameter at 0.05, post-processing at 0.01-2 ppm Au and all other settings at default.

## **2.5 Gold grain separation and analysis**

Sixteen bulk samples (10-30 kg) were collected for separation of heavy minerals, including Au particles, using a Haultain Superpanner. The bulk samples were dried, split to 4.0-4.5 kg subsamples, and washed with 0.01% Triton X-100. This material was processed in the superpanner several times using about 500 g each time. The superpanner is essentially a mechanized version of the prospector's pan to obtain gravity separation. It consists of a 72 cm long shallow v-shaped trough, varying from 12 to 24cm wide, mounted on a 3-point suspension. The trough slope is variable. A cam that gives a bump on each rotation shakes the trough; in addition a variable frequency side shake with independently variable amplitude at each end can be applied.

The superpanner was set to a 284 cam rpm and 7 mm axial bump amplitude. A 10 mm side shake amplitude was applied at each end in opposing sense, to cause rotational oscillation around vertical axis. The trough angle was varied during the treatment. After the dispersion was complete, the pulp was slowly introduced at the middle part of the trough during agitation. With increasing slope of the trough a thin tail of heavy minerals was obtained in the top quarter of the trough. As fractionation progressed, the light mineral fraction was removed by suction into collector and new portion of the pulp was added. This cycle was repeated and the final tail of heavy minerals was collected into small suction flask by vacuum. The trough was then thoroughly washed and wiped clean with damp tissue until there was no discoloration.

The concentrate was transferred into the trough of a micropanner. This trough is 10cm wide and 25cm long and is provided with changeable slope, cross-wise rocking and trough length direction tapping. A combination of varying slope angle and wash rate was used to separate Au from the other minerals. Gold particles were recovered under a binocular microscope by sticky needle and deposited at the slide with two-sided adhesive tape. More than 100 Au particles, 200-300 grains on average, were picked out from every sample. In case of insufficient recovery of Au grains, the separation cycle was repeated with another subsample.

The morphology and size distribution of Au grains were examined and measured using an optical microscope. Following this, selected particles were examined by SEM and their Ag content, and the composition of neighbouring minerals, were determined semi-quantitatively (due to surface effects of the unpolished grain surfaces) using an energy dispersion X-ray system (EDXS). The SEM study was done in backscattered electron mode, using a Jeol JSM-2 instrument fitted with an environmental sample chamber. This permitted the examination of samples without a conductive coating.

Selected Au grains were analysed quantitatively by electron microprobe using a Cameca SX-50 instrument operated at 35 kV and 450 nA. Polished mounts were prepared by totally embedding the grains in epoxy and carefully polishing down to expose the grains. Long count times (100 sec) were used to reduce detection limits. Native gold was analysed for Ag, Al, As, Br, Cl, Cu, Fe, I, S, Si, Te and Zn.

## **2.6 Groundwater sampling and analysis**

Thirty six shallow (15-20 m depth) and one deep (48 m) groundwater samples were collected onsite by bailer in July 1997, with 16 additional deep samples (31-116 m) collected by Hydro Resources and sent to the CSIRO Floreat laboratories in late 1997 (Figure 1). The shallow groundwaters were sampled from 700 to 3000 mN, and therefore span a variety of regolith environments, with the alluvial cover varying from less than 10 m in the north to 100 m at 1600 mN and 800 mN. The main mineralized areas covered by the shallow water sampling particularly include the 3000 mN zone and the 1600 and 800 mN areas, whereas the deep water samples include two in the 3000 mN zone, one in the 800 mN zone and other samples away from mineralization (Figure 1).

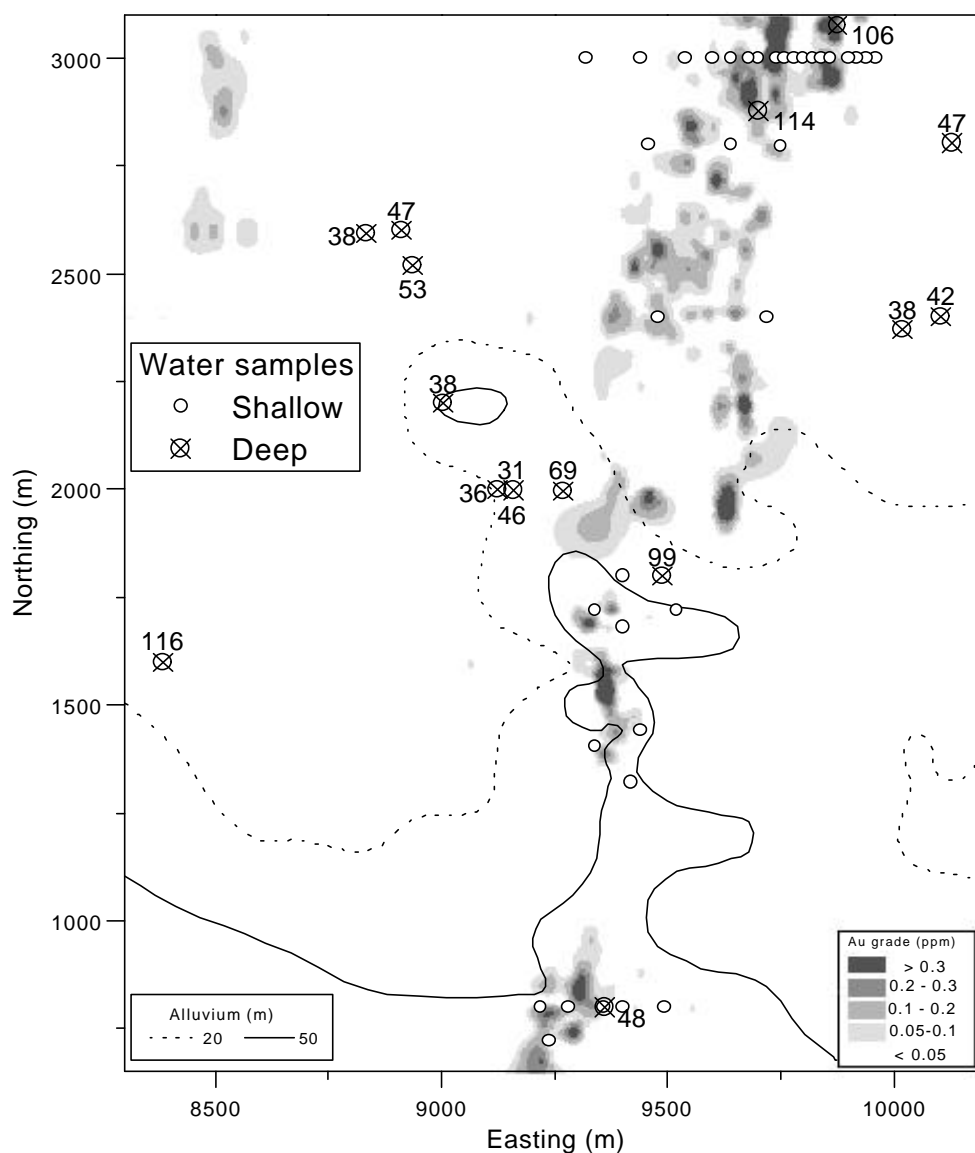


Figure 1: Groundwater sample positions and deep sample depths, showing averaged Au grade and 20 and 50 m alluvium contours.

Waters were analysed for pH, temperature, conductivity and oxidation potential (Eh), at the time of sampling for the bailed waters, and immediately upon arrival for the Hydro Resources samples. A 125 mL aliquot was collected in a polyethylene bottle (with overfilling to remove all air) for  $\text{HCO}_3^-$  analysis by alkalinity titration in the laboratory. About 1.5 L of water was immediately filtered through a  $0.2 \mu\text{m}$  membrane filter. About 100 mL of the filtered solution was acidified [0.1 mL 15 moles/litre (M) nitric acid ( $\text{HNO}_3$ )], and analysed for:

- i. Al, B, Ba, Be, Ca, Cd, Co, Cr, Cu, Fe, K, Li, Mg, Mn, Mo, Na, Ni, P/I (distinction between P and I is difficult due to spectral overlap),  $\text{SO}_4$  (measured as S), Si, Sr, Ti, V and Zn by Inductively Coupled Plasma - Atomic Emission Spectroscopy.
- ii. Ag, Bi, Cd, Ce, Dy, Er, Eu, Ga, Gd, Ge, Ho, La, Mo, Nd, Pb, Pr, Rb, Sb, Sc, Sm, Sn, Tb, Th Tl, Tm, U, W, Y, Yb and Zr by Inductively Coupled Plasma - Mass Spectroscopy.

- iii. Total phosphate by the molybdenum blue colourmetric method (Murphy and Riley, 1962).
- iv. I by subtraction of P from P/I concentration.

About 50 mL of the filtered water was collected separately, without acidification, and analysed for Cl by the Technicon Industrial method (Zall et al., 1956).

A 1 L subsample of the filtered water was acidified with 1 mL 15 M HNO<sub>3</sub> and a 1 g sachet of activated carbon plus 30 g sodium chloride added. The bottle was rolled for eight days in the laboratory and the water discarded. The carbon was then analysed for Au by Instrumental Neutron Activation Analysis (INAA) at Becquerel Laboratories, Lucas Heights. The method was tested by shaking Au standards of varying concentrations, and in varying salinities, with activated carbon (Gray, unpublished data).

The solution species and degree of mineral saturation were computed from the solution compositions using the program PHREEQE (Parkhurst et al., 1980; described in detail in Gray, 1990 and Gray, 1991), which determines the chemical speciation of many of the major and trace elements. To obtain highly accurate speciation data on a limited suite of the major elements (Na, K, Mg, Ca, Cl, HCO<sub>3</sub>, SO<sub>4</sub>, Sr and Ba), the Pitzer specific ion interaction model equations was applied, using the program PHRQPITZ (Plummer and Parkhurst, 1990). These programs calculate the solubility indices (SI) for each water sample for various minerals. If the SI for a mineral equals zero (empirically from -0.2 to 0.2 for the major element minerals, and -1 to 1 for the minor element minerals), the water is in equilibrium with that mineral, under the conditions specified. Where the SI is less than zero, the solution is undersaturated with respect to that mineral, so that, if present, the phase may dissolve. If the SI is greater than zero, the solution is over-saturated with respect to that mineral, which can potentially precipitate from solution. Note that this analysis only specifies possible reactions, as kinetic constraints may rule out reactions that are thermodynamically allowed. Thus, for example, waters are commonly in equilibrium with calcite, but may become oversaturated with respect to dolomite, due to the slow rate of solution equilibration and precipitation of this mineral (Drever, 1982).

The determinations are important in understanding solution processes at a site. They have particular value in determining whether the spatial distribution of an element is correlated with geological phenomena such as lithology or mineralization, or whether they are related to weathering or environmental effects. Thus, if Ca distribution is controlled by equilibrium with gypsum in all samples, then the spatial distribution of dissolved Ca will reflect SO<sub>4</sub> concentration alone and have no direct relation with the presence of primary mineralization.

### 3 REGOLITH STRATIGRAPHY

#### 3.1 Regolith stratigraphy, as defined by Great Central Mines logging

Three major regolith boundaries can be defined according to the GCM logging information from reverse circulation drill cuttings from exploration drilling. The boundaries are:

- i. Unconformity - separates residual from alluvial materials.
- ii. Base of complete oxidation (BOCO) - depth where the recovered material contains negligible unweathered rock fragments.
- iii. Base of weathering - depth where the recovered material is totally constituted of fresh rock fragments.

These boundaries separate four zones: fresh rock; transition; oxide and alluvium (Figure 2). Contours of each of these boundaries are shown in, Figures 3 to 5. The base of weathering and BOCO surfaces are deeper along the mineralized zone. The transported cover is generally less than 10 m thick but in the southern portion of the area, it may reach depths of over 100 m within a palaeochannel running approximately West to East.

The average depths of these boundaries over mineralization in the areas around the 3000 and 800 mN lines, representing the areas with shallow alluvial cover and a deep palaeochannel (Figure 2), show that the base of weathering occurs at similar depths in both areas. However, the residual profile is about 40 m thicker in the 3000 mN area, due to a thicker oxide zone as visualized in Figure 6.

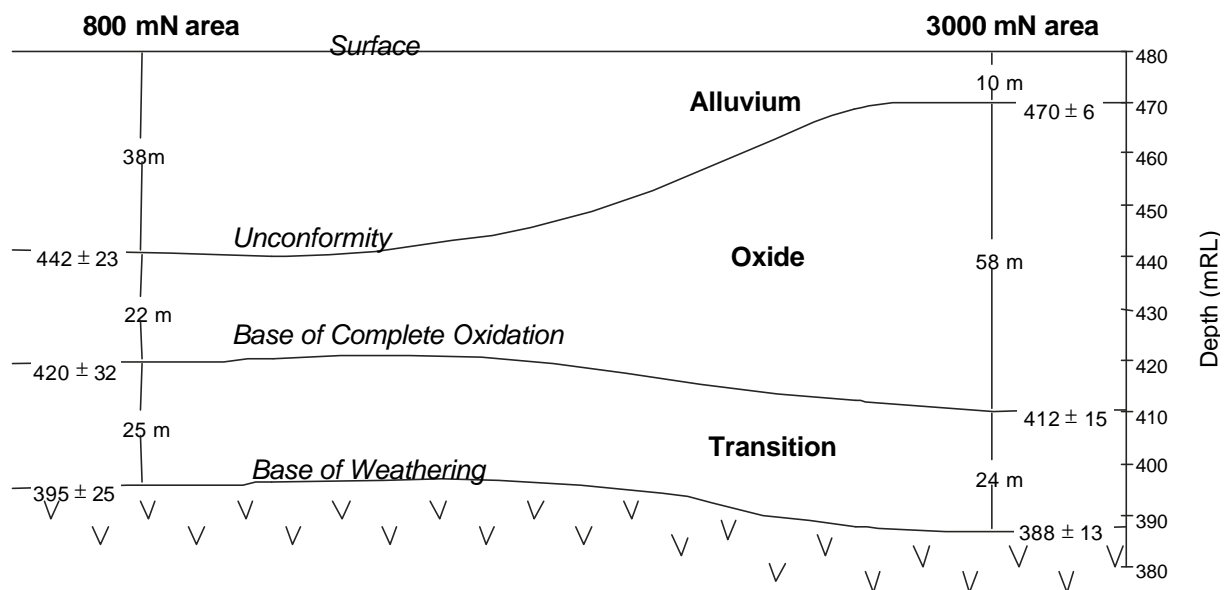


Figure 2: Average depths of weathering front, BOCO and unconformity in the 3000 and 800 mN areas.

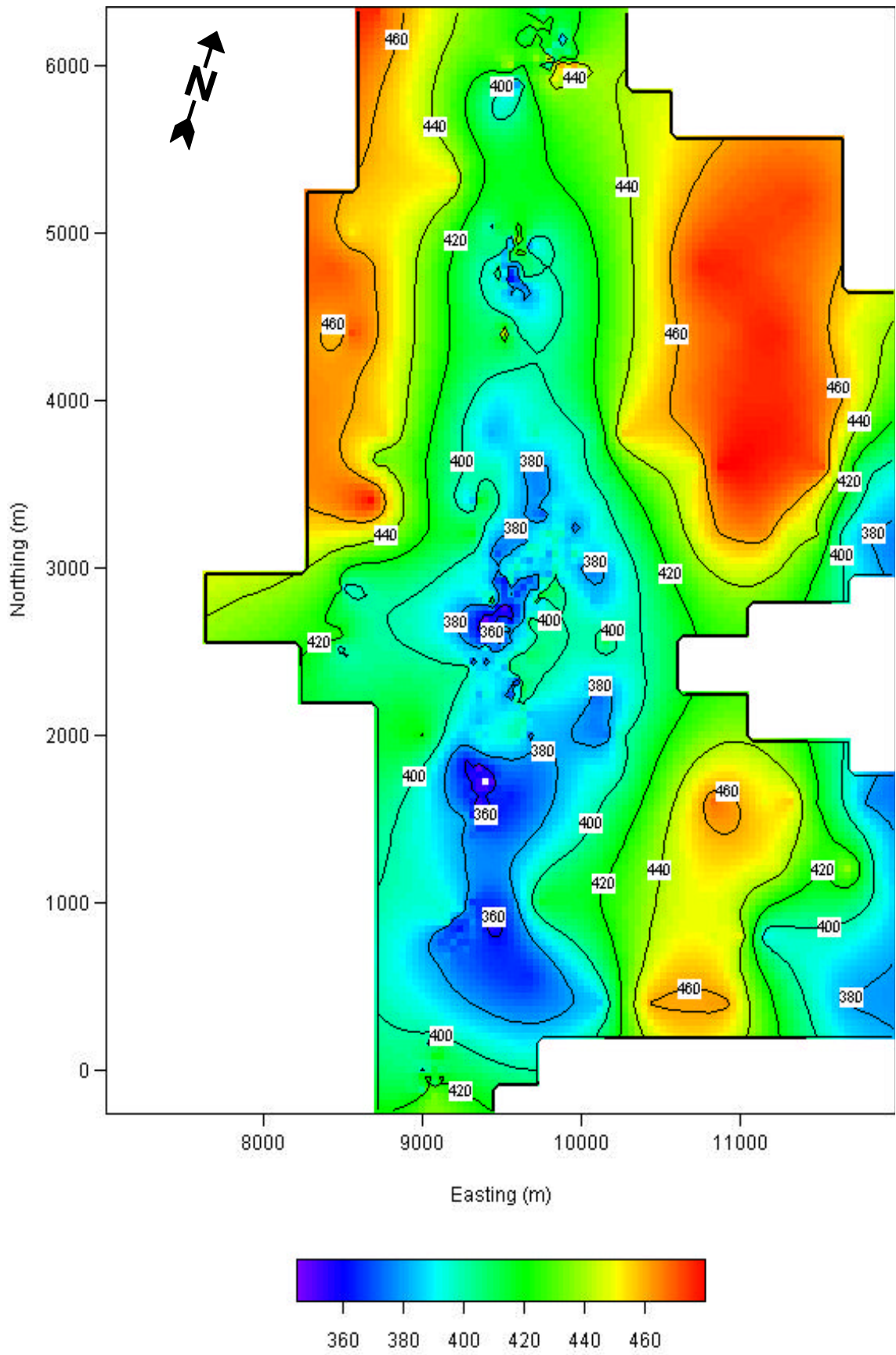


Figure 3: Depth of the base of weathering (mRL).

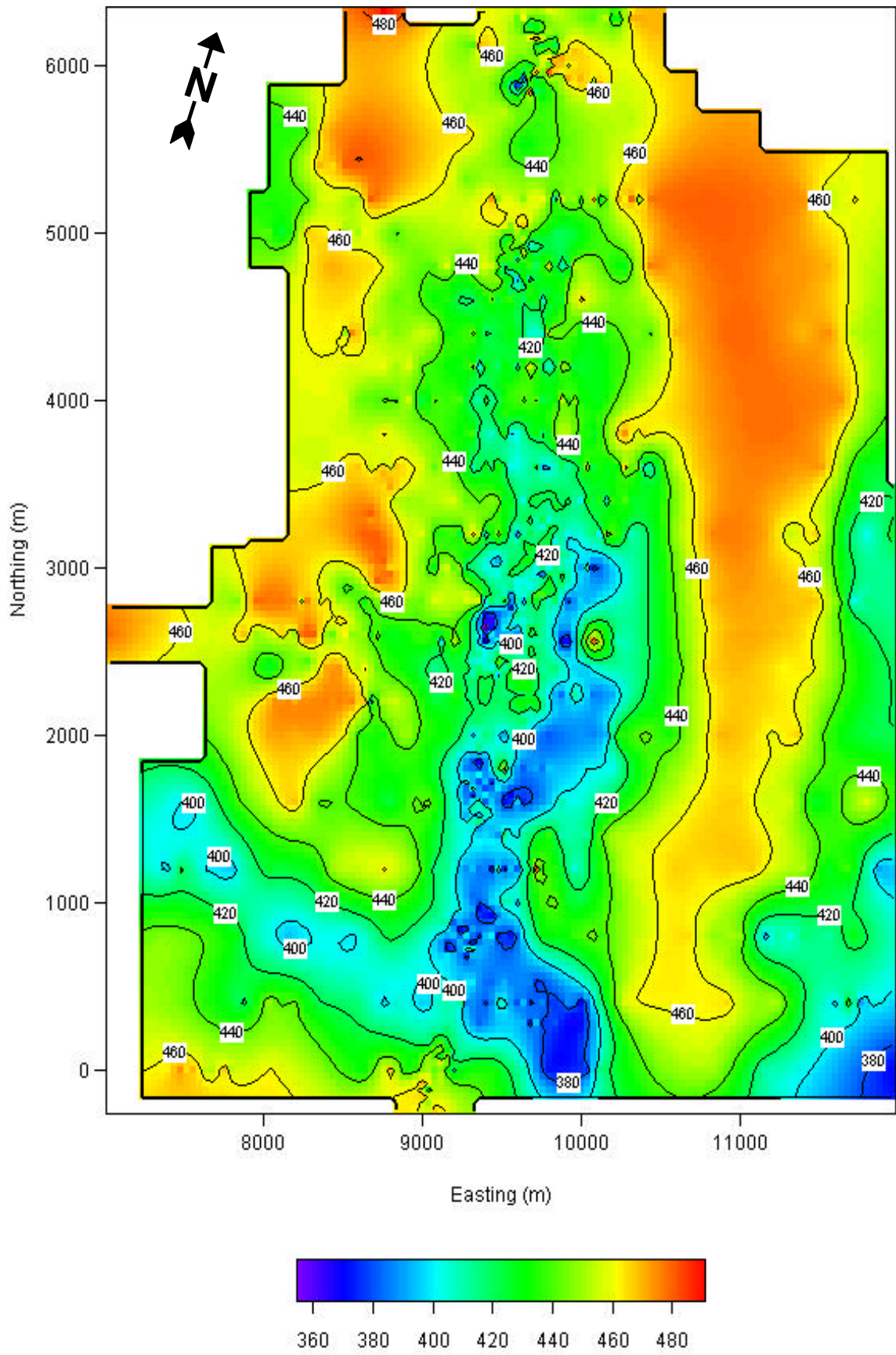


Figure 4: Depth of the base of complete oxidation (BOCO) (mRL).

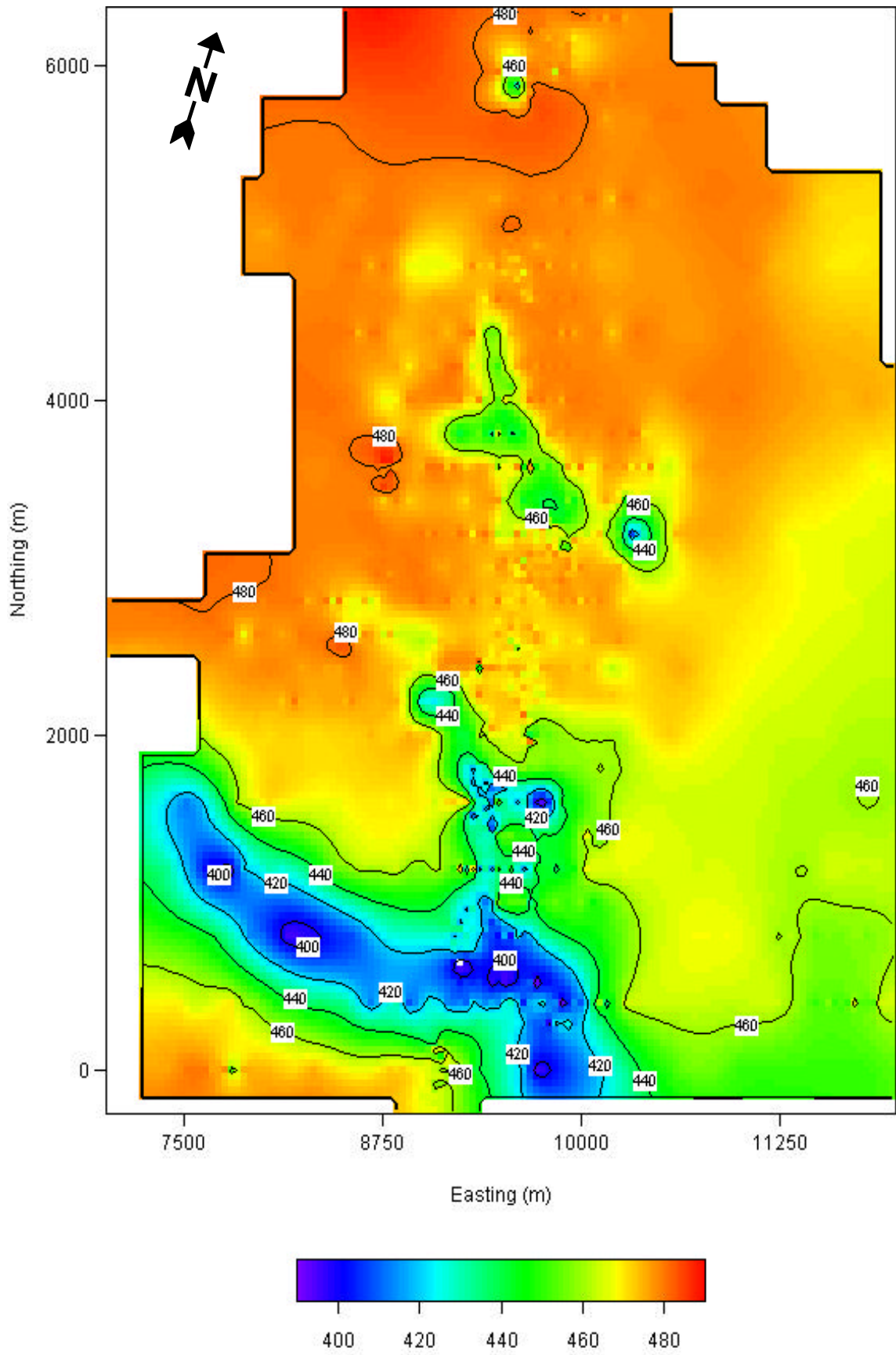


Figure 5: Depth of unconformity (mRL).

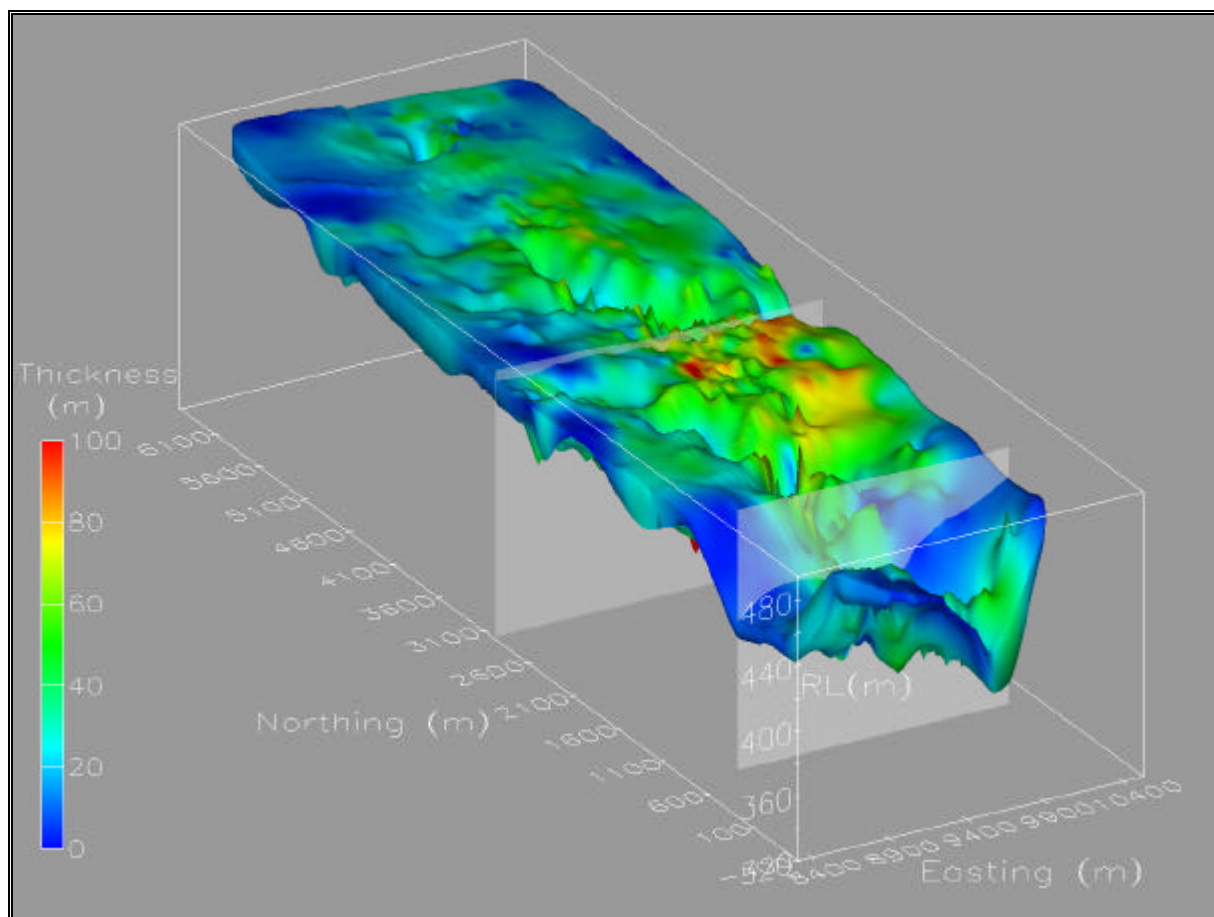


Figure 6: Thickness and elevation of the oxide zone for the Mt Joel study area. Grey planes represent 800 and 3000 mN.

### 3.2 Regolith stratigraphy defined by CRC LEME logging

Further regolith information derives from detailed logging of drill holes in sections 2920 mN, 3000 mN and 800 mN. The logging was based mostly on bulk colour of the samples, guided by the Munsell colour charts, and the nature of coarse fragments obtained by wet sieving of approximately 300 g of each sample. Samples of about 1 to 2 kg were taken from drill spoil at each metre or composited according to geology, weathering features and Au grades.

**SECTION 2920 mN** (Figure 7): Drill holes RC 670, RC 730, RC 453, RC 549 and RC 731 were selected for detailed description of the regolith features and sampling in this section. Detailed logs of drill holes RC453 and RC 670/730 are shown in Figures 8 and 9, respectively, as an example.

The base of weathering is commonly 100 m deep. Above it, a saprock unit has been defined based on the presence of relatively fresh biotite- and chlorite-bearing fragments with greyish colours. It coincides approximately with the transition zone logged by GCM. The saprock grades up into the saprolite, the lower portions of which show paler colours from grey to orange. Upwards, the saprolite becomes more ferruginized and reddish brown, however, colour variation in the saprolite also reflect lithological variations. Biotite and chlorite oxidation imprints a purple colour to the coarse saprolite fragments. Lighter colour intervals may be due to lower abundances of biotite or chlorite. A ferruginous zone with incipient development of yellow cutans over saprolite fragments is present in drill hole RC453 at a depth of about 30 m, and becomes more consistent between 20 m and 10 m (Figure 8) but is not present across the whole section. At depths of about 10 m, the saprolite acquires a more uniform bright reddish

brown colour due to more uniform ferruginization. This is closely accompanied by silicification, which increases upwards and transgresses into the alluvial cover at a depth of 4 to 5 m. The transition to the transported cover is characterized by a change to orange colours, the presence of slightly rounded quartz grain and magnetic Fe nodules without cutans, and the general polymictic nature of the fragments.

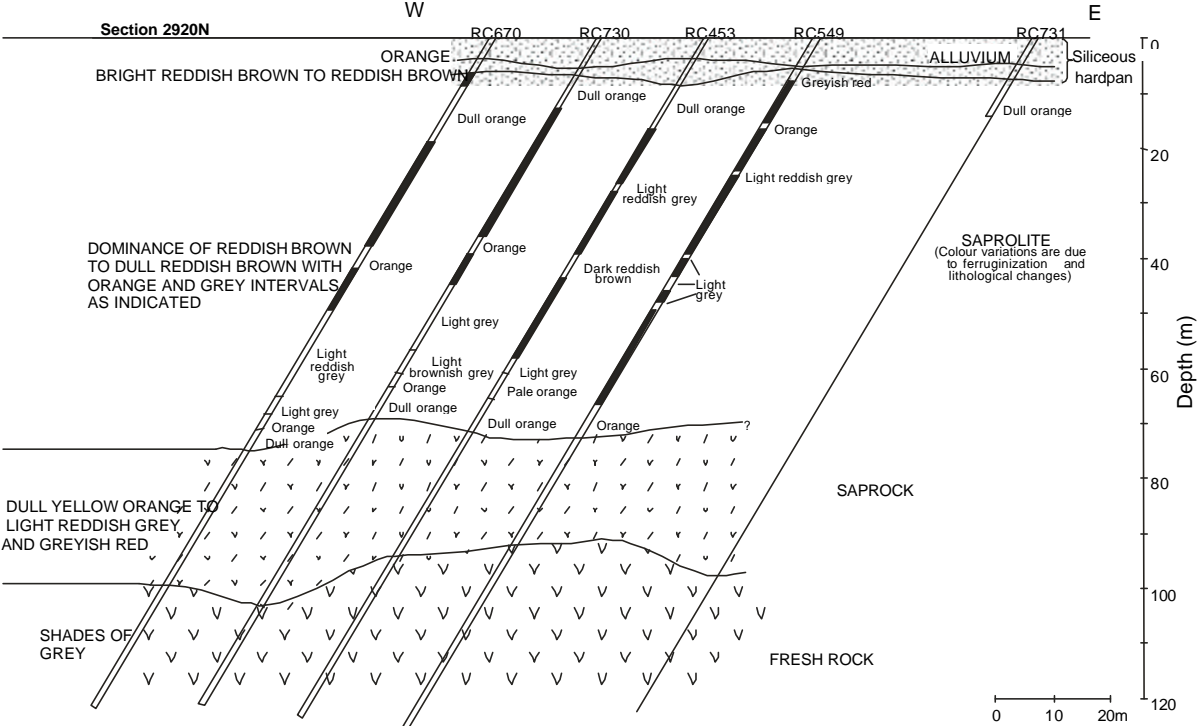


Figure 7: Regolith stratigraphy: Section 2920 mN.

**SECTION 3000 mN (Error! Reference source not found.):** This section was selected to establish the position of the unconformity and investigate lateral geochemical dispersion. Twenty drill holes 20 to 120 m apart were logged along a 800 m long traverse using the same criteria to differentiate the alluvial cover as in the neighboring 2920 mN section. The unconformity is positioned up to 12 m above the one defined by GCM logging. The alluvial cover deepens in the direction of a palaeochannel to the east, where the regolith stratigraphy is similar to the 800 mN area (see below). The unconformity separates lateritic residuum from palaeochannel sediments and the top of the lateritic residuum contains a layer with magnetic nodules and pisoliths, which grade downwards into a nodular zone and then into a ferruginous saprolite.

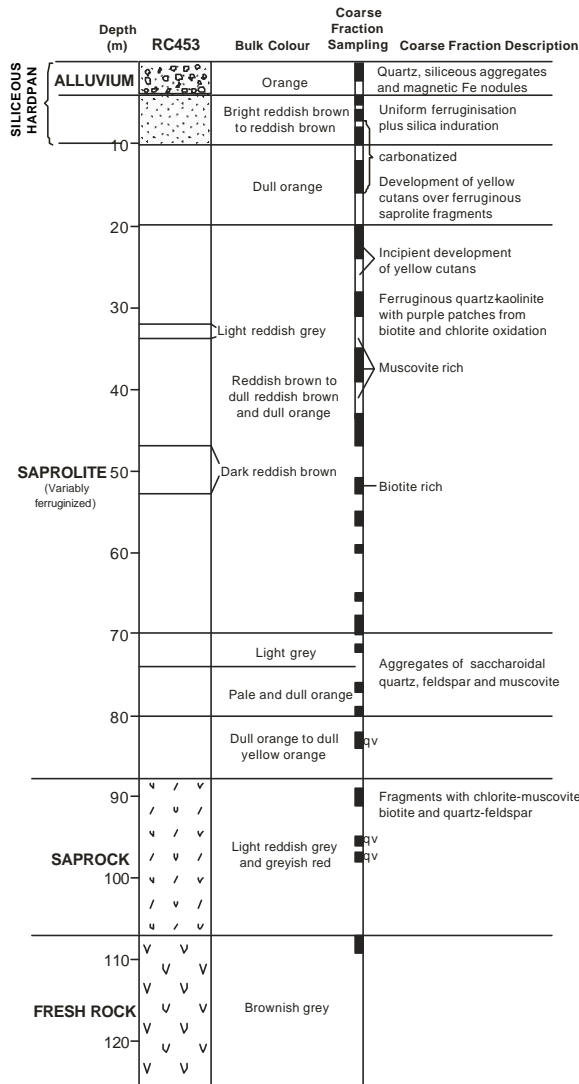


Figure 8: Log of drill hole RC453.

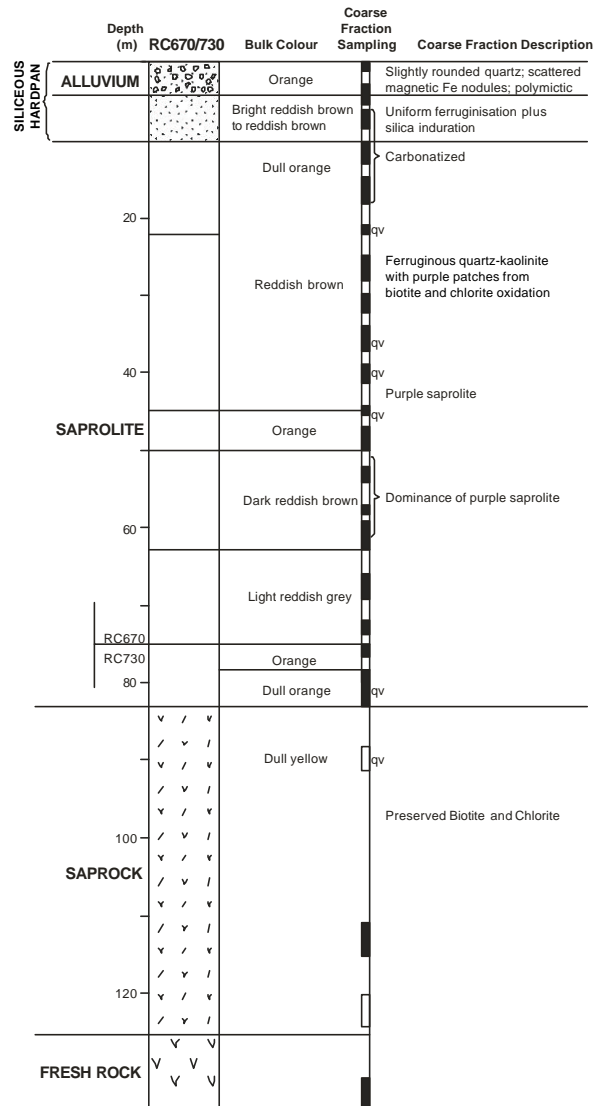


Figure 9: Log of drill hole RC670/730.

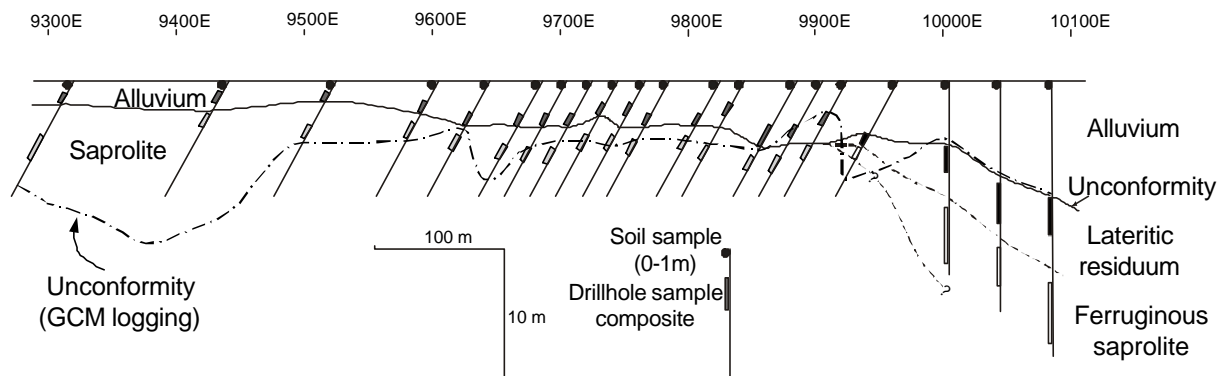


Figure 10: Regolith stratigraphy of section 3000 mN.

**SECTION 800 mN** (Figure 11): Drill holes RC325, RC218, RC326 and RC219, plus selected intervals from neighboring drill holes, especially across the unconformity, were logged to investigate the regolith features and geochemical dispersion in this area.

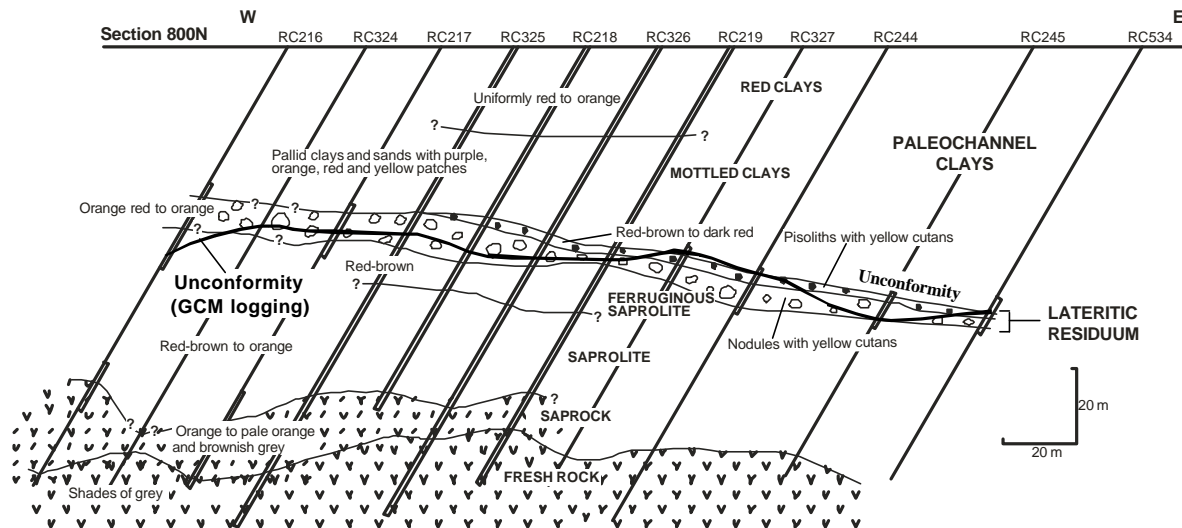


Figure 11: Regolith stratigraphy: Section 800 mN.

A detailed, combined log of drill holes RC326 and RC218 is shown in Figure 12 as an example. The regolith is dominated by a complete laterite profile overlain by 50 m of palaeochannel sediments. The saprock has similar characteristics to section 2920 mN, but the saprolite could be more consistently divided into a lower pale portion and an upper ferruginous portion. Biotite and chlorite oxidation also imprints a purple colour to coarse saprolite fragments. The ferruginous saprolite grades upward into a zone where yellow cutans develop over fragments of purple saprolite, forming a nodular structure in which the primary fabric is partly destroyed by ferruginization. Further upwards is a highly ferruginous zone with pisoliths, which are often magnetic, and where the saprolite fabric is completely destroyed. The transition to the palaeochannel sediments is characterized by the presence of a basal layer of grey clays grading upwards into a mottled clay zone and then into a predominantly red clay zone at the top. The basal gray clay zone contains no magnetic nodules or pisoliths but has slightly rounded quartz grains and rounded purple lithorelics without cutans.

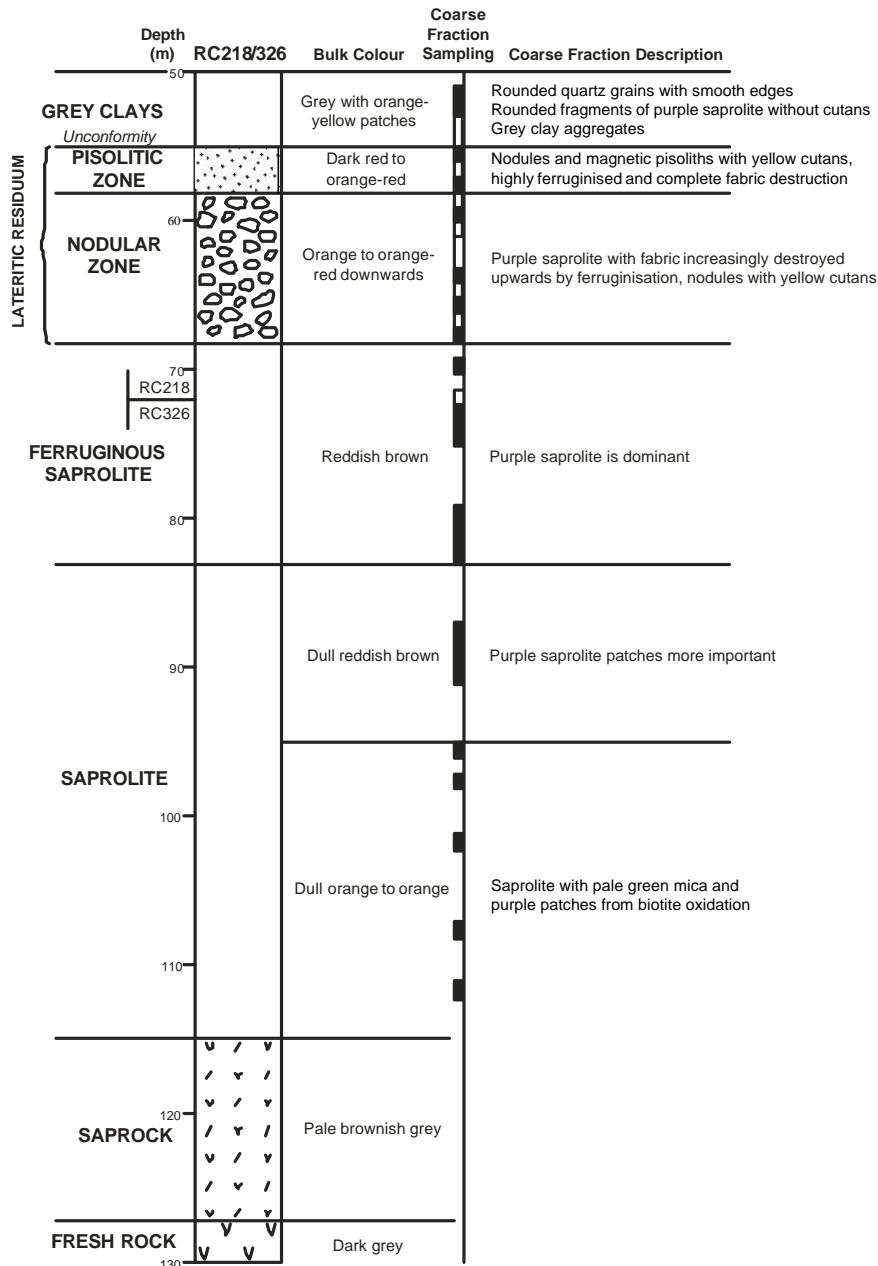


Figure 12: Log of drill holes RC218/326.

### 3.3 Nomenclature used in this report

When referring to data generated by GCM, the terms used to refer to the regolith stratigraphy are *transition zone*, *oxide zone* and *alluvium*. The surfaces that separate these zones are the *base of weathering*, *base of complete oxidation (BOCO)* and *unconformity*. However, during treatment of the Au data (Section 8) it has been found that a distinctly Au enriched zone occurs up to 5 m above and below the unconformity and this interval is then referred to as the *interface zone*. A distinctly Au-depleted zone has also been identified in the oxide zone of the 2400 mN and 3000 mN. It occurs below the interface zone down to 450 mRL, or approximately 30 m below surface. This zone is then referred to as the *leached zone* and the oxide zone between the leached and the transition zone is referred to as the *lower oxide zone*. The terms *leached zone* and *lower oxide* apply only to the 2400 mN and 3000 mN areas since a Au depleted zone is not present in the 0 mN and 800 mN areas. These terms are shown in the first column of Table 1.

When referring to data generated by this research, the terms used to describe the regolith stratigraphy vary according to the area. Where the lateritic profile is preserved and covered by palaeochannel sediments, such as the 800 mN section and eastern portions of the 3000 mN section, the terms applied are the same as those used to describe the regolith stratigraphy of those sections (see third column of Table 1).

In the areas dominated by saprolite and covered by thinner alluvium, such as the 2920 mN section and most of the 3000 mN section, the saprolite was further subdivided based on results of mineralogical, geochemical and Au grade distribution patterns. The *top of saprolite* is defined as the topmost nearly 5 m of the saprolite which is commonly silicified and/or ferruginized and approximately coincides with the Au enriched interface zone. The *leached zone* is a distinctly leached saprolite, which is clay rich and approximately equivalent to the Au-depleted zone defined above. The *lower saprolite* is the saprolite below the leached zone and above saprock and is approximately equivalent to the lower oxide zone defined above. These terms are shown in the second column of Table 1.

The equivalence of the regolith terms defined in this research with those derived from the GCM logging data are summarized in Table 1:

- As the position of the unconformity surface defined by GCM is lower than that logged during this research, the *interface zone* should closely approximate the *top of saprolite* in the 2400 and 3000 mN areas and the upper *lateritic residuum* (probably mostly *pisolitic laterite*) in the 0 and 800 mN areas.
- The *oxide zone* corresponds approximately to the *saprolite* in the 2400 and 3000 mN areas, and to the *saprolite, ferruginous saprolite and lateritic residuum* in the 0 and 800 mN areas.
- In the 2400 and 3000 mN areas the *leached zone* and *lower oxide zone* of GCM corresponds approximately *leached zone* and *lower saprolite* zones defined by this research.
- The *transition zone* corresponds approximately to the *saprock*.

Table 1: Summary of the regolith stratigraphy terms used in this report, S with approximate equivalencies between logging systems.

GCM logging data	This research	
	3000 mN area	800 mN area
Alluvium (with logged unconformity 0-5m below that of LEME)	Alluvium	Alluvium (and palaeochannel sediments)
Interface	Saprolite: Top of saprolite	Laterite: pisolitic zone
Oxide zone: Leached zone 450 mRL → Lower oxide	Leached zone Lower saprolite	? nodular zone Ferruginous saprolite Saprolite
Transition zone	Saprock	Saprock
Fresh rock	Fresh rock	Fresh rock

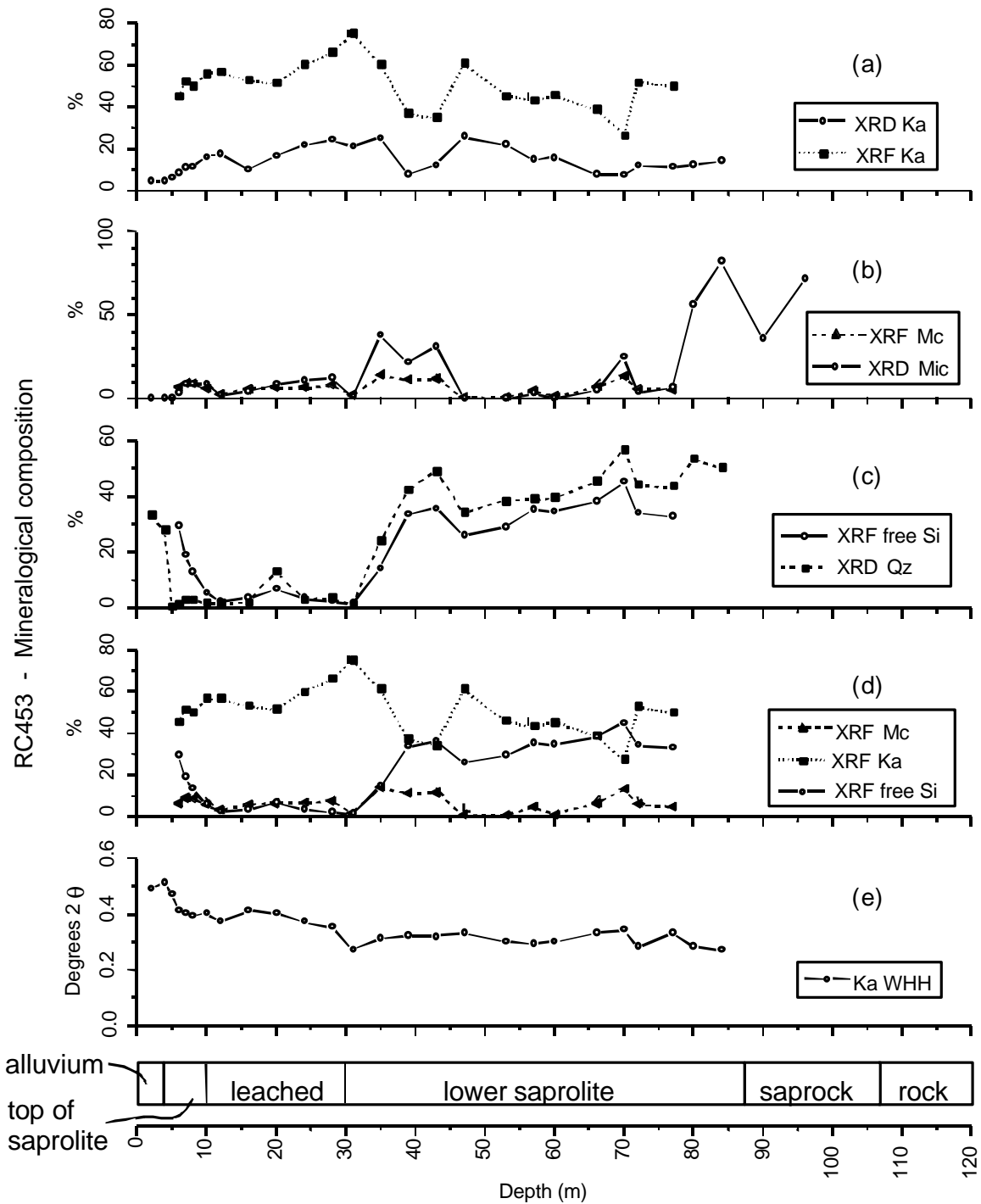
## 4 REGOLITH MINERALOGY

### 4.1 3000 mN area

The results for drill hole RC453 are shown in Figure 13 and Table 2, for drill hole RC670/730 in Figure 14 and Table 3 and for drill hole RC731 in Figure 15 and Table 4. In the saprock, primary minerals such as chlorite, plagioclase, K-feldspar, calcite, dolomite and hornblende are partly preserved. However, these minerals are completely absent in the saprolite, where kaolinite and quartz are the dominant phases. The leached zone is characterized by a significant decrease in the proportion of free silica (which includes quartz and any other SiO<sub>2</sub> phases) and an increase in kaolinite. The percentage of quartz calculated from XRD analysis closely follows the amount of free silica calculated from XRF, with the minor disparity shown by the higher amounts of quartz presumably due to errors inherent to this type of calculation. Despite that, there is a noticeable inversion of this trend at a depth of about 10 m (near the top of saprolite), where the amount of free silica becomes distinctly greater than that of quartz, reflecting a higher abundance of amorphous silica related to the siliceous zone. The amount of quartz increases again in the alluvial cover where feldspars are also present, reflecting the allochthonous nature of the material, whose provenance is possibly granitic rocks a few kilometres to the west. Calcite and dolomite are also present in the upper portions of the saprolite and are generally preferentially concentrated below the siliceous zone.

The amounts of kaolinite and muscovite calculated from XRD and XRF data are similar. However, in many cases XRD analysis could not unequivocally distinguish biotite or phlogopite in the presence of muscovite. Muscovite, however, is more resistant to weathering and its presence in some intervals in the saprolite has been confirmed by XRD in drill holes RC453 (Table 1) and RC670/730 (Table 2).

Goethite and hematite are present throughout the whole regolith, but in the alluvial cover hematite tends to dominate, probably reflecting dehydration close to the surface. On the other hand, goethite is dominant over hematite in the permanently saturated zone close to the weathering front. Kaolinite from the alluvial cover shows a characteristic broader peak, reflecting its poorer crystallinity.



- (a) XRD Ka: kaolinite from XRD corrected for mass absorption  
XRF Ka: kaolinite abundance calculated from XRF data
- (b) XRF Mc: muscovite abundance calculated from XRF data  
XRD Mic: mica from XRD corrected for mass absorption
- (c) XRF free Si: silica as quartz and amorphous calculated from XRF data  
XRD Qz: quartz abundance from XRD corrected for mass absorption and standardised to 100% quartz
- (d) Kaolinite, muscovite and free silica calculated from XRF data [ as for (a), (b) and (c) ]
- (e) Ka WHH: XRD kaolinite  $7\text{\AA}$  peak width at half height

Figure 13: Mineralogical composition by XRD and XRF of drill hole RC453.

Table 2: Mineralogical composition by XRD of drill hole RC453.

Zone	Depth (m)	Quartz	Kaolinite	Chlorite	Mica	Hematite	Goethite	K-feldspar	Plagioclase	Calcite	Dolomite	Rutile
Alluvium	0-2	xxxx	xx		x	x		xx	xx			
	2-4	xxx	xx	x-sm	x	x	x	x	x	x		
	4-5	x	xxx		x	x	x	x				
Top of saprolite	5-6	?	xxx		x	x	xx	?				?
	6-7	?	xxx		x-m	xx	xx					x
	7-8	?	xxx		x-m	xx	xx			xx		x
	8-10	?	xxx		x	xxx	xx			xx		x
Leached zone	10-12		xxx		x	xxx	xxx				x	x
	12-16		xxx		x	xxx	xxx			x	x	x
	16-20	xx	xxx		x	xxx	xxx				x	x
	20-24	?	xxx		x	xx	xxx					x
	24-28	?	xxxx		x	xx	xxx					x
	28-31	x	xxxx		x	xxx	xx					x
Lower saprolite	31-35	xxx	xxxx		xxx-m	x	xx					x
	35-39	xxx	xx		xx-m	xx	xx					
	39-43	xxx	xxx		xx-m	xx	xx					
	43-47	xxx	xxxx			xx	xx					x
	51-53	xxx	xxx			xx	xx					x
	55-57	xxx	xxx		x	xx	xx					x
	59-60	xxx	xxx			xx	xx					x
	65-66	xxx	xxx		x	xx	xx					x
	69-70	xxxx	xxx		xx-m	xx	xx					x
	71-72	xxxx	xxx		x	x	x					x
	76-77	xxxx	xxx		x	x	xx					x
	79-80	xxxx	xxx		xx-m&p		x					x
82-84	xxxx	xxx		xxx-m&p		x						
Saprock	89-90	xxxx	xx	xx-csm	xx-p		x		xx			
	95-96	xxx	xxx	x	xxx-m&p		x	x	x			
	97-98	xxx	xx	x	xxx-m&p		x	x	x			
Fresh	107-109	xx		xxx-chl	xx				xx			

xxxx Predominant

xxx Moderate to high concentration

xx Slight to moderate concentration

x Trace

? Possible trace

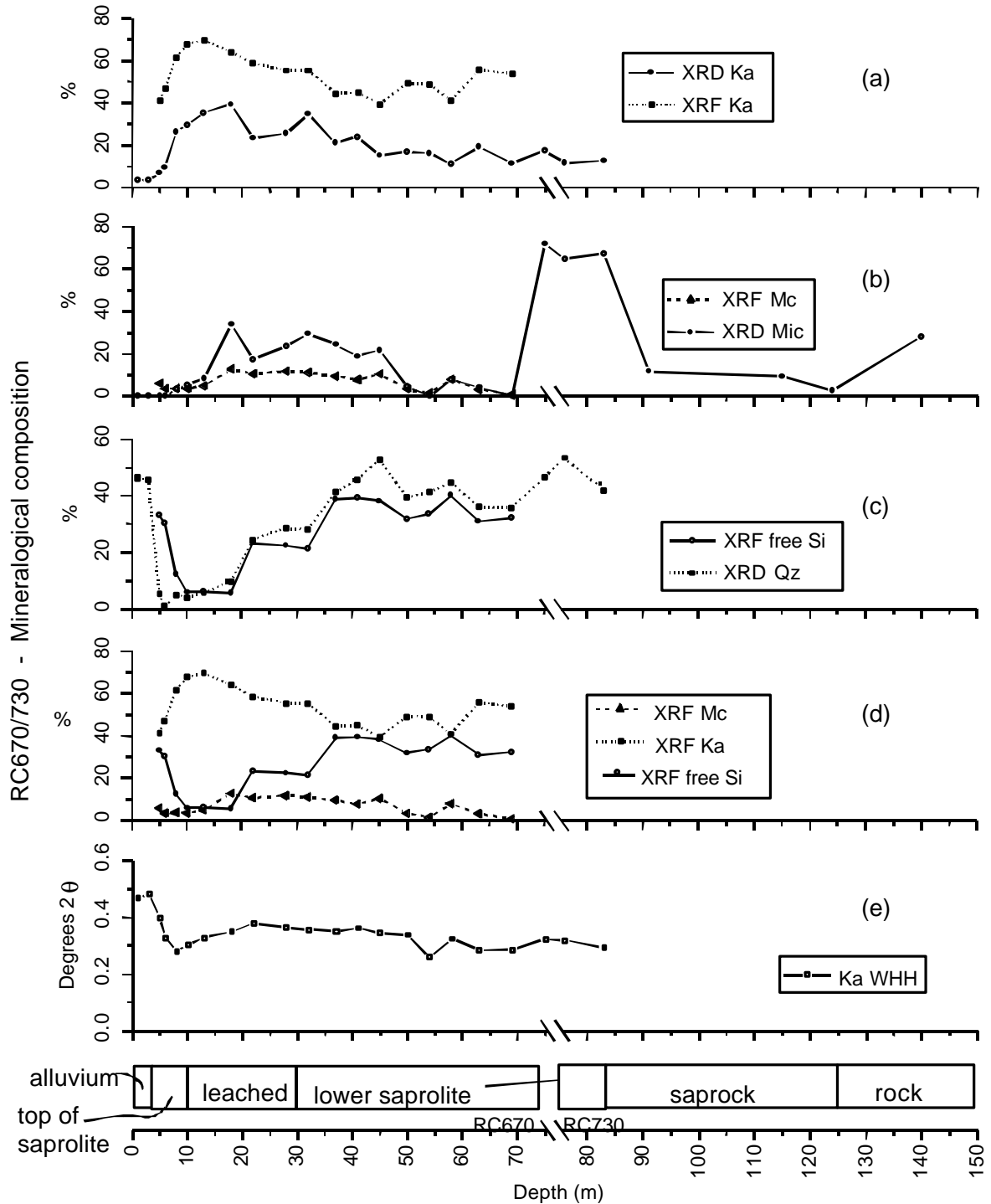
sm - smectite

csm - chlorite/smectite

chl - fresh chlorite

m - muscovite

p - phlogopite



- (a) XRD Ka: kaolinite from XRD corrected for mass absorption  
XRF Ka: kaolinite abundance calculated from XRF data
- (b) XRF Mc: muscovite abundance calculated from XRF data  
XRD Mic: mica from XRD corrected for mass absorption
- (c) XRF free Si: silica as quartz and amorphous calculated from XRF data  
XRD Qz: quartz abundance from XRD corrected for mass absorption and standardised to 100% quartz
- (d) Kaolinite, muscovite and free silica calculated from XRF data [ as for (a), (b) and (c) ]
- (e) Ka WHH: XRD kaolinite 7Å peak width at half height

Figure 14: Mineralogical composition by XRD and XRF of drill hole RC670/730.

Table 3: Mineralogical composition by XRD of drill hole RC670/730.

	Hole	Depth (m)	Quartz	Kaolinite	Mica	Goethite	Hematite	Chlorite	Plagioclase	K-feldspar	Hornblende	Calcite	Dolomite	Vermiculite	Smectite
<b>Alluvium</b>	RC670	0-1	xxxx	x			tr		tr	x					tr
	RC670	1-3	xxxx	x			x		x	x					tr
<b>Top of saprolite</b>	RC670	3-5	x	x		xx	xx								tr
	RC670	5-6	tr	xx		xx	xx								
	RC670	6-8	x	xxxx	tr	xx	xx					xx			
	RC670	8-10	x	xxxx	tr	xx	xx					xx			
<b>Leached zone</b>	RC670	10-13	x	xxxx	tr	xx	x					xx			
	RC670	15-18	x	xxxx	xxx-m	xx	xx					x			
	RC670	21-22	xx	xxx	xxx-m	xx	x								
	RC670	25-28	xxx	xxx	xxx-m	xx	x								
	RC670	30-32	xx	xxxx	xxx-m	xx	x								
<b>Lower saprolite</b>	RC670	34-37	xxxx	xxx	xxx-m	xx	xx								
	RC670	39-41	xxxx	xxx	xx-m	xx	xx								
	RC670	44-45	xxxx	xx	xx-m	xx	x								
	RC670	47-50	xxx	xx	tr	xx	xx								
	RC670	52-54	xxx	xxx		xx	xx								
	RC670	57-58	xxxx	xx	tr	xx	xx								
	RC670	59-63	xxx	xxx	tr	xx	xx								
	RC670	66-69	xxx	xx		xx	x								
	RC670	74-77	xxxx	xxx	xxxx-p	xx	x								
	RC730	71-76	xxxx	xx	xxxx-p	xx	x								
	RC730	78-83	xxx	xx	xxxx-p	xx	x								
<b>Saprock</b>	RC730	88-91	xxx		x	tr	x	xx							
	RC730	111-115	xx		x			xxx	x						
	RC730	120-124	xx		tr			xx	xx		xx	x	x	x	
<b>Fresh</b>	RC730	135-140	xx		x			x	xx		x	xx	xx		

xxxx Predominant  
xxx Moderate to high concentration  
xx Slight to moderate concentration  
x Trace

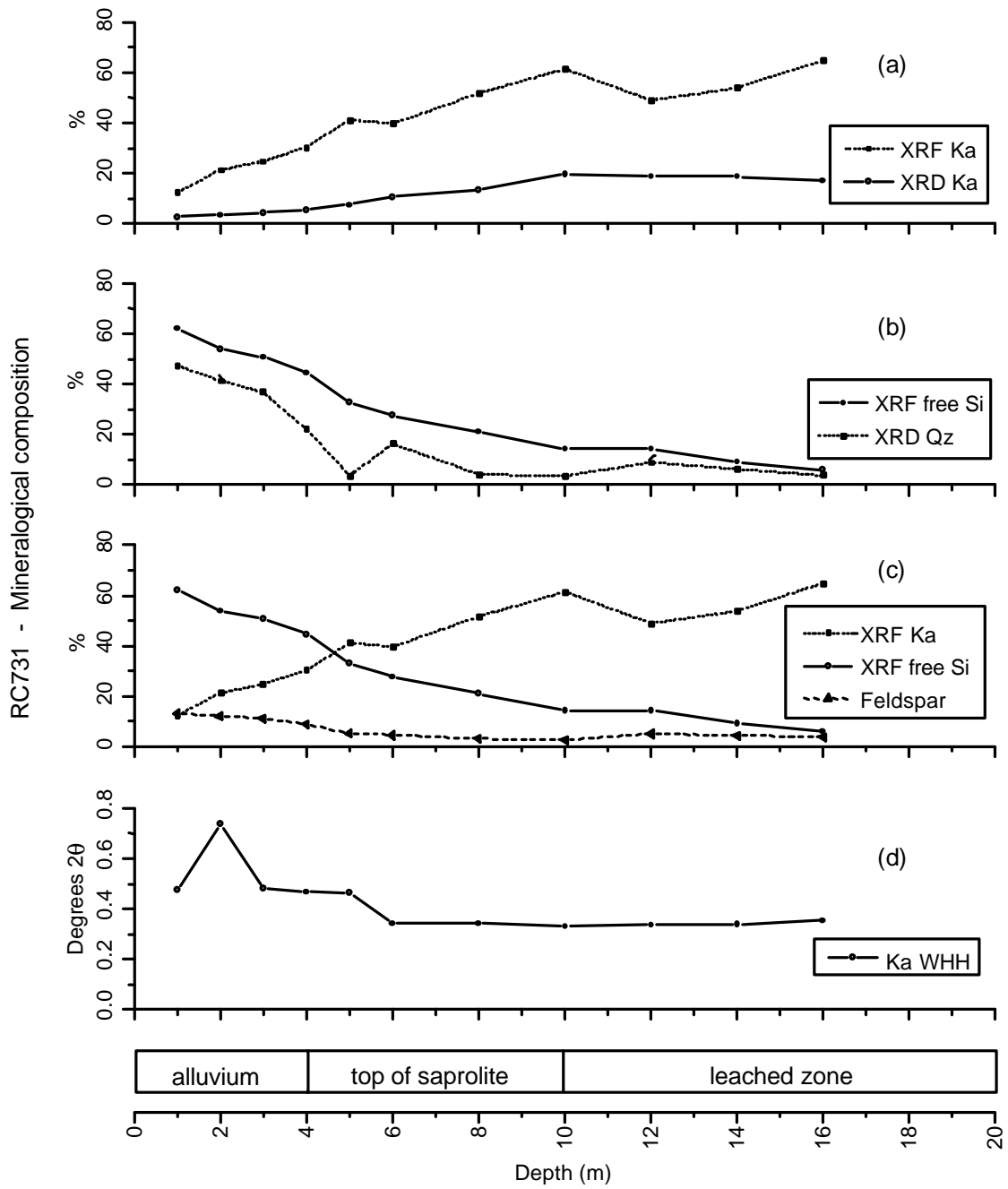
? Possible trace  
m - muscovite  
p - phlogopite

Table 4: Mineralogical composition by XRD of drill hole RC731.

	Depth (m)	Quartz	Kaolinite	Mica	Goethite	Hematite	Plagioclase	K-feldspar	Calcite	Smectite
<b>Alluvium</b>	0-1	xxx	x			tr	xx	xx		tr
	1-2	xxx	x			tr	xx	xx		tr
	2-3	xxx	x			tr	xx	x		tr
	3-4	xx	x		tr	x	x	x		tr
	4-5	tr	x		x	x				tr
<b>Top of saprolite</b>	5-6	x	x	tr	xx	xx				
	7-8	tr	xx		xxx	xx				
	9-10	tr	xxx		xxx	x				x
<b>Leached zone</b>	11-12	x	xxx	tr	xx	xx			tr	
	13-14	x	xxx	tr	xx	xx			xx	
	15-16	x	xxx		x	xx			xx	

xxxx Predominant  
 xxx Moderate to high concentration  
 xx Slight to moderate concentration

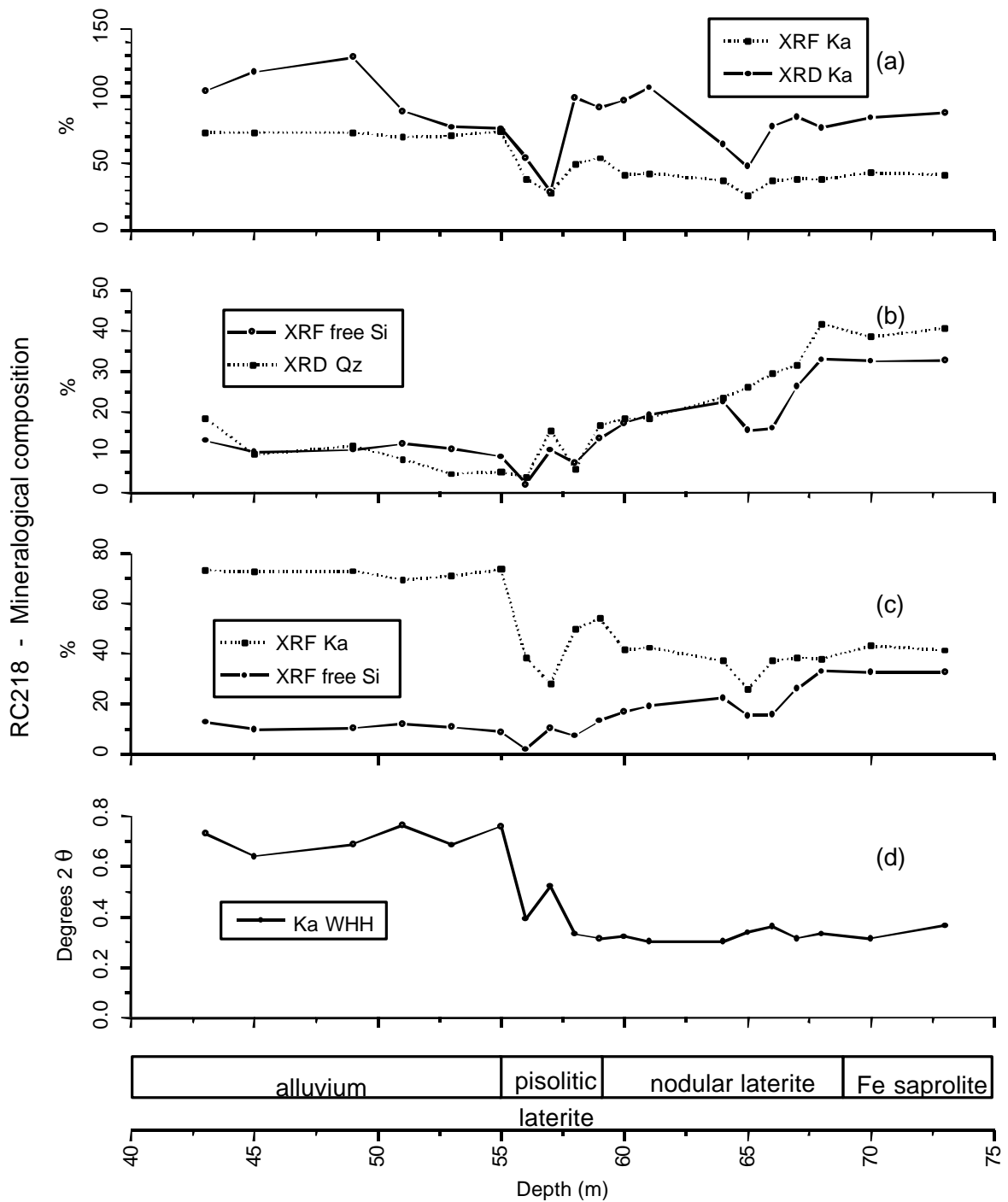
x Trace  
 ? Possible trace



- (a) XRF Ka: kaolinite abundance calculated from XRF data  
XRD Ka: kaolinite from XRD corrected for mass absorption
- (b) XRF free Si: silica as quartz and amorphous calculated from XRF data  
XRD Qz: quartz abundance from XRD corrected for mass absorption and standardised to 100% quartz
- (c) Feldspar: feldspar abundance calculated from XRF data, with kaolinite and free silica as per (a) and (b)
- (d) Ka WHH: XRD kaolinite 7Å peak width at half height

Figure 15: Mineralogical composition by XRD and XRF of drill hole RC731.





- (a) XRF Ka: kaolinite abundance calculated from XRF data  
XRD Ka: kaolinite from XRD corrected for mass absorption
- (b) XRF free Si: silica as quartz and amorphous calculated from XRF data  
XRD Qz: quartz abundance from XRD corrected for mass absorption and standardised to 100% quartz
- (c) Kaolinite and free silica calculated from XRF data [as for (a) and (b)]
- (d) Ka WHH: XRD kaolinite 7Å peak width at half height

Figure 16: Mineralogical composition by XRD and XRF of drill hole RC218/326.

## 5 PIMA SURVEY

### 5.1 Introduction

The Portable Infrared Mineral Analyzer (PIMA-II) is a compact spectrometer which allows rapid and cost effective mineralogical analyses. It measures the reflected radiation, resulting in absorption features, from the surface of samples in the short wavelength infrared (SWIR) range from 1300 to 2500 nm. The characteristic absorption features of clay minerals are related to the presence of OH, H<sub>2</sub>O, Al-OH, Fe-OH and Mg-OH molecules, which produce absorptions around the 1400 nm, 1900 nm, 2200 nm, 2250 nm and 2330 nm wavelengths, respectively.

The sharpness and depth of diagnostic absorption features generally increase with increasing degree of crystallinity. Composition variations are typically represented by shifts in the wavelength of diagnostic absorption features. A range of geological environments can be distinguished by properly treating the absorption features related to kaolinite and water (Pontual and Merry, 1996; Gray and Cudahy, 1996). In these studies, a series of ratios of reflectance intensities at specific wavelengths were tested and deconvolution of the spectrum into its component gaussian curves were also obtained to extract spectral parameters of potential significance in the study of regolith materials. The ratio of reflectances are generally easier to obtain than curve parameters such as area and peak position, and are therefore of more practical use for logging regolith materials.

At Mount Joel, the ratios of reflectance intensities that produced the best results were: 1414/1395; 2160/2177; 2205/2160; and 2380/2320. The 1414/1395 ratio is related to kaolinite crystallinity, but may be influenced by the presence of mica, talc or chlorite. The other ratios relate more specifically to kaolinite crystallinity.

Deconvolution of the absorption features in the range 1300-1600 nm has been performed to obtain the gaussian curves of the kaolinite diagnostic peaks at 1390 nm and 1414 nm, plus two additional peaks at approximately 1430 nm and 1460 nm, presumably related to "bound water" (i.e. H<sub>2</sub>O molecules firmly attached to minerals). An example is shown in Figure 17. The spacing between the 1390 nm and 1414 nm peaks correlates positively with degree of disorder in kaolinite (Pontual and Merry, 1996). Since the 1414 nm peak for kaolinite is fixed, only the wavelength of the 1390 nm peak need be used to estimate kaolinite disorder. The deconvoluted 1460 nm peak area was also calculated to estimate the amount of "bound water" in the samples. Deconvolution was also applied to the water absorption curve in the range 1800-2100 nm which gives better water only discrimination, with the 1910 nm peak area calculated for comparison with the results from the 1460 nm peak.

### 5.2 Results

The wavelength of the deconvoluted kaolinite 1390 nm peak from samples of drill holes RC453 and RC218/326 are plotted in Figures 18 and 19 respectively. There is a clear shift in the peak positions to lower wavelengths in the samples near the alluvial cover on both drill holes. XRD results on the same samples confirm the presence of more disordered kaolinite in the alluvial cover (Figures 13 and 16).

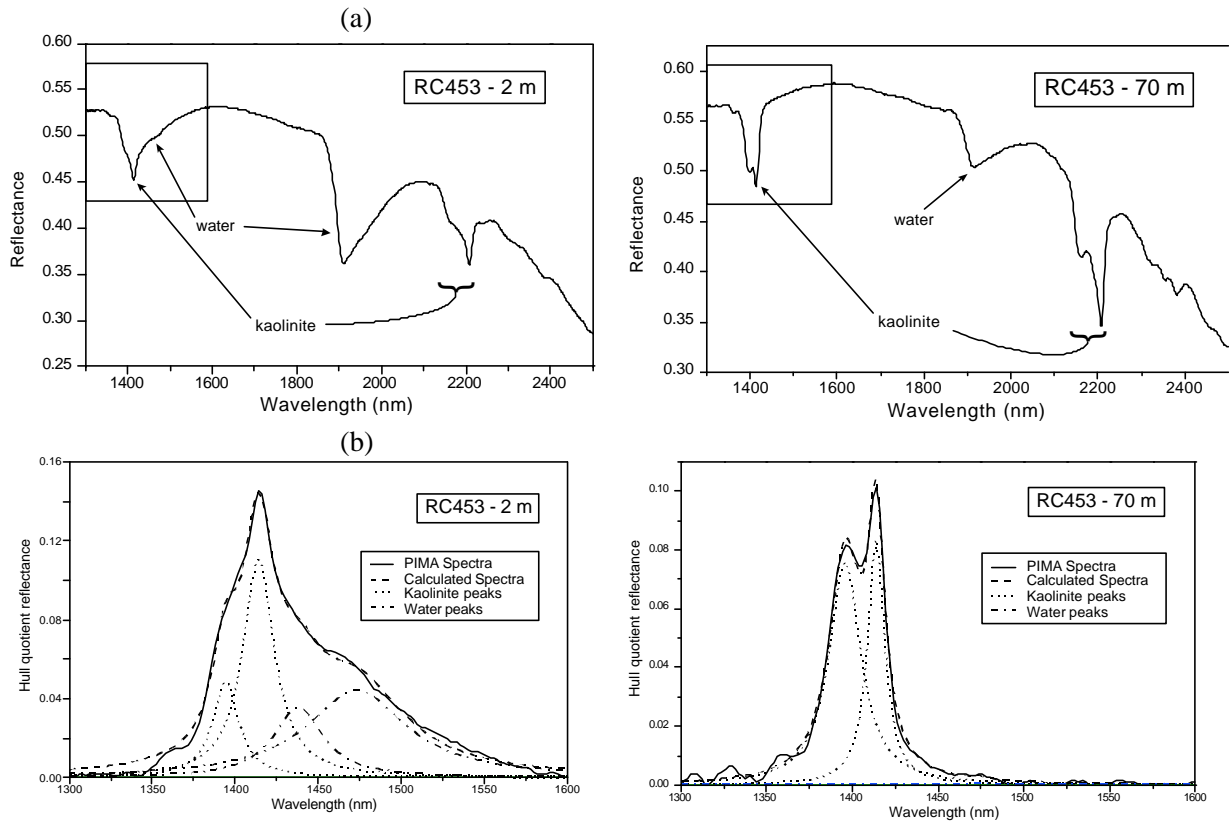


Figure 17: Example deconvolutions for  $H_2O$  rich (RC453, 2 m) and  $H_2O$  poor (RC453, 70 m) samples: (a) Whole uncorrected reflectance with region used for deconvolution (1300-1600 nm) highlighted; and (b) deconvolution of hull corrected 1300-1600 nm region.

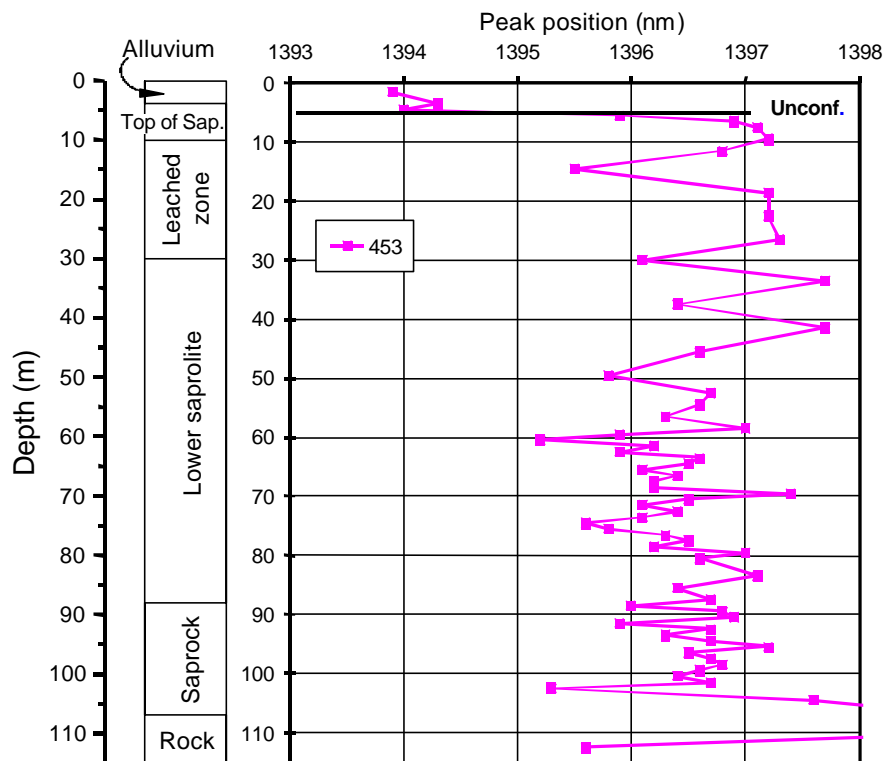


Figure 18: Wavelength of the 1390 nm kaolinite peak in drill hole RC453.

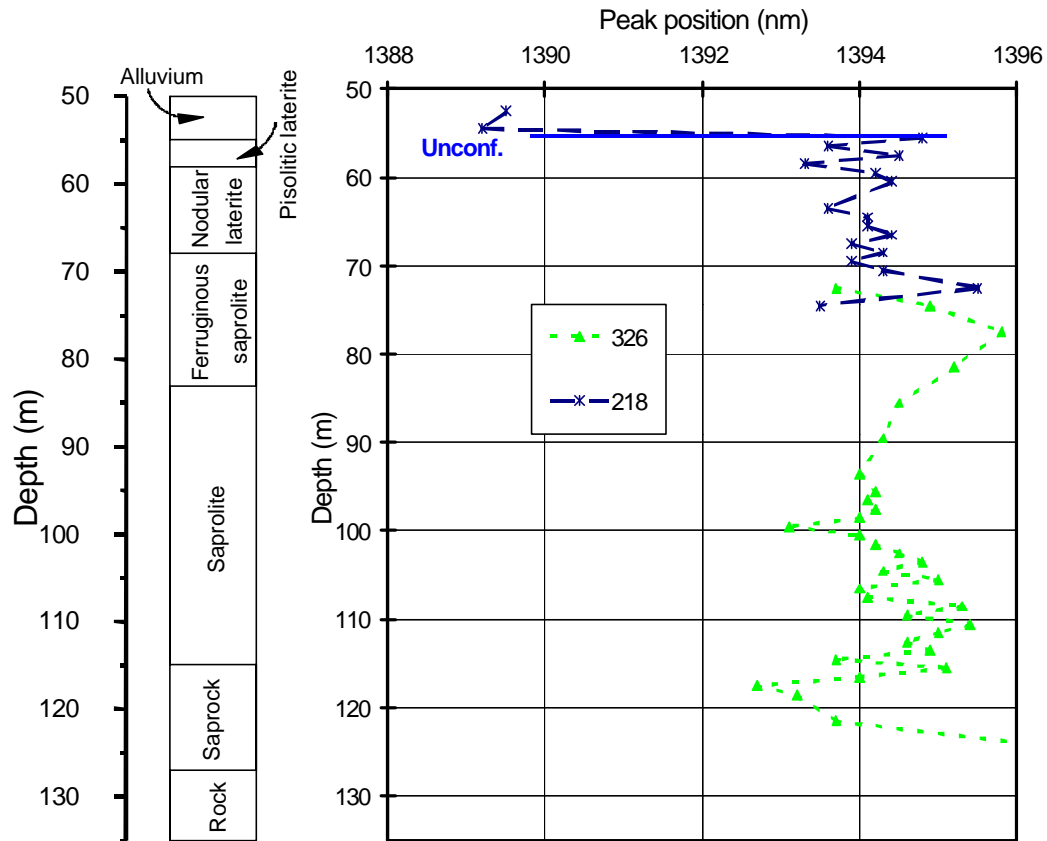


Figure 19: Wavelength of the 1390 nm kaolinite peak in drill hole RC218/326

The measured areas of the deconvoluted “bound water” peaks at 1460 nm and 1910 nm are plotted for drill holes RC453 (Figure 20) and RC218/326 (Figure 21). The results for both peaks are generally in good agreement but the 1460 nm peak is virtually zero in most samples below the leached zone. This is probably due to an artefact derived from deconvolution which tends to suppress the water peak when it is very low. The water peak is stronger at 1910 nm and remains after deconvolution so it is a better indicator for bound water in the samples. For the samples from drill holes RC670/730, RC731 and for the 3000 mN traverse, only the 1910 nm peak area was measured and these results are plotted in Figures 22, 23 and 24 respectively. In all drill holes, the amount of “bound water” is clearly higher in the alluvial samples, commonly in the first few metres of the top of saprolite. For this reason the samples from top of saprolite/base of alluvium could not be discriminated in the 3000 mN traverse (Figure 24). It can also be observed that the leached zone from drill holes RC453 and RC670/730 tend to be richer in “bound water” compared to the lower saprolite samples. This may be due to the higher amount of kaolinite, which can attract more water to its surface. This is not observed in drill hole RC218/326 in the 800 mN area.

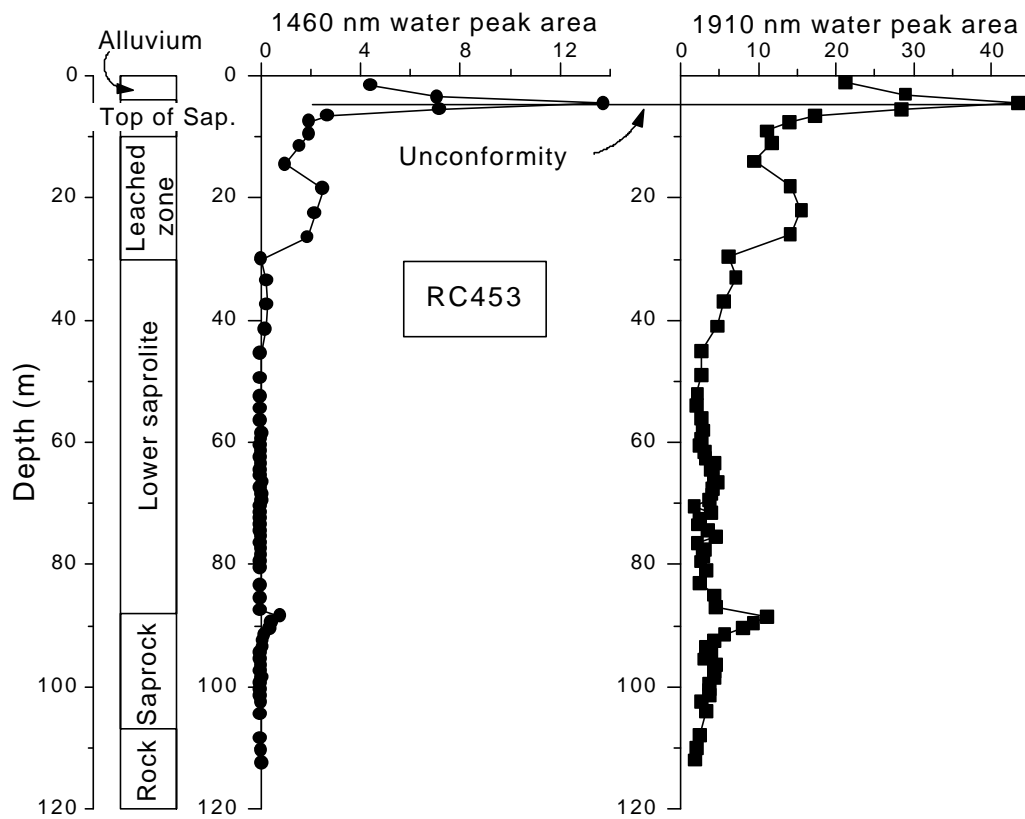


Figure 20: Area of water peak at 1460 nm and 1910 nm in drill hole RC453.

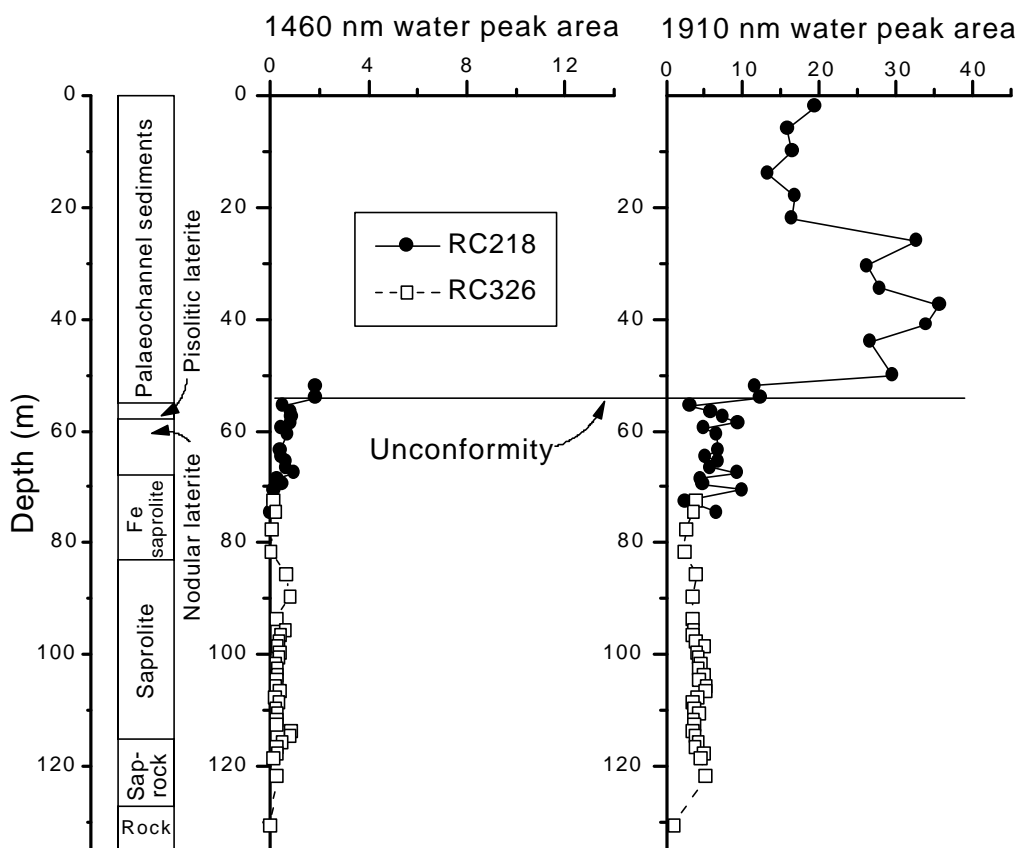


Figure 21: Area of water peak at 1460 nm and 1910 nm in drill hole RC218/326.

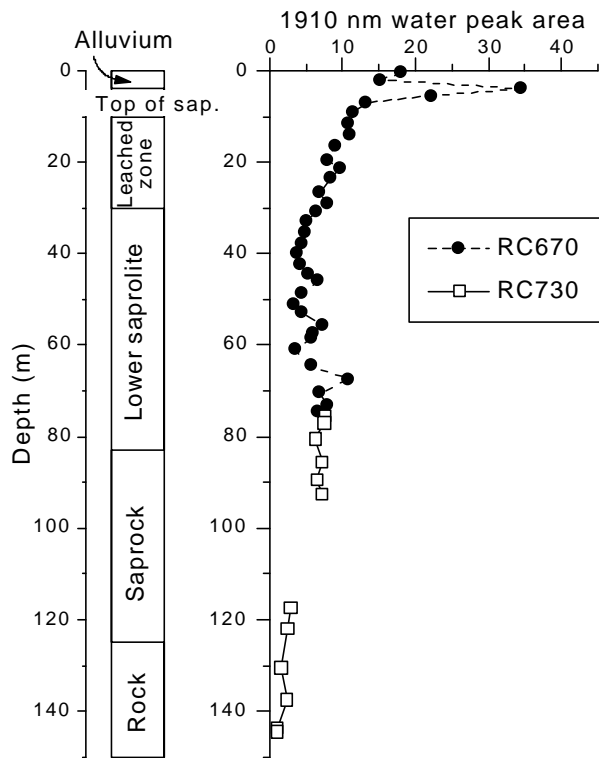


Figure 22: Area of water peak at 1910 nm in drill hole RC670/730.

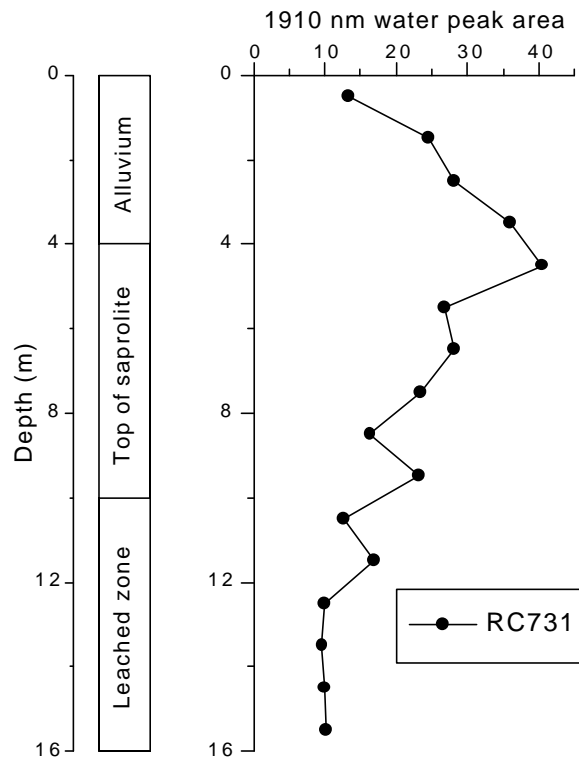


Figure 23: Area of water peak at 1910 nm in drill hole RC731.

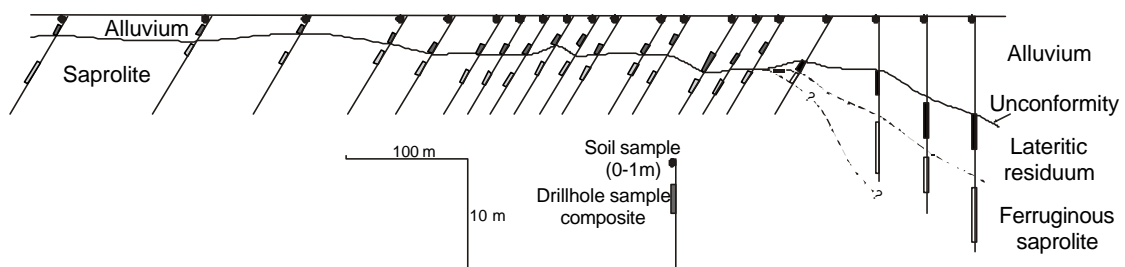
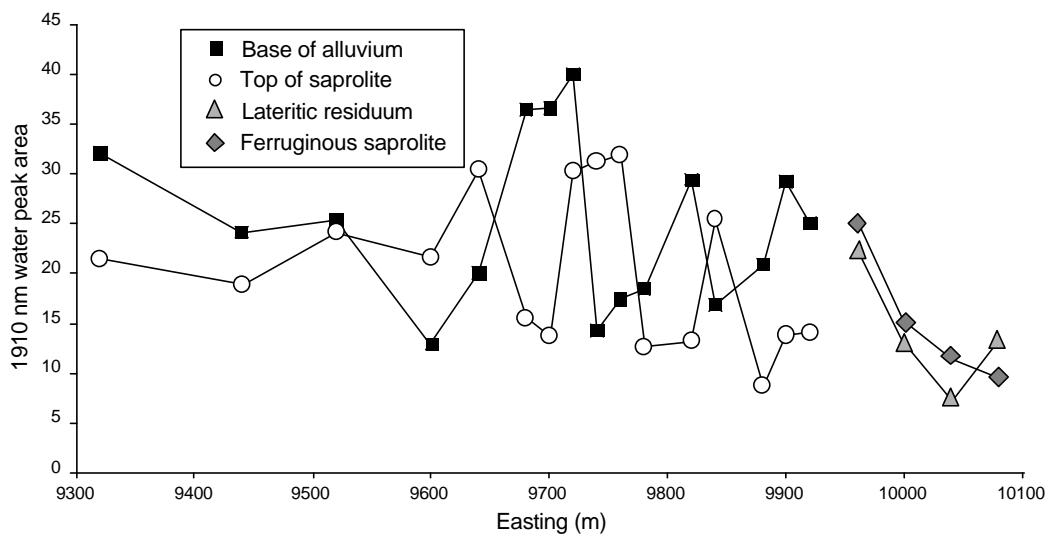


Figure 24: Area of water peak at 1910 nm in traverse 3000 mN.

The results obtained with the ratio of reflectance intensities for drill holes RC453 (Figure 25), RC670/730 (Figure 26), RC731 (Figure 27) and RC218/326 (Figure 28), and for the 3000 mN traverse (Figure 29), show that alluvium and residual samples are best discriminated using the ratio of 2160/2177 nm, which is related to kaolinite crystallinity (Pontual and Merry, 1996).

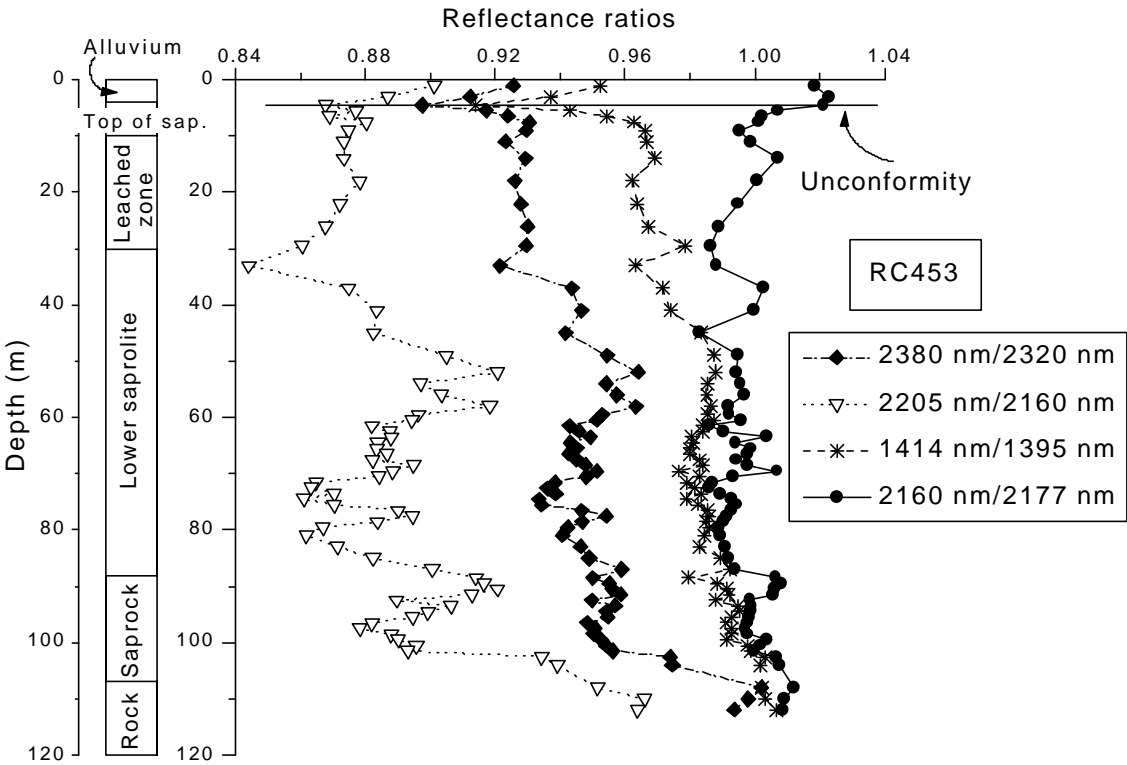


Figure 25: Ratio of reflected intensities in drill hole RC453.

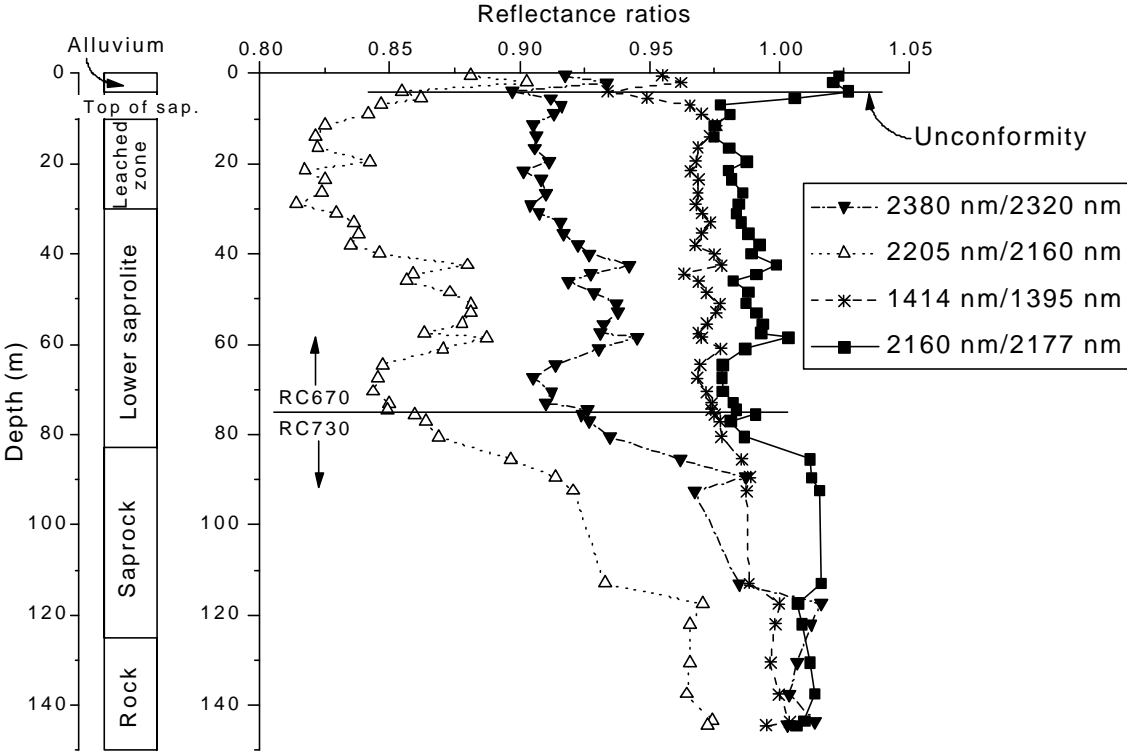


Figure 26: Ratio of reflected intensities in drill hole RC670/730.

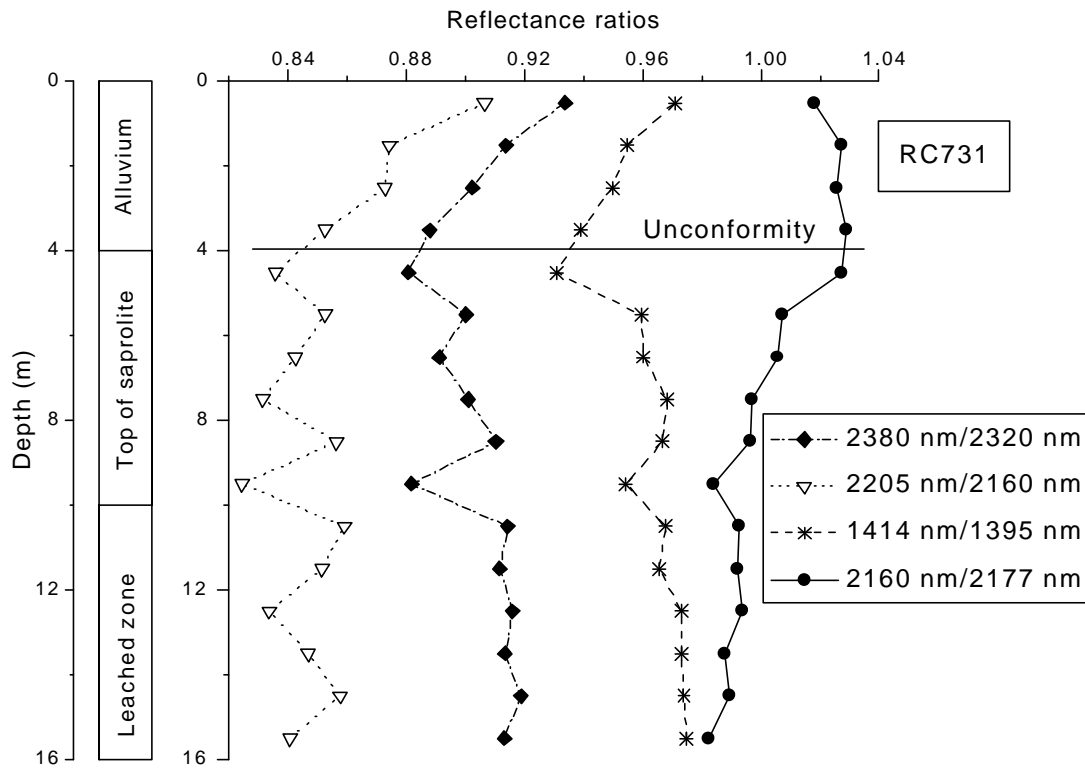


Figure 27: Ratio of reflected intensities in drill hole RC731.

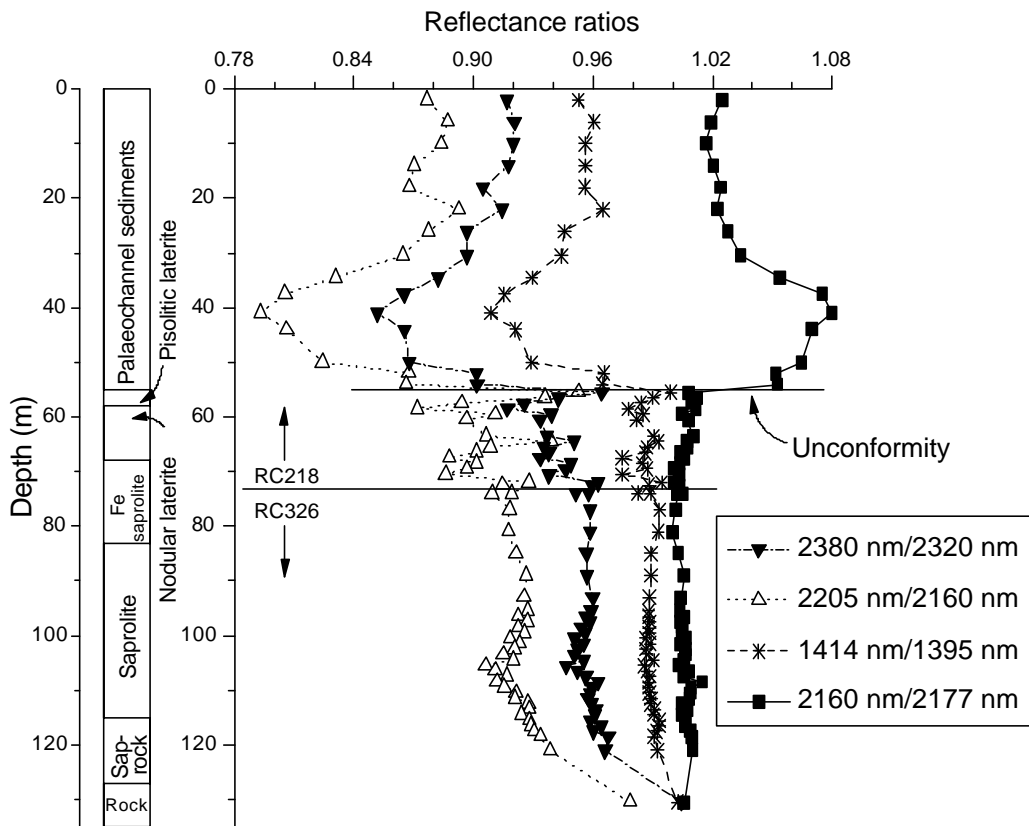


Figure 28: Ratio of reflected intensities in drill hole RC218/326.

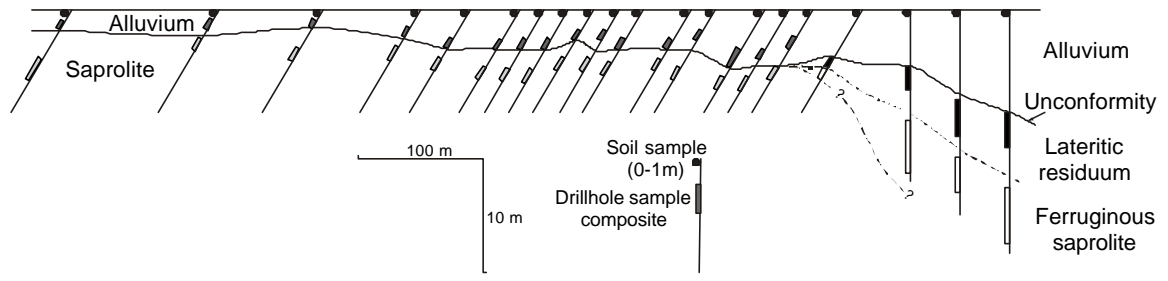
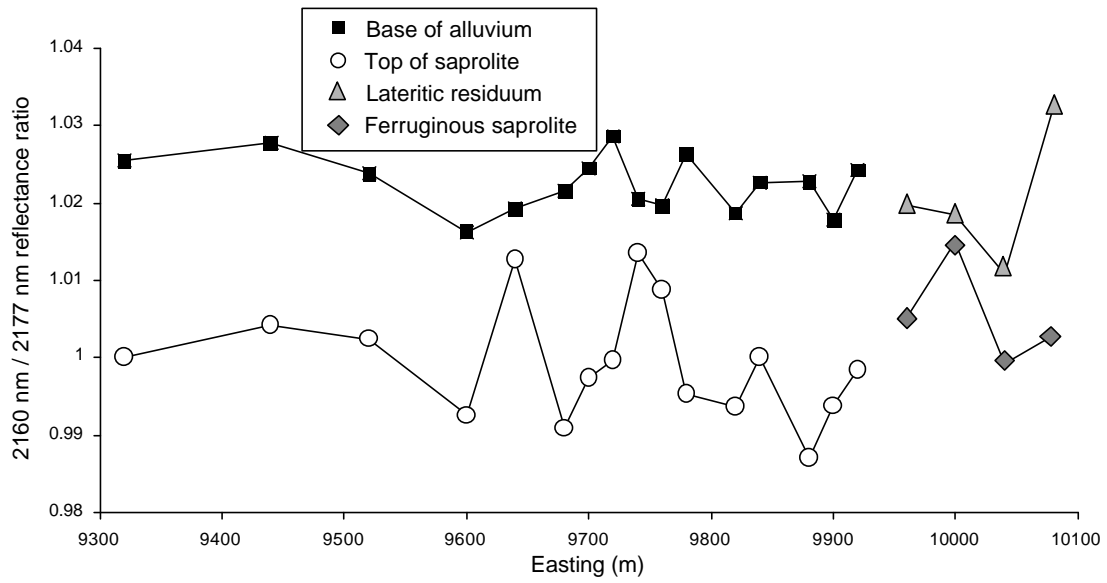


Figure 29: Ratio of reflected intensities in traverse 3000 mN.

## 6 REGOLITH GEOCHEMISTRY

### 6.1 Sample distribution and data treatment

In the 3000 mN area, 151 samples from drill holes RC453, RC670, RC730 and RC731 were analysed by INAA; 128 of these samples were also analysed by XRF. In addition, 42 samples from the 3000 mN traverse were analysed by INAA.

In the 800 mN area, the compositions of 54 samples from drill hole RC218/326 were determined by INAA and 21 of these samples were also analysed by XRF.

Bedrock geochemistry was determined by INAA on 32 samples from drill hole RC272, located approximately half way between the two areas, and on 7 samples from drill holes RC453 and RC730. Only 5 of these samples were also analysed by XRF. Results for bedrock geochemistry were complemented using a geochemical database provided by GCM, which contained XRF results for major oxides for 21 samples from several drill holes in the area.

Geochemical profiles for each of the drill holes are plotted in Appendix 1 and the results from the 3000 mN section are plotted in Appendix 2. To observe major geochemical variations in each area, box and whisker plots were produced for 40 elements according to the regolith zones and these results are plotted in Appendix 3. Cluster analysis has been applied to the geochemical results from the drill holes of the 3000 mN area where a sufficient number of analyses were available (Figures 30 to 35). These results are discussed below.

### 6.2 Major oxides: Si, Fe, Al

(Box and whisker plots, Figures A3.1 to A3.4)

#### *3000 mN area*

(3000 mN section plotted in Figure A2.1a for Fe. Geochemical profiles for drill holes: RC453 in Figure A1.1.1; RC670/730 in Figure A1.2.1; and RC731 in Figure A1.3.1)

Concentrations of Si increase slightly in the lower saprolite (mean of 55% SiO<sub>2</sub>), possibly due to residual concentration (Figure A3.1). In the leached zone Si concentrations drop markedly to about 40 % SiO<sub>2</sub> and this is coincident with the lower concentrations of quartz (see section 4). This trend has been observed in drill holes RC453 (Figure A1.1.1c) and RC670/730 (Figure A1.2.1c) and at the moment it is not clear whether this is a weathering effect or a lithological variation. The top of saprolite contains higher concentrations of Si (mean of 45 % SiO<sub>2</sub>) presumably due to silicification. Aluminium concentration increases upward from about 15 % Al<sub>2</sub>O<sub>3</sub> in the fresh rock to 27 % in the kaolinite rich leached zone (Figure A3.2). Such enrichment could be residual due to loss of other elements but it is also possible that it results from reprecipitation of kaolinite dissolved from above. The decrease in Al concentration in the top of saprolite may be due to kaolinite dissolution and dilution by silicification and ferruginization. Iron is leached from the lower saprolite, but its concentration increases slightly in the leached zone and top of saprolite, resulting in incipient cutan development as observed in the leached zone of drill hole RC453.

There is a sharp increase in Si concentration in the alluvium due to its sandy composition. In the 3000 mN traverse, Fe concentration diminishes from the top of saprolite to base of the alluvium and soil, but in the palaeochannel area to the east both the lateritic residuum and ferruginous saprolite are richer in Fe (Figure A2.1a).

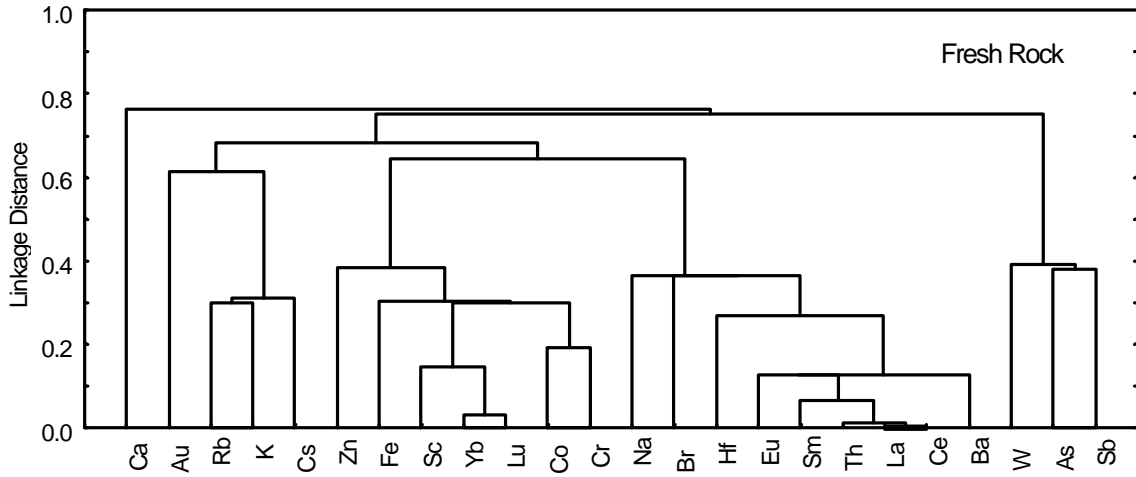


Figure 30: Cluster analysis from 39 fresh rock samples - 3000 mN area, using single linkage, Pearson correlation coefficients.

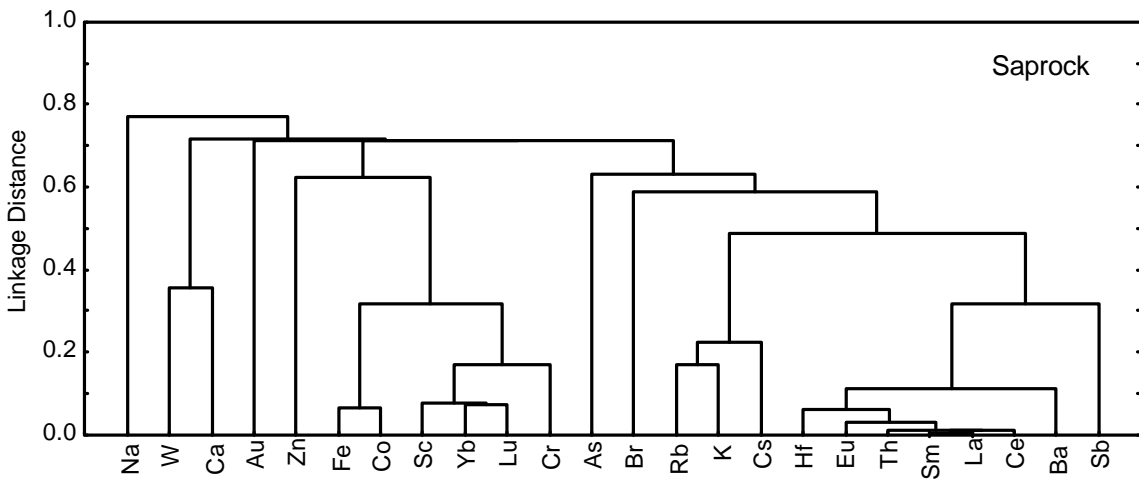


Figure 31: Cluster analysis from 40 saprock samples, 3000 mN area, using single linkage, Pearson correlation coefficients.

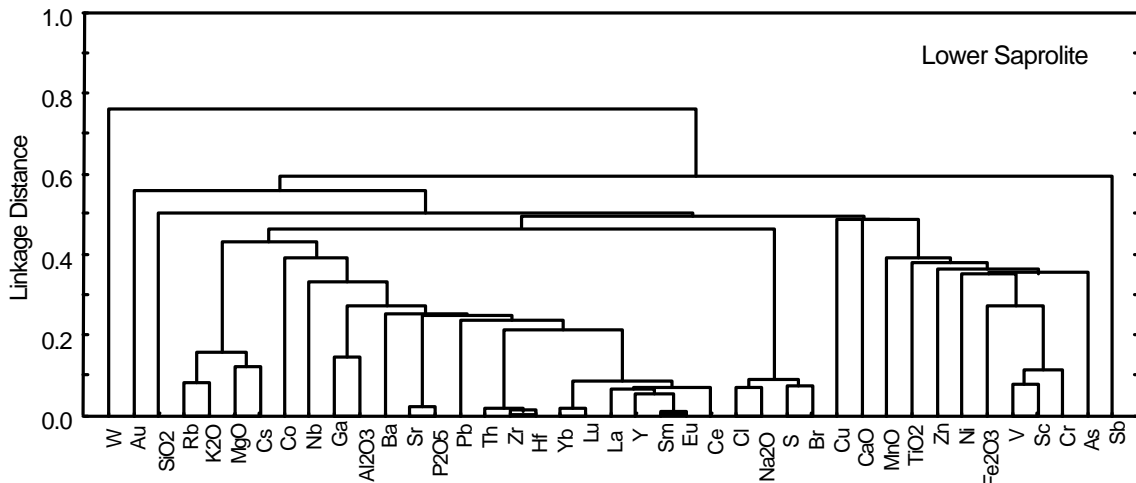


Figure 32: Cluster analysis from 35 lower saprolite samples, 3000 mN area, using single linkage, Pearson correlation coefficients.

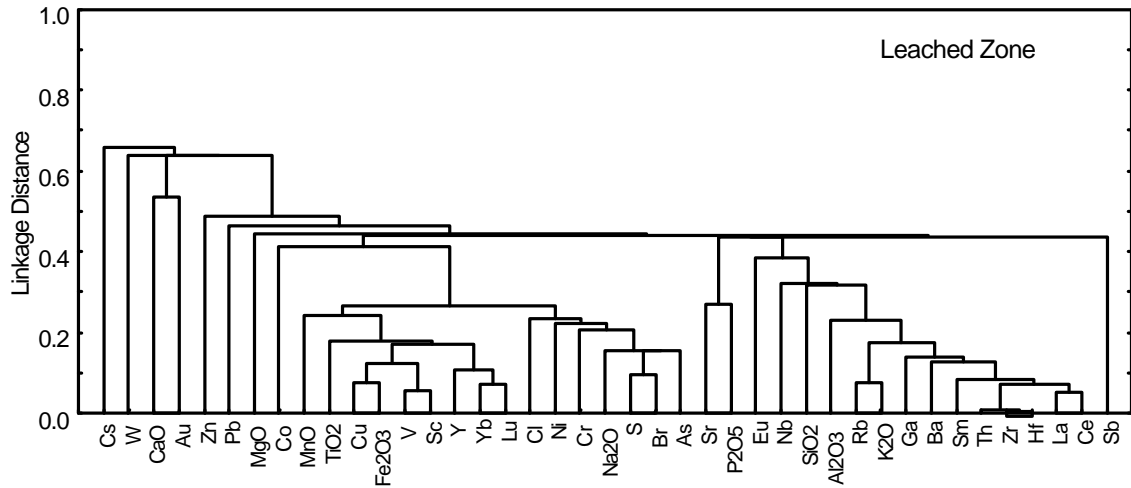


Figure 33: Cluster analysis from 24 leached zone samples, 3000 mN area, using single linkage, Pearson correlation coefficients.

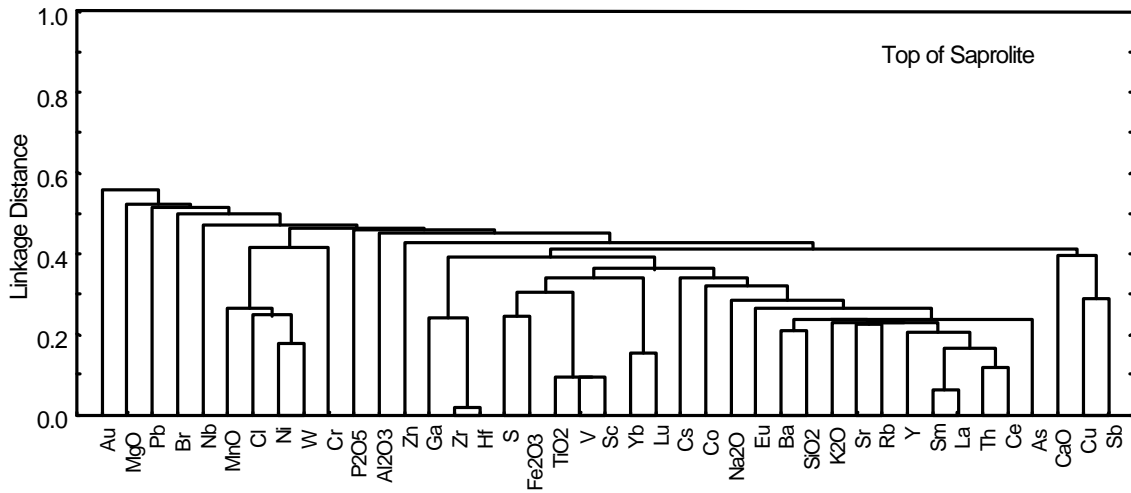


Figure 34: Cluster analysis from 18 top of saprolite samples, 3000 mN area, using single linkage, Pearson correlation coefficients.

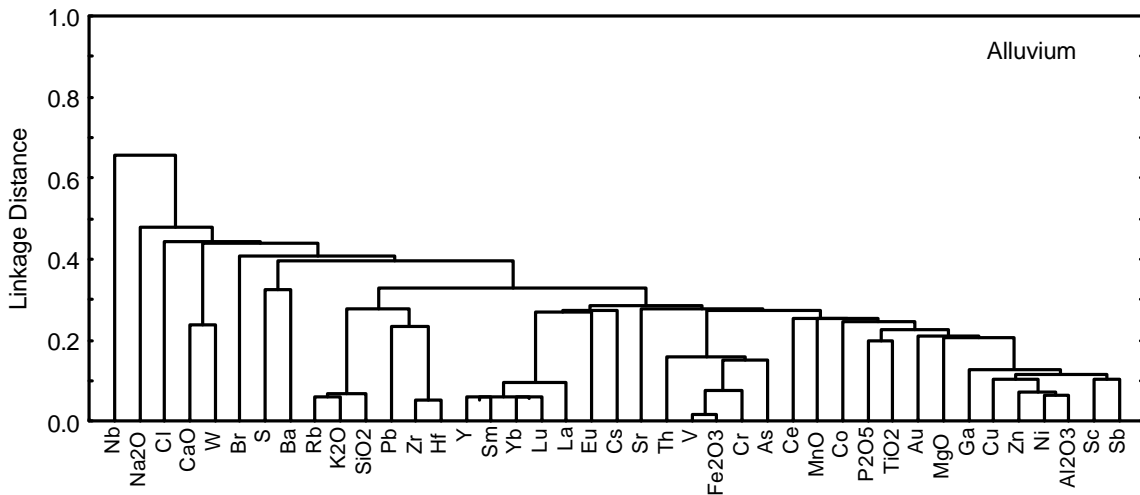


Figure 35: Cluster analysis from 14 alluvium samples, 3000 mN area, using single linkage, Pearson correlation coefficients.

### **800 mN area**

(Geochemical profiles for drill hole RC218/326 in Figure A1.4.1.)

Silicon is strongly depleted in the ferruginous zones. Distribution of Al is more variable but is apparently retained in the ferruginous zones. Iron is retained up to the saprolite and strongly enriched in the ferruginous zones, probably by addition.

The alluvium is Fe-poor but Si and Al concentration are higher with the dominance of kaolinite.

### **6.3 Alkaline earth elements: Mg, Ca, Ba, Sr**

(Box and whisker plots, Figures A3.4 to A3.10)

#### **3000 mN area**

(3000 mN section plotted in Figures A2.1b and c. Geochemical profiles for drill holes: RC453 in Figure A1.1.2; RC670/730 in Figure A1.2.2; RC731 in Figure A1.3.2.)

Magnesium and Ca concentrations in the bedrock are in the vicinity of 5 and 8%, respectively (Figures A3.4 to A3.6). Magnesium concentrations are basically unchanged in the saprock, where parent minerals are partly preserved, but highly leached upwards. Calcium, however, is leached in the saprock because it dominantly occurs in primary carbonates. Calcium is enriched in the leached zone and top of saprolite (5 to 6 % CaO) as a result of later carbonate precipitation near the surface. Strontium is more stable and is depleted only in the leached zone. Its close association with P in the lower saprolite suggests it is hosted mostly in phosphates. Barium shows a more irregular distribution, which may indicate lithological variations, with a slight depletion from the lower saprolite upwards.

In the alluvium, Ba concentration increases and its close association with S (Figure 35) suggests it is present as barite, particularly at the base of alluvium in the 3000 mN traverse (Figure A2.1c).

#### **800 mN area**

(Geochemical profiles for drill hole RC218/326 in Figure A1.4.2)

The depletion of Mg, Ca and Sr is stronger compared to the 3000mN area, especially in the ferruginous zones. Barium distribution is more irregular but tends to be more leached from the lower profile and enriched in the ferruginous zones.

### **6.4 Alkali metals: Na, K, Rb, Cs**

(Box and whisker plots, Figures A3.11 to A3.17)

#### **3000 mN area**

(3000 mN section plotted in Figure A2.2. Geochemical profiles for drill holes RC453 in Figure A1.1.3; RC670/730 in Figure A1.2.3; and RC731 in Figure A1.3.3)

Potassium concentration increases markedly from about 0.5% K<sub>2</sub>O in the bedrock to 1.8% in the saprock (Figure A3.11). This may reflect lithological changes, since K is closely associated with Rb and Cs, reflecting the presence of muscovite (Figure 31). This association is maintained only up to the lower saprolite. Upwards, K is slightly depleted but its variable concentration still reflects lithological variations. Sodium is strongly depleted except in the saprock.

In the alluvium, K and Rb are closely associated (Figure 35) and higher concentrations (1.2% and 80ppm, respectively) reflect the presence of K-feldspar. Their distribution in the 3000 mN traverse show that they tend to be more strongly concentrated in the soil than in the base of alluvium.

### **800mN area**

(Geochemical profiles for drill hole RC218/326 in Figure A1.4.3)

In the ferruginous zone, the much lower concentrations of K<sub>2</sub>O (<0.2%), Rb (<5ppm) and Cs (<1ppm) reflect the more unstable conditions for muscovite or dilution by Fe precipitation. Sodium concentrations are relatively higher (1%) in the saprolite, probably due to the presence of halides, as indicated by the high values of Cl and Br (Figures A3.34 and A3.35).

### **6.5 Elements associated with gold mineralization: Au, As, Sb, W**

(Box and whisker plots, Figures A3.39 to A3.42)

#### **3000 mN area**

(3000 mN section plotted in Figures A2.7c and A2.8. Geochemical profiles for drill holes RC453 in Figure A1.1.9; RC670/730 in Figure A1.2.9; and RC731 in Figure A1.3.9.)

The distribution of W and Au are naturally extremely variable. However, it can be observed that the leached zone, which is typically depleted in Au, is not similarly depleted in W. Tungsten occurs in resistate minerals and maintains its variable distribution pattern in the leached zone, although with low concentrations (up to 50 ppm). The top of saprolite is typically enriched in gold and a slight enrichment tendency for W is also observed (up to 200 ppm). Concentrations of Au and W in the alluvial cover are visibly lower but still anomalous.

Results of the Au and W distribution in the 3000 mN traverse are discussed in the Section 9.2.

The As-Sb-W association detected in fresh rock (Figure 30) does not include Au, probably due to the scale of observation. In the saprock, this association disappears as As and Sb sulphides are readily oxidized (Figure 31). Arsenic concentrations in the bedrock are of the order of 10 to 20 ppm but may reach up to 200 ppm (Figure A3.29). Arsenic is leached from the lower saprolite whereas Sb tends to stay in the regolith due to its lower mobility, however, its concentration rarely exceeds 5 ppm. Arsenic is the only element showing some enrichment in the leached zone and top of saprolite (up to 50 ppm) and this is probably influenced by the Fe distribution. Arsenic distribution in the 3000 mN traverse is highly concentrated in the lateritic residuum to the east showing a strong affinity for Fe. Antimony is more concentrated in the top of saprolite but is also enriched in the lateritic residuum.

### **800 mN area**

(Geochemical profiles for drill hole RC218/326 in Figure A1.4.9.)

The pisolitic laterite is distinctly enriched in As (up to 100 ppm) and Sb (up to 15 ppm) but the association with Fe in the ferruginous zones is more apparent for As. Gold is enriched in the nodular and pisolitic laterite but W and other immobile trace elements, such as Zr and Hf, are not. This suggests that Au enrichment in the lateritic zones is probably of chemical origin, as commonly observed in other lateritic zones in Western Australia (Butt, 1989).

### **6.6 Base metals: Cu, Pb, Zn, Ni, Co**

(Box and whisker plots, Figures A3.33 to A3.38)

#### **3000 mN area**

(3000 mN section plotted in Figures A2.7a and b. Geochemical profiles for drill holes RC453 in Figure A1.1.8; RC670/730 in Figure A1.2.8; and RC731 in Figure A1.3.8.)

The low concentrations of these elements in the regolith reflect their low abundances in primary mineralization (of the order of 100 ppm for Cu, Zn, and Ni; 50 ppm for Co; and 5 ppm for Pb), which is generally poor in sulphide minerals. It is probable that a significant proportion of these elements is hosted in silicates. Cobalt shows a good correlation with Fe up to the transition zone, reflecting its association with mafic minerals, but is strongly leached upwards. Nickel and Zn are also depleted

upwards but to a lesser extent. Copper distribution is very variable but it tends to concentrate in the transition zone and lower saprolite, and becomes depleted above. Lead is the only base metal enriched in the regolith.

#### **800 mN area**

(Geochemical profiles for drill hole RC218/326 in Figure A1.4.8)

Cobalt, Ni and Cu tend to be enriched with Fe in the ferruginous zones, although Ni and Cu concentrations decrease upwards from the ferruginous saprolite. Zinc and Pb concentrations are basically unchanged.

### **6.7 Other Transition metals: Cr, Sc, Ti, V**

(Box and whisker plots, Figures A3.29 to A3.32)

#### **3000 mN area**

(3000 mN section plotted in Figure A2.6. Geochemical profiles for drill holes RC453 in Figure A1.1.7; RC670/730 in Figure A1.2.7; and RC731 in Figure A1.3.7.)

These metals tend to be associated with Fe in fresh rock, reflecting the occurrence of more mafic lithologies (Figure 30). However, in the regolith Cr and Sc tend to be leached whereas Ti and V are concentrated upwards. Chromium and Sc are probably hosted in more unstable Fe-Mg minerals whereas Ti and V are hosted in more resistate phases such as magnetite, rutile or ilmenite.

The alluvial cover contains lower concentrations of these elements, reflecting the more felsic derivation of these sediments. However, the concentration of Cr and Sc increases markedly in the lateritic zones to the east of the 3000 mN traverse.

#### **800 mN area**

(Geochemical profiles for drill hole RC218/326 in Figure A1.4.7)

Chromium and Sc tend to be retained with Fe in the ferruginous zones, and are strongly enriched in the pisolitic laterite. The same is observed for V but Ti shows a slight depletion tendency in the ferruginous zones. In the alluvial cover, only Ti occurs in higher concentrations.

### **6.8 Immobile elements: Zr, Hf, Th, Nb**

(Box and whisker plots, Figures A3.25 to A3.28)

#### **3000 mN area**

(3000 mN section plotted in Figure A2.5. Geochemical profiles for drill holes RC453 in Figure A1.16; RC670/730 in Figure A1.2.6; and RC731 in Figure A1.3.6.)

The strong Zr-Hf-Th association across the regolith reflects the presence of zircon; a Th-REE correlation suggests some Th is hosted in monazite. The concentrations of Zr, Hf and, particularly, Th are very variable, possibly reflecting lithological variations. In general, their abundances tend to increase gradually upwards and are essentially maintained in the leached zone (Figures A3.25 and A3.26). This probably results from residual enrichment with the possible exception of Th which tends to be more leached following the behaviour of REE due to their presence in monazite. Only at the top of saprolite does the concentration of these elements decrease. The distribution of Nb is more erratic and likely influenced by poor analytical results close to detection of the XRF instrument.

The alluvial shows higher and more uniform concentrations of Zr, Th and Hf (means of 130, 4 and 13 ppm respectively). This is probably due to the presence of zircon and monazite as resistate minerals. In the 3000 mN traverse, these elements are more strongly concentrated in the soil than in the base of alluvium, which may reflect aeolian contribution (Figure A2.5).

### ***800 mN area***

(Geochemical profiles for drill hole RC218/326 in Figure A1.4.6.)

The concentrations of these immobile elements are essentially maintained across the regolith, with clear enrichment in the alluvial cover.

### **6.9 Rare earth elements: La, Ce, Sm, Eu, Lu, Yb, Y**

(Box and whisker plots, Figures A3.18 to A3.24)

#### ***3000mN area***

(3000 mN section plotted in Figures A2.3 and A2.4. Geochemical profiles for drill holes RC453 in Figures A1.1.4 and A1.1.5; RC670/730 in Figures A1.2.4 and A1.2.5; and RC731 in Figures A1.3.4 and A1.3.5.)

In the saprock and lower saprolite, the concentration of light rare earth elements (LREE) are very variable but in general tend to be several orders of magnitude higher than the fresh rock. Lithological variations are probably influencing this distribution pattern but there may be some supergene enrichment, since LREE are lower in the leached zone. The more aggressive leaching conditions may have destabilized the hosts of LREE (probably phosphates) with dissolution of the LREE and reprecipitation below. The heavy rare earth elements (HREE) concentrations are less variable and tend to be associated with Fe, being slightly depleted in the regolith.

The concentration of the LREE increases slightly in the alluvium, reflecting the presence of resistate minerals such as monazite. This enrichment is more pronounced in the base of alluvium of the 3000 mN traverse.

### ***800 mN area***

(Geochemical profiles for drill hole RC218/326 in Figures A1.4.4 and A1.4.5.)

All REE show a strong tendency for enrichment in the ferruginous zones, this is more pronounced for the HREE, reflecting their higher affinity for Fe. However, this pattern is not repeated in the lateritic residuum on the eastern portions of the 3000 traverse.

### **6.10 Other elements: P, Cl, Br, Ga, Mn**

(Box and whisker plots, Figures A3.43 to A3.47)

#### ***3000 mN area***

(Geochemical profiles for drill holes RC453 in Figures A1.1.10 and A1.1.11; RC670/730 in Figures A1.2.10 and A1.2.11; and RC731 in Figures A1.3.10 and A1.3.11.)

Phosphorus is enriched in the saprock, possibly reflecting lithologies originally richer in apatite and other phosphates, or supergene enrichment, as proposed for the enrichment of LREE in this zone. Upwards, P is increasingly leached due to the instability of apatite, which probably contains the bulk of the P, whereas monazite and other REE-bearing phosphates remain stable.

### **800 mN area**

(Geochemical profiles for drill hole RC218/326 in Figures A1.4.10 and A1.4.11.)

Phosphorus tends to be leached from the ferruginous zones. Concentrations of Cl and Br are higher in the lower parts of the regolith, reflecting the presence of salts. Manganese is increasingly leached upwards although it tends to concentrate in the ferruginous saprolite of the 800 area. Gallium distribution is closely related to Al.

### **6.11 Summary of geochemical trends in the 3000 mN area**

A number of elements are increasingly enriched upwards by residual concentration. Hafnium, Zr and Th are hosted in zircons with the large variability of their concentrations probably reflecting lithological variations. Titanium and V are probably hosted in magnetite, rutile and ilmenite. Aluminium and Ga reflect the kaolinite distribution, but the enrichment of Al in the leached zone may result from reprecipitation. These elements generally show lower concentrations at the top of saprolite, probably due to dilution by silicification and ferruginization.

Magnesium, Ca and Na are partly retained in the saprock and strongly leached upwards; some Ca is enriched in upper horizons due to carbonate precipitation. Phosphorus, S, Co and Mn are also strongly leached; whereas leaching of Cr, Sc, HREE, Ni and Zn are less pronounced.

Silicon is residually concentrated in the lower saprolite but leached in the leached zone, due to quartz dissolution. The large variability of Ba, K, Rb, and Cs in each weathering zone reflects lithologies with variable amounts of muscovite. Depletion of these elements in the leached zone reflects instability of muscovite. The variations in LREE probably also reflect lithological changes although supergene enrichment may also be possible since they are leached from the leached zone probably reflecting instability of the hosting phosphates.

Arsenic tends to be leached from the lower saprolite but is enriched upwards, even in the leached zone, due to its affinity for Fe. Antimony is less mobile and tends to be retained in the lower saprolite and is also enriched upwards, following Fe and As.

Elements enriched in the alluvial cover include Si, Ba, K, Rb, Zr, Th, Hf and LREE, due to detrital accumulation of minerals such as quartz, feldspar, micas, zircon and monazite. Potassium, Rb, Th and Hf concentrations are higher in the soil compared to the base of alluvium and the opposite is observed for Ba and LREE. This probably reflects aeolian accumulation of zircon and, possibly, muscovite in the soil and concentration of monazite and barite by mechanical transport at the base of alluvium.

### **6.12 Summary of geochemical trends in the 800 mN area**

Due to the smaller number of samples analysed in this area (see box and whisker plots, Appendix 3), interpretation of the geochemical patterns observed are more difficult. Therefore only broad trends are mentioned and only for the elements which showed a consistent pattern.

Leaching of elements such as Si, Mg, Ca, Sr, K, Na, Rb, Cs and P is stronger than in the 3000 mN area, probably due to the more intense ferruginization conditions in which muscovite, for example, is more unstable. In contrast to the 3000 mN area, the concentrations of Al, Zr, Th, Hf and Ga in the regolith are similar to those in to fresh rock. The lack of residual enrichment may be due to the addition of Fe, especially in the ferruginous zones.

Elements enriched in the ferruginous zones include Fe, As, LREE, HREE, Co, Cr, Sc, V and Sb. Elements enriched in the alluvial cover include Si, Al, Hf, Th, Zr, Nb, Ti and Ga. This basically reflects the concentration of kaolinite, zircon and Ti bearing heavy minerals.

## 7 HYDROGEOCHEMISTRY

### 7.1 Introduction

A primary justification given for the use of hydrogeochemistry in mineral exploration is that groundwater anomalies may be broader and more regular than the mineralization and secondary dispersion halo in the regolith, thus enhancing the geochemical signature. In addition, areas of high chemical reactivity (e.g., faults and shear zones) may have distinct hydrogeochemical signatures even where they are unremarkable, in terms of elemental abundances, and where petrographic study is difficult. However, such effects may also be counter-productive, as interpretation may become complicated by various factors.

Hydrogeochemical studies also provide information on how various materials are weathering. This enhances understanding of active dispersion processes and assists in the development of weathering and geochemical models, which are essential for effective exploration in regolith-dominated terrain.

The aims of this hydrogeochemical study were, therefore:

- i. To yield data on dispersion processes and to assist in interpretation of geochemical data.
- ii. To provide information on whether groundwater can be used successfully as an exploration medium in this area in particular and, in conjunction with other studies, in the northern Yilgarn in general.
- iii. To contribute to a groundwater database on the characteristics of groundwaters at various sites and to enhance our understanding of groundwater processes in mineralized zones.

The scope of this investigation includes the effect of underlying lithology on the observed water chemistry, thermodynamic modeling, mapping of the data and comparison with results from other Western Australian sites.

### 7.2 Compilation of results and comparison with other sites

The concentrations of various ions at Mt Joel and other sites are plotted versus total dissolved solids (TDS) or pH in Appendix 4. The sea water data (Weast, 1983) are used to derive the line of possible values (denoted as the sea water line) if sea water were diluted with freshwater or concentrated by evaporation. The line is shown on each figure except when the concentration in sea water is too low, relative to the concentration of the element in groundwaters. The plots of concentration vs TDS only extend to TDS = 40000 mg/L, so as to allow viewing of the Mt Joel data. The results from Mt Joel can be compared with those from other sites in south WA, which are grouped as follows:

- i. *Northern groundwaters* (N Yilgarn and margins):  
Lawlers (Gray, 1994) and Baxter (Gray, 1995).  
Groundwaters in these areas are fresh and neutral, trending more saline in the valley floors.
- ii. *Central groundwaters* (close to and north of the Menzies line):  
Granny Smith (Gray 1993a); Golden Delicious (Bristow et al., 1996); Mt. Gibson (Gray, 1991); and Boags (Gray, 1992a).  
Groundwaters are neutral and brackish (commonly < 1% TDS) to saline (about 3% TDS).  
They commonly increase in salinity with depth and trend to hypersaline (10-30% TDS) at the salt lakes.

- iii. *Kalgoorlie groundwaters:*  
Golden Hope mine, (Gray, 1993b); Wollubar palaeochannel (Gray, 1993b); Panglo deposit (Gray, 1990); Baseline mine, Mulgarrie palaeochannel (Gray, 1992b); Steinway palaeochannel (Lintern and Gray, 1995a); and Argo palaeochannel (Lintern and Gray, 1995b). These groundwaters are commonly acid (pH 3-5), except where buffered by extremely alkaline materials (e.g., ultramafic rocks), and saline within the top part of the groundwater mass. They trend towards being more neutral (pH 5-7) and hypersaline at depth and when within a few kilometres of various salt lakes in the region.
- iv. *Mulga Rock:*  
Mulga Rock palaeodrainage system (Douglas et al., 1993). Groundwaters are saline to hypersaline and neutral to acid. The major ion chemistry is similar to that of the Kalgoorlie region, but the dissolved concentration of many other ions is low, due to the presence of lignite in the channel sediments

Wollubar, Baseline, Panglo and Yalanbee are acid groundwater systems, whereas the other sites have dominantly neutral groundwater. Comparisons with other sites may be useful in indicating the significance of any particular element anomaly and whether the groundwater composition is affected by particular lithological interactions. Specific descriptions of the varying sites can be found in the referenced reports, with generalized descriptions of the hydrogeochemistry of the Yilgarn Craton given in Gray (1996) and Butt et al. (1997).

Solubility index (SI) values for various minerals (Section 2.6) are plotted in Appendix 5. The equilibrium point is shown as the dashed line. The shaded area denotes the zone in which waters may be in equilibrium with that mineral. Note, that where a mineral has a very broad zone, there is significant uncertainty in the thermodynamic data for this mineral and/or calculation problems - i.e., samples within that zone are not necessarily at equilibrium, though samples above or below the zone are definitely out of equilibrium. Spatial distributions of element concentrations and some relevant SI values for the shallow groundwaters (i.e., sampled at 13-17 m below surface) are plotted in Appendix 6, with the data for deep groundwaters mapped in Appendix 7.

### **7.3 Acidity and oxidation potential**

An Eh-pH plot of waters from Mt Joel and other sites is shown in Figure 36. Groundwaters are combined into the various groundwater groups, as described in Section 7.2. The shallow Mt Joel groundwaters are neutral (pH 7.0-7.6) and range from moderately oxidizing to reducing, similar to the pH and Eh range of other northern groundwaters. The deeper groundwaters have a larger pH range (pH 6.3-8.0), suggesting heterogeneous characteristics.

### **7.4 Salinity effects and major element hydrogeochemistry**

Data are plotted in Appendix 4, Figures A4.1 to A4.12. With the exception of some of the saline deeper groundwaters, the Mt Joel groundwaters closely match other northern groundwaters. The shallow groundwaters have low salinities (400-3200 mg/L), whereas the salinities of the deeper groundwaters are highly variable, ranging from fresh to greater than sea water (1000-38600 mg/L). The Mt Joel groundwaters are enriched in Ca, SO<sub>4</sub> and Sr relative to the concentrations expected if the groundwater had been diluted sea water (Figures A4.4, A4.6 and A4.11). The deeper groundwaters show considerable heterogeneity.

The particular characteristics of the groundwaters at Mt Joel are demonstrated by a plot of pH vs TDS (Figure 37); most of the shallow and deep groundwaters are in the same range as the northern groundwaters. However, the four most saline deep groundwaters are five times more saline than the most saline northern groundwater. This may affect the concentration of various minor elements, including Au, as discussed below.

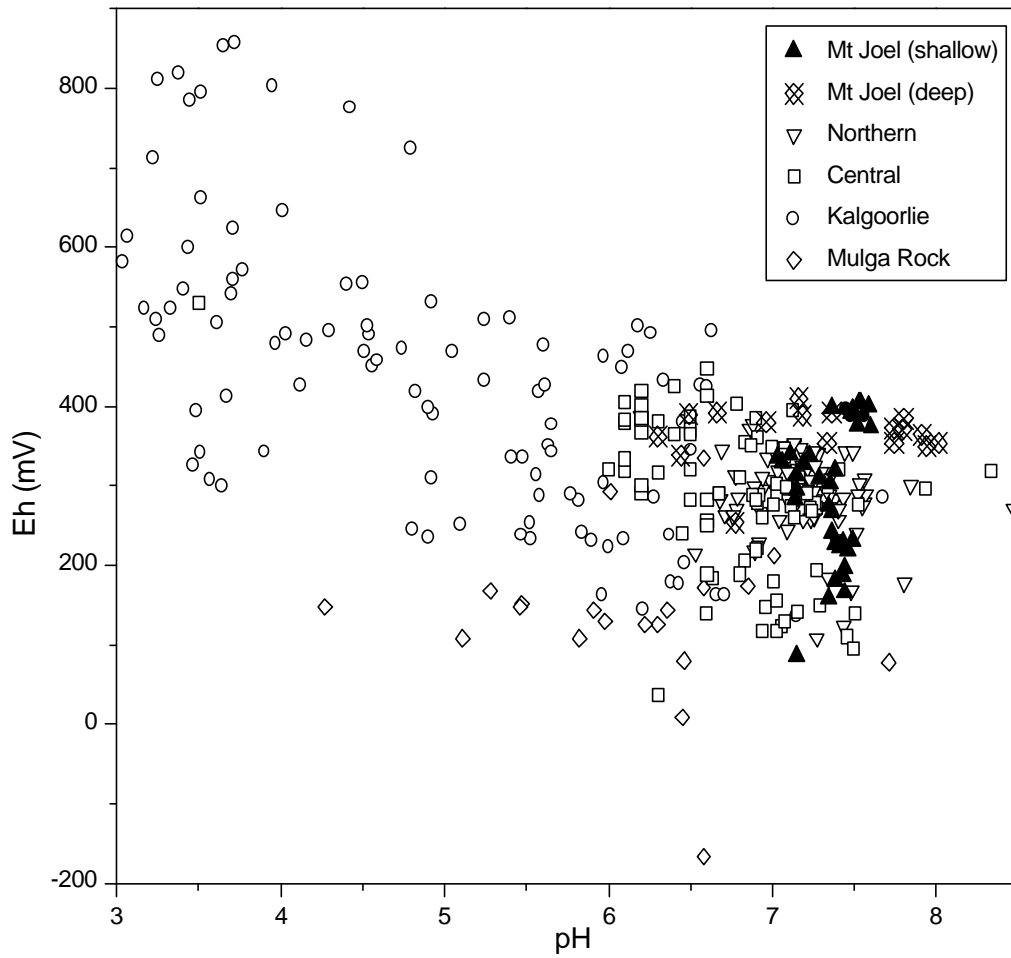


Figure 36: Eh vs pH for groundwaters from Mt Joel and other sites.

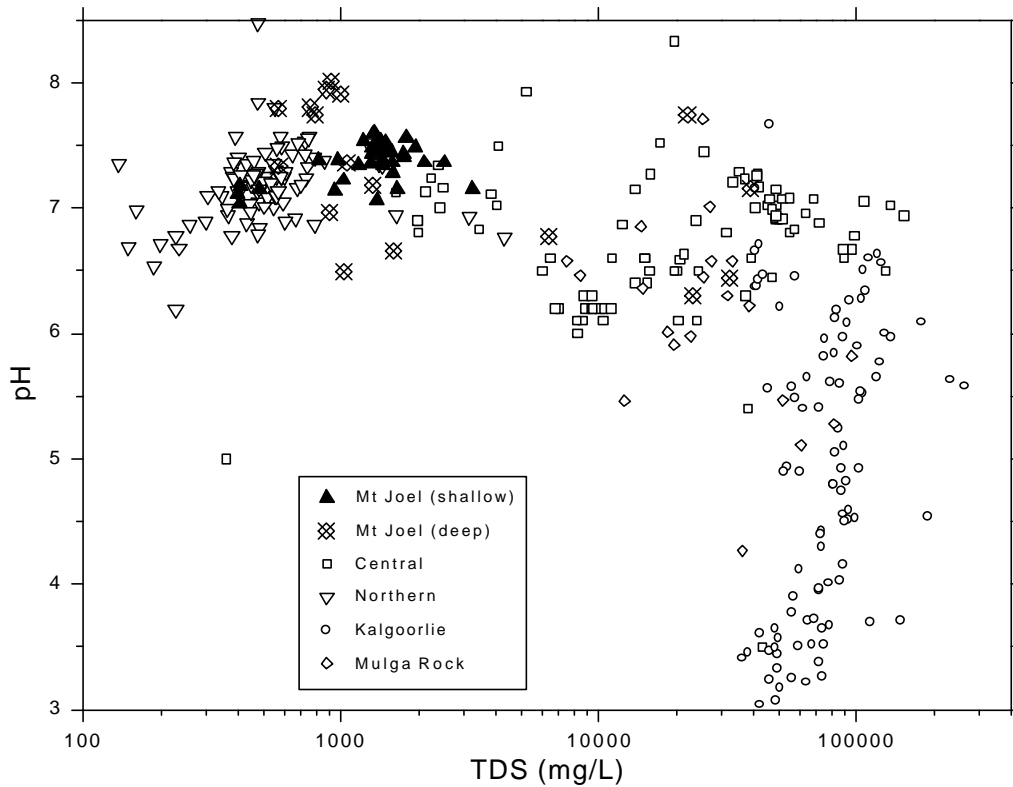


Figure 37: pH vs TDS for groundwaters from Mt Joel and other sites.

The potential for dissolution or precipitation of minerals from the Mt Joel groundwaters has been tested by speciation analysis (Section 2.6). The range, mean and standard deviation of the SI values of the water samples for a number of relevant solid phases are given in Table 6, with SI values plotted in Appendix 5. As discussed in detail in Section 2.6, in general a SI of zero indicates the solution is saturated with respect to that mineral, a SI less than zero indicates under-saturation and a SI greater than zero indicates the solution is over-saturated with respect to the mineral phase.

Table 6: SI values for the Mt Joel groundwaters, for a number of relevant solid phases.

Mineral	Formula	Shallow samples				Deep samples			
		Min	Max	Mean	St. Dev.	Min	Max	Mean	St Dev
Halite	NaCl	-6.4	-4.5	-5.3	0.5	-5.9	-2.5	-4.6	1.1
Gypsum	CaSO <sub>4</sub> ·2H <sub>2</sub> O	-2.2	-1.0	-1.4	0.3	-1.6	-0.3	-1.1	0.4
Celestine	SrSO <sub>4</sub>	-2.7	-1.5	-1.9	0.3	-2.2	-0.8	-1.6	0.5
Barite	BaSO <sub>4</sub>	-0.7	0.3	-0.2	0.2	-0.8	0.7	-0.1	0.3
Calcite	CaCO <sub>3</sub>	-1.4	-0.1	-0.5	0.4	-1.3	0.2	-0.5	0.6
Dolomite	CaMg(CO <sub>3</sub> ) <sub>2</sub>	-2.5	0.1	-0.7	0.8	-2.4	1.0	-0.6	1.1
Magnesite	MgCO <sub>3</sub>	-1.9	-0.6	-1.0	0.4	-1.9	0.2	-0.9	0.6
Quartz	SiO <sub>2</sub>	0.8	1.2	1.0	0.1	0.0	1.1	0.9	0.3
Amorphous silica	"	-0.5	-0.1	-0.2	0.1	-1.3	-0.2	-0.4	0.3
Gibbsite	Al(OH) <sub>3</sub>	-0.1	1.3	0.4	0.4	0.1	1.8	1.0	0.5
Amorphous alumina	"	-2.4	-1.0	-1.9	0.4	-2.2	-0.5	-1.3	0.5
Kaolinite	Al <sub>2</sub> Si <sub>2</sub> O <sub>5</sub> (OH) <sub>4</sub>	2.8	5.3	3.6	0.7	3.1	6.0	4.5	0.9
Sepiolite	Mg <sub>2</sub> Si <sub>3</sub> O <sub>7.5</sub> (OH)·3H <sub>2</sub> O	-2.8	0.2	-1.0	0.9	-4.8	1.6	-1.4	2.4
Siderite	FeCO <sub>3</sub>	-2.2	-0.5	-1.5	0.6	-3.3	-1.1	-2.0	0.7
Rhodochrosite	MnCO <sub>3</sub>	-2.8	0.3	-1.9	0.9	-3.0	0.0	-1.4	0.7
Tenorite	Cu(OH) <sub>2</sub> ·H <sub>2</sub> O	-1.1	-1.1	-1.1	-	-3.4	-3.4	-3.4	-
Smithsonite	ZnCO <sub>3</sub>	-4.1	-2.8	-3.5	0.3	-3.9	-2.2	-3.1	0.6
Cerussite	PbCO <sub>3</sub>	-1.7	-1.7	-1.7	0.0	-2.2	0.3	-0.9	1.8
Sphaerocobaltite	CoCO <sub>3</sub>	-2.9	-2.9	-2.9	0.0	nd	nd	nd	nd
Theophrasite	Ni(OH) <sub>2</sub>	-4.5	-3.4	-3.9	0.3	nd	nd	nd	nd
Eskolaite	Cr <sub>2</sub> O <sub>3</sub>	4.7	8.4	7.0	1.1	nd	nd	nd	nd
Au metal	Au	1.8	6.4	3.8	1.5	nd	nd	nd	nd
Carnotite	KUO <sub>2</sub> VO <sub>4</sub>	-2.6	-1.5	-1.9	0.3	nd	nd	nd	nd
	CaMoO <sub>4</sub>	-2.4	-1.4	-1.7	0.3	-2.1	-1.0	-1.5	0.3
	FeWO <sub>4</sub>	-5.4	-5.4	-5.4	-	-5.0	-5.0	-5.0	-
Chervitite	Pb <sub>2</sub> V <sub>2</sub> O <sub>7</sub>	-0.8	-0.6	-0.7	0.2	nd	nd	nd	nd

- standard deviation not calculated (single value)

nd not determined (analyses not completed)

The groundwaters at Mt Joel have salinities well below that required for halite saturation (Figure A5.1). Although, some of the other major elements appear to be controlled by equilibration with respect to a number of other minerals in some or all of the groundwaters, namely:

- Mg: sepiolite (Figure A5.9) dolomite and/or magnesite (Figures A5.6 and A5.7).
- Ca: calcite (Figure A5.5).
- Ba: barite (Figure A5.4).
- Si: amorphous silica (Figure A5.8) and/or sepiolite (Figure A5.9) (commonly precipitated within valley calcretes; Mann and Horwitz, 1979).

Concentrations of these elements (with the exception of Mn, for which groundwaters show a large SI range from highly unsaturated to saturated) are therefore fundamentally controlled by salinity and pH effects and are unlikely to show any effects from rock type or presence of mineralization.

### 7.5 Minor element hydrogeochemistry

In general, the concentrations of the minor elements (Table 7) are similar to other northern groundwaters, as expected for a fresh/neutral environment. Base metals and REE have low dissolved concentrations, in comparison with the very high contents in the acidic Kalgoorlie groundwaters. This effect must be considered if comparing results for groundwaters from different regions.

Compared with other northern sites, the Mt Joel groundwaters are relatively enriched in V, U, As and Mo. Because of the greater dissolved V and U concentrations, carnotite ( $\text{K}_2\text{UO}_7$ ) is more readily precipitated than at the other previous study sites (Figure A5.26). Arsenic and Mo are both indicators for Au mineralization and/or weathering sulphides and these relative enrichments may be regional indicators for mineralization. The distribution of these elements within the Mt Joel area will be discussed in Section 7.7.

Most of the minor elements are highly undersaturated with respect to their least soluble secondary mineral phase (Table 6), with the following exceptions:

- Mn: rhodochrosite (Figure A5.15);
- Pb/V: chervitite (Figure A5.20);
- Mo:  $\text{CaMoO}_4$  (Figure A5.23)

Groundwaters are also strongly oversaturated with respect to eskolaite ( $\text{Cr}_2\text{O}_3$ , Figure A5.22). This may be due to dissolved Cr being present as  $\text{CrO}_4^{2-}$ , which has a much higher mobility than  $\text{Cr}^{3+}$  (Gray, 1996).

Table 7: Median minor element compositions of groundwaters.

	Mt Joel		Northern	Central	Kal-goorlie	Mulga Rock	Sea Water	Controls
	Shallow	Deep						
I	0.6 ± 0.5	nd	0.2	5	5.8	0.32	0.06	S/Sal ?
Li	<0.005	0.02 ± 0.04	<0.005	<0.005	0.9	nd	0.18	Ac ?
Rb	0.012 ± 0.003	nd	0.013	0.051	0.032	nd	0.12	Min ?
Ba	0.04 ± 0.02	0.03 ± 0.04	0.04	0.02	0.04	0.03	0.013	Eq/Min
Sc	<0.005	<0.005	0.009	0.017	0.019	nd	0.000006	Ac/Min
V	0.012 ± 0.005	0.007 ± 0.018	0.007	<0.005	<0.005	nd	0.002	?
Cr	0.009 ± 0.012	0.002 ± 0.002	0.01	<0.005	0.003	0.002	0.0003	Um
Mn	0.001 ± 0.27	0.03 ± 1.15	0.01	0.1	2	0.3	0.0002	Mf/Um/Ac
Fe	0.01 ± 0.16	0.02 ± 0.03	0.003	0.05	0.1	1	0.002	S
Co	<0.001	<0.005	<0.0005	0.002	0.16	<0.002	0.00002	Um/Mf/Ac
Ni	0.001 ± 0.004	0.005 ± 0.009	0.002	0.001	0.26	0.020	0.00056	Ac/Mf/Um
Cu	<0.005	<0.005	0.003	0.003	0.05	0.00	0.00025	Ac/Mf
Zn	0.003 ± 0.001	0.019 ± 0.016	0.006	0.01	0.05	0.04	0.0049	Ac/Mf
Ga	<0.001	nd	0.002	<0.005	0.006	nd	0.00003	S
As	0.004 ± 0.002	nd	<0.0002	0.09	<0.02	<0.02	0.0037	S
Mo	0.041 ± 0.015	0.050 ± 0.055	0.001	0.009	<0.01	nd	0.01	S
Ag	<0.001	nd	<0.001	0.0005	0.001	nd	0.00004	?
Cd	<0.001	nd	<0.002	0.001	<0.002	<0.001	0.00011	?
Sb	<0.001	nd	<0.0003	0.001	<0.001	<0.0004	0.00024	S
REE	<0.001	nd	<0.002	<0.008	0.8	0.013	0.000013	Ac
W	<0.001	nd	<0.0002	0.001	0.001	nd	0.0001	S
Au	0.004 ± 0.004	0.006 ± 0.003	0.004	0.03	0.05	0.001	0.004	Min
Hg	<0.001	nd	<0.0002	<0.001	0.002	<0.001	0.00003	S
Tl	<0.001	nd	<0.0002	0.001	<0.002	0.0005	0.000019	S
Pb	<0.001	nd	<0.001	0.001	0.06	0.012	0.00003	Ac/Min
Bi	<0.001	nd	<0.0002	0.001	<0.001	<0.002	0.00002	S ?
Th	<0.001	nd	<0.0002	<0.001	<0.002	<0.001	0.000001	?
U	0.013 ± 0.006	nd	0.0003	0.002	0.004	<0.002	0.0032	Ac

All concentrations in mg/L (ppm), except Au in µg/L (ppb)

nd: not determined

Eq mineral equilibrium

Min enriched in waters contacting Au mineralization

Ac enriched in acid groundwaters  
sulphides

S enriched in waters contacting weathering

Um enriched in waters contacting ultramafic rocks

Sal enriched in saline groundwaters

Mf enriched in waters contacting mafic rocks

? not clearly defined

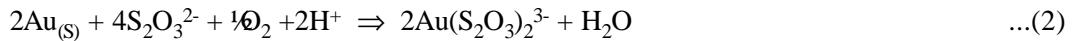
## 7.6 Gold chemistry

The low salinity of most of the groundwaters at this site means that the dominant mechanism for the mobilization of Au in the southern Yilgarn, namely as the chloride complex ( $\text{AuCl}_2^-$ ):



is not expected to be significant for the shallow groundwaters at Mt Joel. Two other mechanisms for Au solubilization are as an organic complex, which is not expected to be important in the organic-poor groundwaters occurring at this site, and as the thiosulphate complex  $[\text{Au}(\text{S}_2\text{O}_3)_2]^{3-}$ :

Therefore, observed minor element enrichments in groundwater may well represent effects of release from weathering minerals, and groundwater distributions (Appendix 6) may well relate to lithological changes, or differing chemistry of mineralized zones.



Generation of this later complex is controlled by the production of thiosulphate:



which primarily occurs during oxidation of sulphides, when minerals such as carbonates buffer acid production. Previous investigations (Butt et al., 1993; Gray, 1994) have indicated that this is only significant for groundwaters sampled at the weathering front, and will have little effect on Au solubility for shallower groundwaters. Therefore, dissolved Au concentrations at Mt Joel are expected to be very low, as is observed (Figure A4.42). This suggests that Au is not being actively dispersed in the regolith, and therefore will not produce a useful dispersion halo in groundwater or in juvenile soils. However, at this site, elements other than dissolved Au can be associated with Au mineralization and may act as effective pathfinders.

### 7.7 Mapping of the shallow groundwater data

Element distributions of shallow groundwaters are given in Appendix 6. The area of alluvium > 50 m is distinguished in having groundwater pH predominantly between 7.0 and 7.2 (Figure A6.1). In contrast, the northern half of the study area has pH between 7.3 and 7.6. Surprising, Eh gives very good areal separation (Figure A6.2): all deep alluvium samples have Eh values between 265 and 340 mV; the intermediate areas and the eastern part of the 3000 mN samples have lower Eh (85 to 240 mV); and the rest of the 3000 mN line have high Eh (370-405 mV). This Eh discrimination is not understood at present, but it should be noted that such clear spatial discrimination in Eh has not been previously observed.

The highest salinities (1740-3220 mg/L) are observed in the three most western groundwaters of the 3000 mN line and in the 2800 mN line (Figure A6.3). This high salinity in the three 3000 mN samples is also matched by enrichments in I (1.2-2.7 mg/L; Figure A6.9), Li (0.006-0.022 mg/L; Figure A6.5) and Mn (0.003-0.027 mg/L; Figure A6.15). The southern part of the study area, with deep alluvium and possibly an actively flowing palaeochannel system, has very **low** salinity (400-1200 mg/L) at surface, though with higher salinity (6400 mg/L) at depth. Consequently, the present day shallow palaeochannel groundwaters are not conducive to mobilizing Au (Section 7.6). Element concentrations which are also lower in the shallow palaeochannel groundwaters are B (0.79-0.91 mg/L; Figure A6.8), As (0.001-0.003 mg/L), Mo (0.009-0.017 mg/L) and Au ( $\leq$  0.001  $\mu\text{g/L}$ ) (Figures A6.19 to A6.21), whereas dissolved Si is high (29-44 mg/L; Figure A6.12). Additionally, the shallow palaeochannel groundwaters are undersaturated with respect to the minerals calcite, sepiolite and barite (Figures A6.23-A6.25).

Vanadium (0.014-0.023 mg/L), As (0.003-0.008 mg/L), Mo (0.041-0.063 mg/L), Au (up to 0.019  $\mu\text{g/L}$ ) and possibly U (0.012-0.016 mg/L) (Figures A6.13, A6.19 to A6.22) are highest in groundwaters at, and near, the Au-rich zones at 3000 mN, and, for Au (up to 0.007  $\mu\text{g/L}$ ) and U (0.015-0.018 mg/L) at 1600 mN. This is consistent with previous observations indicating enrichments of these elements in the vicinity of Au deposits (Gray, 1996; Butt et al., 1997). These elements are **not** enriched in the shallow groundwaters above mineralization at 700 mN (V, 0.008-0.013 mg/L, U  $\leq$  0.003 mg/L, concentrations of other elements given in previous paragraph). Thus, there is no evidence of diffusion of V, As, Mo and Au into the shallow groundwaters in the palaeochannel from the buried mineralization.

The low dissolved Au content and poor diffusion into the palaeochannel groundwaters indicates very low present-day activity. Any observed redistribution of Au in the regolith may be due to the long timescale of regolith formation, and/or past periods when Au solubility was greater (possibly due to higher salinities).

## 7.8 Mapping of the deep groundwater data

Element distributions of deep groundwaters are given in Appendix 7. The mineralized zone has slightly acidic groundwaters (Figure A7.1), possibly due to the presence of weathering sulphides. In contrast to the shallow groundwaters, Eh gave no clear pattern for the deep groundwaters. This could be due to the analyses being done on samples sent to the Floreat laboratories rather than in the field, as Eh is highly sensitive to environmental changes, including light (Gray, unpublished data).

The highest salinities (6420-32000 mg/L) are observed in the deep groundwaters along strike of the mineralization at Mt Joel (Figure A7.3). In contrast, the deep groundwaters in the background areas have salinities similar to or less than those for the shallow groundwaters (Figure 38). Thus, the hydrology of the area can be considered in terms of (at least) three aquifers: a deep saline aquifer associated with the mineralized strike, with potential for dissolving Au as a halide complex if acid/oxidizing conditions are ever generated; a fresh groundwater system close to the surface; and fresh groundwaters, even at depth, away from the mineralized zone.

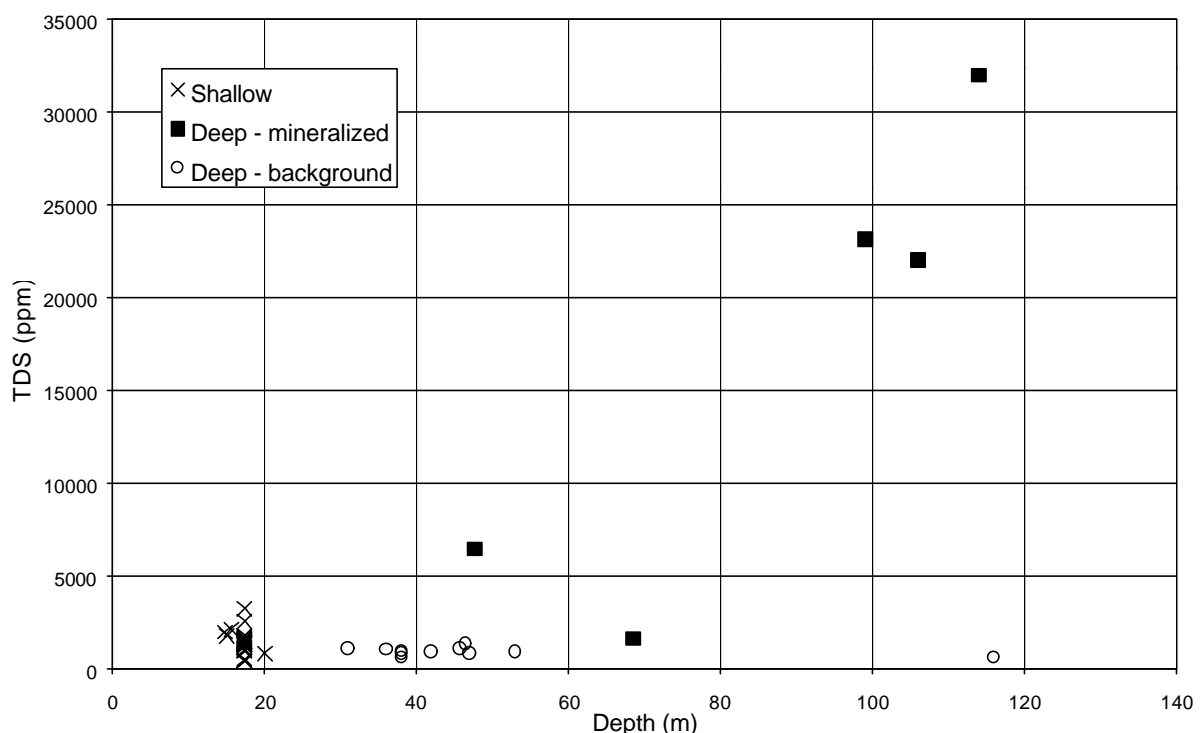


Figure 38: Salinity vs depth for Mt Joel groundwaters.

Very few elements showed any clear distribution patterns. Vanadium was relatively enriched in the NW of the study area (Figure A7.13; 0.012-0.057 mg/L) and this is reflected in groundwater possibly reaching saturation with respect to carnotite ( $\text{KUO}_2\text{VO}_4$ ; Figure A7.34). Carnotite mineralization has been observed in valley calcrete systems in this region, e.g. Lake Maitland (Butt et al., 1977; Cavaney, 1984). Element concentrations which are also lesser in the shallow palaeochannel groundwaters are B (0.79-0.91 mg/L; Figure A6.8), As (0.001-0.003 mg/L), Mo (0.009-0.017 mg/L) and Au ( $\leq 0.001 \mu\text{g/L}$ ) (Figures A6.19 to A6.21), whereas dissolved Si is high (29-44 mg/L; Figure A6.12). Additionally, the shallow palaeochannel groundwaters are undersaturated with respect to the minerals calcite, sepiolite and barite (Figures A6.23 to A6.25). Of the elements enriched within the mineralized zones in the shallow groundwaters (Au, As, Mo and possibly U; Section 7.7), only As showed any tendency to be enhanced near mineralization in the deep groundwaters (Figure A7.19; up to 0.11 mg/L). Dissolved Au, Mo and U showed **no** enhancement with mineralization (Figures A7.20 to A7.22), but dissolved Hg was possibly enhanced in mineralized groundwaters (Figure A7.25; up to 0.09 mg/L). Possible oversaturation with

respect to barite was observed in groundwater along the mineralized strike (Figure A7.30) - this has been observed coincident with mineralization elsewhere in the Yilgarn Craton (Gray, 1996) and is postulated to be due to dissolution of carbonates releasing Ba faster than it reprecipitates as barite.

## 7.9 Summary

The hydrology of the Mt Joel area can be considered in terms of (at least) three aquifers:

- i. A deep saline (6420-32000 mg/L) aquifer associated with the mineralized strike, with potential for dissolving Au as a halide complex if acid/oxidizing conditions are ever generated.
- ii. Fresh groundwaters, even at depth, away from the mineralized zone.
- iii. A fresh shallow groundwater system throughout the area.

The shallow Mt Joel groundwaters are neutral (pH 7.0-7.6), range from moderately oxidizing to reducing, and have low salinities (400-3200 mg/L), similar to other northern groundwaters. The deeper groundwaters have a higher pH (6.3-8.0) and salinity (1000-38600 mg/L) range, suggesting heterogeneous characteristics, as discussed above. The four deepest saline groundwaters, associated with the mineralized strike, are five times more saline than the most saline other northern groundwater.

Concentrations of the minor elements are generally similar to other northern groundwaters, as expected for a fresh/neutral environment. However, compared with other northern sites, the Mt Joel groundwaters are relatively enriched in V, U, As and Mo. Because of the greater dissolved V and U concentrations, carnotite ( $KUO_2VO_4$ ) is more readily precipitated than at the other previous study sites in this region (e.g., Lawlers and Baxter; Gray, 1994, 1995). Arsenic and Mo are both indicators for Au mineralization and/or weathering sulphides and these relative enrichments may be regional indicators for mineralization. Dissolved Au concentrations at Mt Joel are, as expected, very low, suggesting that Au is not being actively dispersed in the regolith, and therefore will not produce a useful dispersion halo in groundwater or in juvenile soils. However, at this site, elements other than dissolved Au can be associated with Au mineralization and may act as effective pathfinders. Vanadium, As, Mo, Au and possibly U are highest in shallow groundwaters at and near the Au-rich zones at 3000 mN, and, for Au and U, at 1600 mN. These elements are **not** diffused into the shallow groundwaters in the palaeochannel from buried mineralization at the 800 mN Au-rich zone. This southern part of the study area has very low salinity at surface and these shallow palaeochannel groundwaters are not conducive to mobilizing Au. Any observed redistribution of Au in the regolith may be due the long timescale of regolith formation, and/or past periods when Au solubility was greater (possibly due to higher salinities).

Of the elements enriched within the mineralized zones in the shallow groundwaters, only As showed any tendency to be enhanced near mineralization in the deep groundwaters, with dissolved Au, Mo and U showing **no** enhancement with mineralization. Dissolved Hg was possibly enhanced in mineralized deep groundwaters (Figure A7.25; up to 0.09 mg/L). Possible over-saturation with respect to barite was observed in groundwater along the mineralized strike.

## 8 DISTRIBUTION OF GOLD

### 8.1 Sample distribution

The distribution of Au was investigated using a database provided by GCM which included Au assay results and logging from exploration drilling in an area delineated by the -200 m and 4000 m N and 9000 m and 10000 m E local coordinates. Most drilling within this area was concentrated in five potential ore zones along the mineralized N-NE trend, known as the 0 mN, 800 mN, 1600 mN, 2400 mN and 3000 mN areas, following their approximate locations.

For each of these areas, the Au data was treated by MVS software as described in Section 2.4. Various plots are included as JPG files in the accompanying CD, in separate directories, as described briefly below, and listed in Appendix 10:

The CD is divided into five folders for the five deposits, namely the “0”, “800”, “1600”, “2400” and “3000” mN areas, along with the “ALL” directory, which includes plots of layer thicknesses for the entire study area. Each area directory contains three sub-directories:

- i. The SLICES directory includes vertical slices mainly at constant northing, named according to the particular northing. Thus a slice through 3000 mN is named 3000mN.JPG.
- ii. The LAYERS directory includes the various layers, either merged together to show the true stratigraphy (TOGETHER.JPG), exploded so as to show the characteristics of the various layers (EXPLODED.JPG), or with a particular Au grade cut-off.
- iii. The PLANS directory includes plans of calculated Au grade at a particular RL (e.g., the plot of the calculated Au concentrations at 300 mRL is named 300.JPG) at a particular surface (e.g., the plot of the calculated Au grade at the base of weathering is named B\_WEATH.JPG) or at a set vertical distance from a weathering surface (e.g., the plot of the calculated Au grade 2 m below the unconformity is named UNCON-2.JPG).

### 8.2 Visualization of gold distribution

Examination of several MVS plans below surface in the 3000 and 2400 mN areas (e.g., Figure 39) show that the patterns of Au distribution in the fresh rock, transition zone and lower oxide zones are very similar, reflecting Au distribution in primary mineralization. In some levels, such as the transition zone (Figure 39b) the grades seem locally greater. This may represent zones of higher grades in primary mineralization or some supergene enrichment. However, a much more noticeable change occurs at approximately 30 m below surface (about 450mRL), within the oxide zone, where Au concentration is distinctly lower marking the presence of a Au leached zone (Figure 39c). This pattern persists upwards to about 20 m below surface (about 460mRL), where the Au anomaly becomes increasingly stronger and more widespread in the interface zone just below the unconformity (Figure 39d).

The plots produced for the 800 mN and 0 mN areas show that primary mineralization is more confined (Figure 40a) than in the 3000 mN and 2400 mN areas. It also shows that Au distribution in the transition zone (Figure 40b) and oxide zone (Figure 40c) tend to become more widespread. Gold depleted zones were not identified but an enriched zone is apparent in the lateritic residuum close to the unconformity, where lateral dispersion follows the direction of the palaeochannel (Figure 40d).

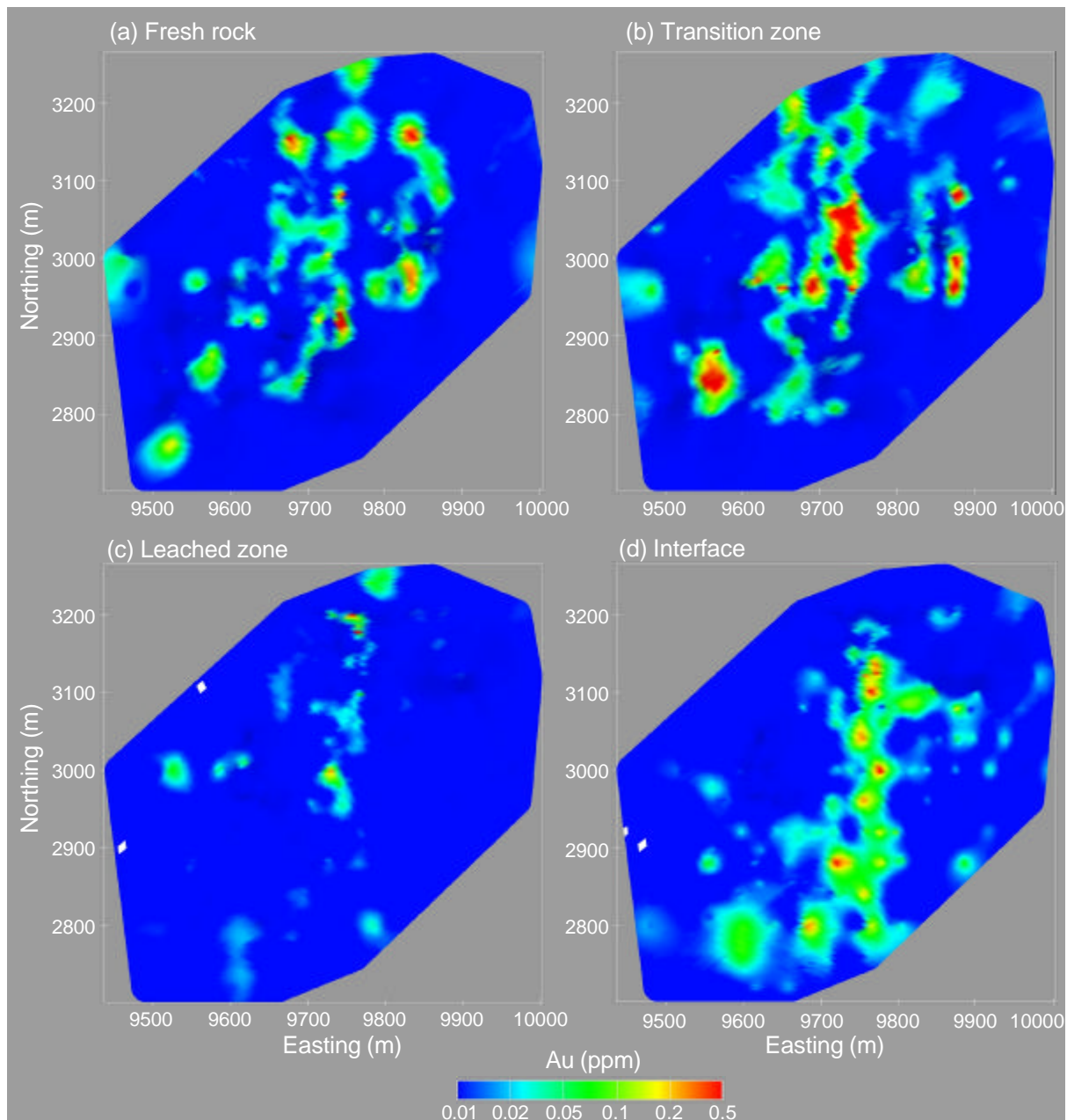


Figure 39: Gold distribution in the 3000 mN area for: (a) fresh rock (5 m below base of weathering); (b) transition zone (10 m above base of weathering); (c) leached zone (20 m below unconformity); and (d) interface (2 m below unconformity).

### 8.3 Statistical analysis

#### 8.3.1 Sample distribution

Statistical analysis was performed combining the data into two groups in order to improve sample representation: 800 and 0 mN areas were combined to represent areas with palaeochannel sediments overlying lateritic residuum, and 3000 and 2400 mN areas were combined to represent areas with thinner alluvial cover dominated by saprolite.

For each group of areas, several layers (2 to 10 m thick) were constructed upwards and downwards from the unconformity, BOCO and base of weathering. Statistical analysis were then performed with the Au grades from the samples contained within those layers.

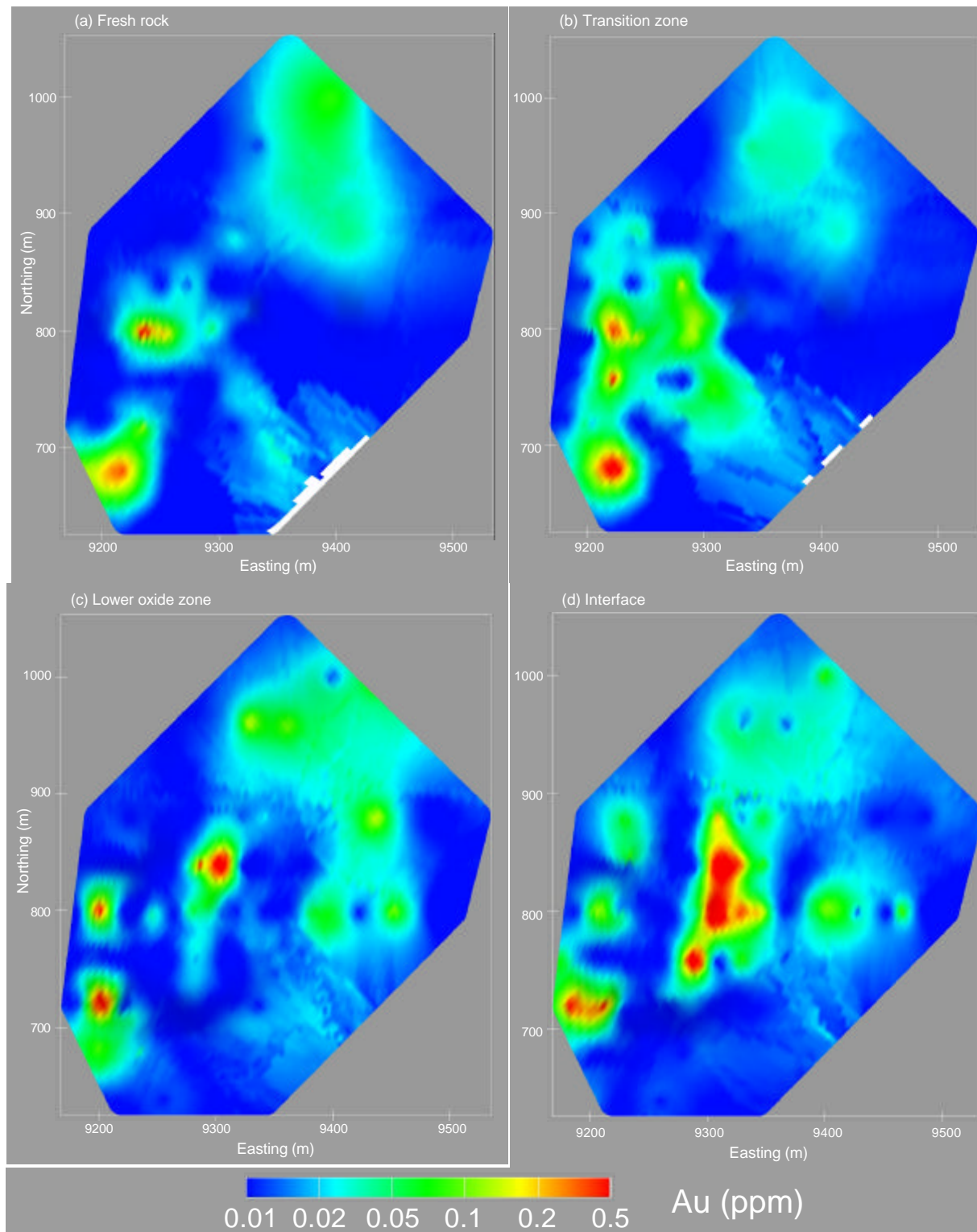


Figure 40: Gold distribution in the 800 mN area for: (a) fresh rock (10 m below base of weathering); (b) transition zone (15 m above base of weathering); (c) lower oxide zone (20 m below unconformity); and (d) interface with laterite (2 m below unconformity).

### 8.3.2 Results for 3000 and 2400 mN areas

The results for the 3000 and 2400 mN areas are shown in Tables 8 to 10 and the geometric and arithmetic means of each data set are plotted graphically in Figures 41 to 46. These same results are plotted as histograms and cumulative frequency plots in Appendix 8.

The results in Table 8, Figures 41 and 42 show that the enrichment associated with the GCM logged unconformity at the base of alluvium apparently varies between 5 m above and below the unconformity. As discussed in Section 3.3, this enriched zone, according to CRC LEME logging, is equivalent mostly to the top of saprolite. This zone is also characterized by a less skewed Au distribution, with almost 50% of the data concentrated in the range 0.02-0.5 ppm (Table 8). This more homogeneous Au distribution results from a significant Au mobilization. The underlying leached zone, down to 25 m below the unconformity, is characterized by a decrease in the mean Au grades with a minimum of 0.012 ppm (geometric mean) and only 0.7% of the data above 0.5 ppm. In the lower oxide zone, Au concentrations increase sharply. The average Au concentration in the alluvium is invariably low (<0.02 ppm).

Table 8: Statistics of Au grades relative to the unconformity surface (3000 and 2400 mN areas).

Depth (m)	No.	Au (ppm)			Coeff. Var.	Grade Distribution (%)		
		Geom. Mean	Arith. Mean	Std. Dev.		<0.02 ppm	0.02-0.5 ppm	≥0.5 ppm
+25 to surface	134	0.011	0.012	0.009	0.7	96.3	3.7	0.0
+15 to 25	339	0.011	0.015	0.036	2.3	95.6	4.4	0.0
+10 to 15	496	0.012	0.015	0.022	1.4	88.1	11.9	0.0
+5 to 10	1500	0.014	0.020	0.037	1.8	77.3	22.5	0.2
+2 to 5	1472	0.019	0.043	0.178	4.2	60.5	38.9	0.6
0 to 2	813	0.025	0.077	0.302	3.9	51.3	46.5	2.2
0 to -2	823	0.028	0.088	0.297	3.4	47.6	49.7	2.7
-2 to -5	1634	0.020	0.067	0.239	3.6	61.3	35.7	3.0
-5 to -10	2432	0.015	0.063	0.563	8.9	76.0	22.5	1.5
-10 to -15	2066	0.013	0.056	0.822	14.6	82.0	17.1	0.8
-15 to -25	4767	0.012	0.035	0.405	11.6	88.7	10.6	0.7
-25 to -40	6550	0.016	0.120	0.909	7.6	79.3	17.0	3.7
-40 to BOCO	8649	0.017	0.105	0.671	6.4	72.9	23.2	3.9
Transition	11264	0.018	0.108	0.678	6.3	70.9	25.4	3.7
Fresh	14586	0.014	0.094	0.887	9.4	78.6	19.0	2.4
Total	57525	0.016	0.088	0.713	8.1	75.6	21.8	2.7

Geom. Mean – Geometric mean  
Arith. Mean – Arithmetic mean

Std. Dev. – Standard deviation  
Coeff. Var. – Coefficient of variation, calculated for arithmetic mean

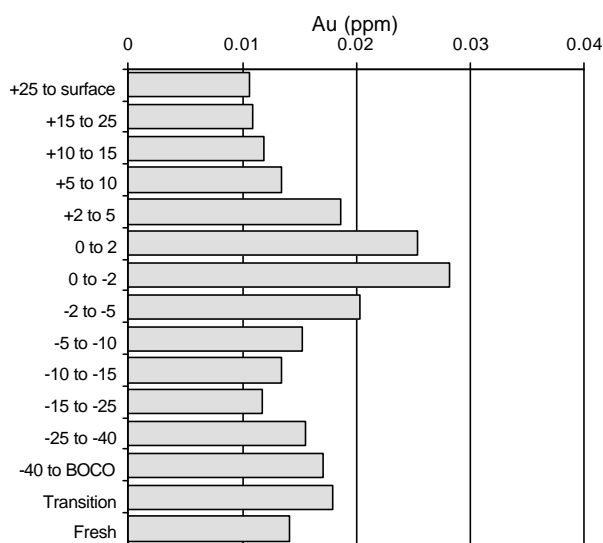


Figure 41: Geometric mean of Au grades relative to unconformity (3000 and 2400 mN areas).

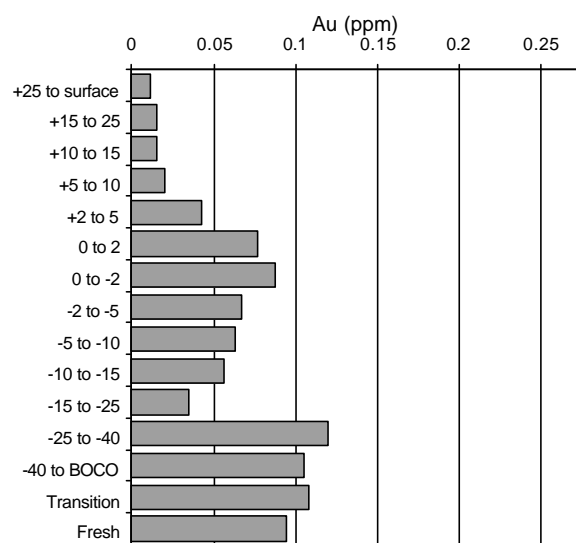


Figure 42: Arithmetic mean of Au grades relative to unconformity (3000 and 2400 mN areas).

Only minor changes in Au distribution take place across the BOCO (Table 9, Figures 43 and 44). In the transition zone, the proportion of values below 0.01 ppm decreases slightly followed by a concomitant increase in the values between 0.01 and 0.5 ppm, whereas the proportion of values above 0.5 ppm remains mostly unchanged. This more homogeneous distribution is reflected in a slight increase in the geometric mean in the transition zone. At the base of weathering there is a slight, but constant, increase of the geometric means accompanied by a lower spread of values in the transition zone compared to fresh rock (Table 10, Figures 45 and 46). These results suggest that some Au redistribution has taken place in the transition zone.

Table 9: Statistics of Au grades relative to the BOCO surface (3000 and 2400 mN areas).

Depth (m)	No.	Au (ppm)			Coeff. Var.	Grade Distribution (%)		
		Geom. Mean	Arith. Mean	Std. Dev.		<0.02 ppm	0.02-0.5 ppm	≥0.5 ppm
Alluvium	4448	0.016	0.034	0.158	4.7	71.7	27.8	0.5
+30 to Unconf.	12380	0.014	0.050	0.467	9.3	80.0	18.6	1.4
+25 to 30	2234	0.015	0.107	0.853	8.0	78.6	18.3	3.2
+20 to 25	2256	0.016	0.124	0.880	7.1	77.3	18.9	3.8
+15 to 20	2267	0.017	0.129	0.798	6.2	74.6	21.0	4.4
+10 to 15	1943	0.016	0.122	1.059	8.7	75.9	20.5	3.6
+5 to 10	2271	0.017	0.104	0.820	7.9	74.9	21.2	3.9
0 to 5	2350	0.019	0.120	0.522	4.4	69.3	25.8	4.9
0 to -5	2265	0.022	0.122	0.519	4.2	64.7	29.9	5.3
-5 to -10	2125	0.018	0.095	0.490	5.1	68.9	27.2	3.9
-10 to -15	1585	0.019	0.144	0.784	5.5	69.3	26.1	4.7
-15 to -20	1606	0.017	0.102	0.684	6.7	71.2	25.2	3.5
-20 to -25	1268	0.017	0.120	1.016	8.5	74.7	22.8	2.5
-25 to BoW.	2415	0.015	0.081	0.652	8.0	77.3	20.7	2.1
Fresh	14460	0.014	0.095	0.891	9.4	78.4	19.1	2.5

Geom. Mean – Geometric mean  
Arith. Mean – Arithmetic mean

Std. Dev. – Standard deviation  
Coeff. Var. – Coefficient of variation, calculated for arithmetic mean

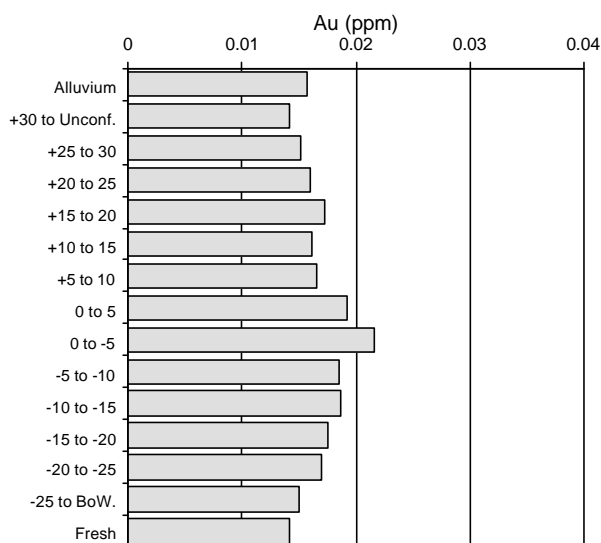


Figure 43: Geometric mean of Au grades relative to the BOCO surface (3000 and 2400 mN areas).

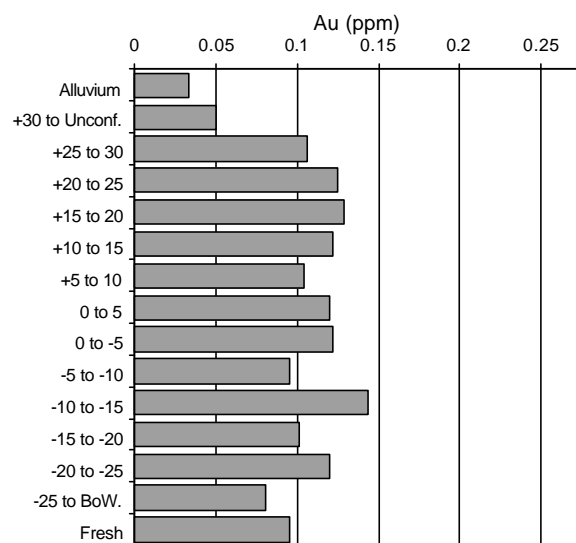


Figure 44: Arithmetic mean of Au grades relative to the BOCO surface (3000 and 2400 mN areas).

Table 10: Statistics of Au grades relative to the base of weathering (3000 and 2400 mN areas).

Depth (m)	No.	Au (ppm)			Coeff. Var.	Grade Distribution (%)		
		Geom. Mean	Arith. Mean	Std. Dev.		<0.02 ppm	0.02-0.5 ppm	≥0.5 ppm
Alluvium	3662	0.016	0.028	0.062	2.2	71.8	27.9	0.3
Oxide	20989	0.015	0.078	0.666	8.5	78.1	19.5	2.4
+30 to BOCO	799	0.019	0.105	0.463	4.4	67.2	28.0	4.8
+25 to 30	723	0.018	0.085	0.354	4.2	68.7	27.2	4.0
+20 to 25	1035	0.019	0.106	0.558	5.3	70.9	24.6	4.4
+15 to 20	1329	0.017	0.084	0.404	4.8	73.5	23.3	3.2
+10 to 15	1319	0.017	0.131	1.080	8.2	71.7	25.5	2.7
+5 to 10	1748	0.019	0.124	0.687	5.5	70.3	25.7	3.9
0 to 5	1869	0.017	0.098	0.697	7.1	74.3	22.8	2.9
0 to -5	1836	0.015	0.069	0.447	6.5	76.9	20.9	2.2
-5 to -10	1624	0.016	0.147	1.670	11.4	77.7	19.3	3.0
-10 to -15	1231	0.015	0.124	1.305	10.5	76.6	20.6	2.8
-15 to -20	1307	0.014	0.084	0.550	6.5	79.1	18.7	2.1
-20 to -25	1206	0.016	0.117	0.826	7.0	77.1	19.7	3.2
-25 down	7256	0.013	0.083	0.671	8.1	79.4	18.3	2.3

Geom. Mean – Geometric mean  
Arith. Mean – Arithmetic mean

Std. Dev. – Standard deviation  
Coeff. Var. – Coefficient of variation, calculated for arithmetic mean

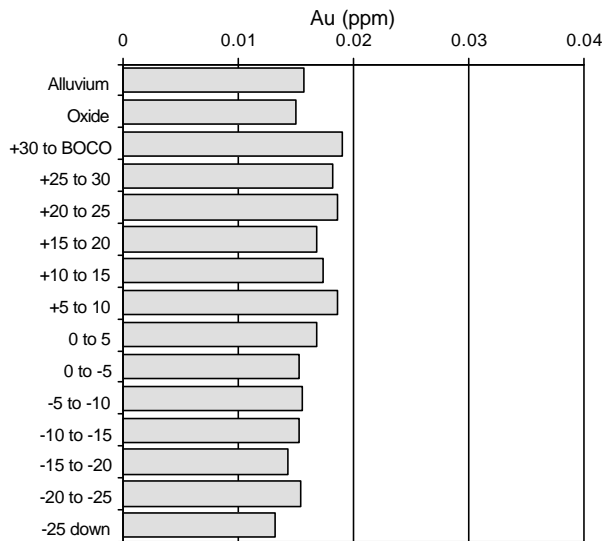


Figure 45: Geometric mean of Au grades relative to base of weathering (3000 and 2400 mN areas).

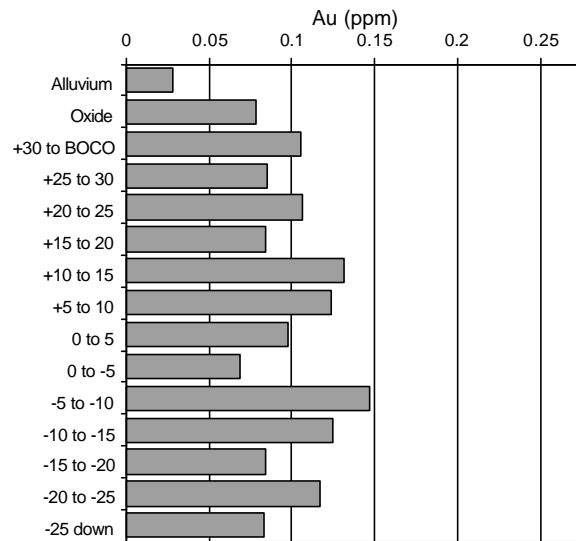


Figure 46: Arithmetic mean of Au grades relative to base of weathering (3000 and 2400 mN areas).

The Au statistics for the 3000 and 2400 mN area have been recalculated for the main weathering zones, including the interface and leached zones. For the purpose of this calculation the leached zone was considered to lie between 450 mRL and 5 m below the unconformity (Table 11). The Sichel's mean has been derived to give a better estimate of the mean values of Au data sets (Sichel, 1966). The Sichel's mean is the geometric mean corrected by a factor, which increases with the variance and the number of samples of the data set. It generally lies between the geometric mean and arithmetic mean of a given log normal data set. These results confirm that Au is slightly enriched and more homogeneously distributed in the transition zone. It also shows the presence of a distinctly Au-depleted zone in the leached zone and a distinctly Au-enriched interface zone where Au distribution is more homogeneous.

Table 11: Statistics of Au grades from whole 3000 and 2400 mN areas.

Zone	No.	Au means (ppm)			Coeff. Var.	Grade distribution (%)		
		Geom.	Sichel's	Arith..		<0.02 ppm	0.02-0.5 ppm	>0.5 ppm
Alluvium	3041	0.014	0.019	0.023	1.8	76	22	2
Interface	1249	0.026	0.052	0.067	3.2	51	47	2
Leached	3885	0.010	0.009	0.022	16.5	83	16	1
Lower Oxide	20361	0.015	0.027	0.078	8.7	78	19	3
Transition	8822	0.018	0.040	0.107	6.4	72	24	4
Fresh Rock	12740	0.015	0.027	0.101	9.3	78	19	34

Geom. – Geometric mean

Sichel's – Sichel's mean

Arith. – Arithmetic mean

Coeff. Var. – Coefficient of variation, calculated for arithmetic mean

### 8.3.3 Results for 800 and 0 mN areas

The results for the 800 mN and 0 mN areas are shown in Tables 12 to 14 and the geometric and arithmetic means of each data set are plotted graphically in Figures 47 to 52. These same results are plotted as histograms and cumulative frequency plots in Appendix 8.

A very distinct Au-enriched zone, 5 m above and below the unconformity (interface zone) is also present in this area (Table 12, Figures 47 and 48). As discussed in Section 3.3 this enriched zone mostly corresponds to the upper parts of the lateritic residuum, which is dominantly pisolitic. This zone is also characterized by a less skewed Au distribution, with up to 40% of the data concentrated in the range 0.02-0.5 ppm, indicating homogenization of the grades. Below this zone, no consistent trend in grade variation is apparent. The Au concentration in the alluvium is also close to the detection limit of 0.01 ppm except for the first few intervals above the unconformity, which may contain anomalous Au results. However, this may be because the GCM-logged unconformity varies slightly from the CRC LEME-logged unconformity (Figure 11).

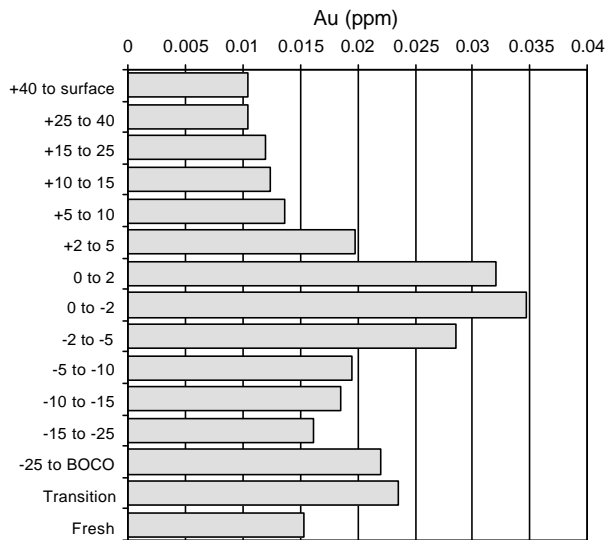


Figure 47: Geometric mean of Au grades relative to the unconformity (800 and 0 mN areas).

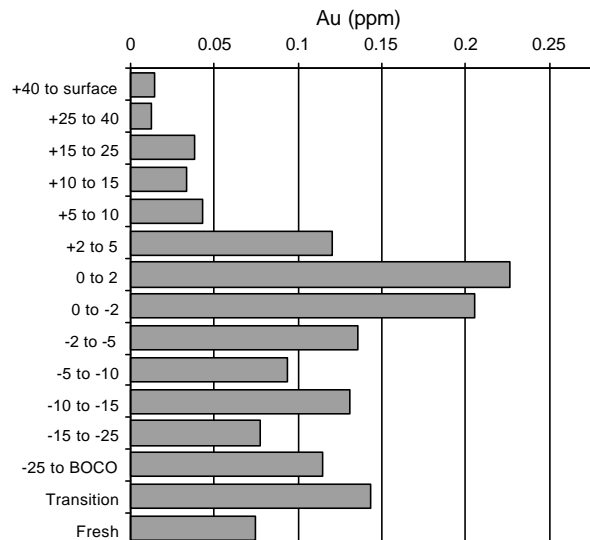


Figure 48: Arithmetic mean of Au grades relative to the unconformity (800 and 0 mN areas).

Table 12: Statistics of Au grades relative to the unconformity surface (800 and 0 mN areas).

Depth (m)	No.	Au (ppm)			Coeff. Var.	Grade Distribution (%)		
		Geom. Mean	Arith. Mean	Std. Dev.		<0.02 ppm	0.02-0.5 ppm	≥0.5 ppm
+40 to surface	1352	0.010	0.014	0.052	3.7	96.7	3.1	0.2
+25 to 40	1026	0.011	0.012	0.016	1.3	94.9	5.1	0.0
+15 to 25	888	0.012	0.038	0.199	5.2	90.4	7.7	1.9
+10 to 15	603	0.012	0.033	0.150	4.5	88.2	10.4	1.3
+5 to 10	719	0.014	0.043	0.207	4.8	83.7	15.0	1.3
+2 to 5	487	0.020	0.120	0.415	3.4	70.8	22.8	6.4
0 to 2	244	0.032	0.226	0.675	3.0	57.8	31.6	10.7
0 to -2	224	0.035	0.205	0.626	3.1	53.6	38.4	8.0
-2 to -5	416	0.029	0.135	0.381	2.8	56.5	36.3	7.2
-5 to -10	569	0.019	0.093	0.404	4.3	69.4	26.5	4.0
-10 to -15	431	0.018	0.131	0.755	5.7	69.8	26.2	3.9
-15 to -25	723	0.016	0.078	0.404	5.2	75.9	20.5	3.6
-25 to BOCO	821	0.022	0.115	0.393	3.4	67.6	26.8	5.6
Transition	3179	0.023	0.143	0.578	4.0	65.9	26.9	7.2
Fresh	3406	0.015	0.074	0.405	5.5	74.4	23.1	2.5
Total	15088	0.017	0.086	0.421	4.9	76.1	20.1	3.8

Geom. Mean – Geometric mean

Std. Dev. – Standard deviation

Arith. Mean – Arithmetic mean

Coeff. Var. – Coefficient of variation, calculated for arithmetic mean

Changes in Au distribution across the BOCO surface are minor (Table 13, Figures 49 and 50). However, a significant grade increase is observed in the transition zone compared to fresh rock (Table 14, Figures 51 and 52).

Table 13: Statistics of Au grades relative to the BOCO surface (800 and 0 mN areas).

Depth (m)	No.	Au (ppm)			Coeff. Var.	Grade Distribution (%)		
		Geom. Mean	Arith. Mean	Std. Dev.		<0.02 ppm	0.02-0.5 ppm	≥0.5 ppm
Alluvium	5126	0.013	0.044	0.238	5.4	88.2	10.0	1.8
+30 to Unconf.	540	0.024	0.152	0.585	3.8	61.3	33.0	5.7
+25 to 30	247	0.017	0.123	0.878	7.1	70.9	25.9	3.2
+20 to 25	290	0.013	0.035	0.133	3.8	83.4	15.2	1.4
+15 to 20	391	0.020	0.103	0.279	2.7	71.9	21.2	6.9
+10 to 15	416	0.026	0.124	0.446	3.6	62.5	33.7	3.8
+5 to 10	552	0.022	0.115	0.415	3.6	65.9	28.1	6.0
0 to 5	622	0.022	0.123	0.474	3.9	64.6	29.7	5.6
0 to -5	701	0.025	0.161	0.597	3.7	62.2	30.1	7.7
-5 to -10	612	0.024	0.167	0.575	3.4	67.8	23.5	8.7
-10 to -15	446	0.025	0.137	0.420	3.1	63.7	28.7	7.6
-15 to -20	450	0.024	0.119	0.382	3.2	62.4	31.1	6.4
-20 to -25	359	0.026	0.198	1.052	5.3	64.3	26.5	9.2
-25 to BoW	611	0.019	0.090	0.327	3.6	73.2	22.4	4.4
Fresh	3400	0.015	0.074	0.406	5.5	74.4	23.1	2.5

Geom. Mean – Geometric mean

Std. Dev. – Standard deviation

Arith. Mean – Arithmetic mean

Coeff. Var. – Coefficient of variation, calculated for arithmetic mean

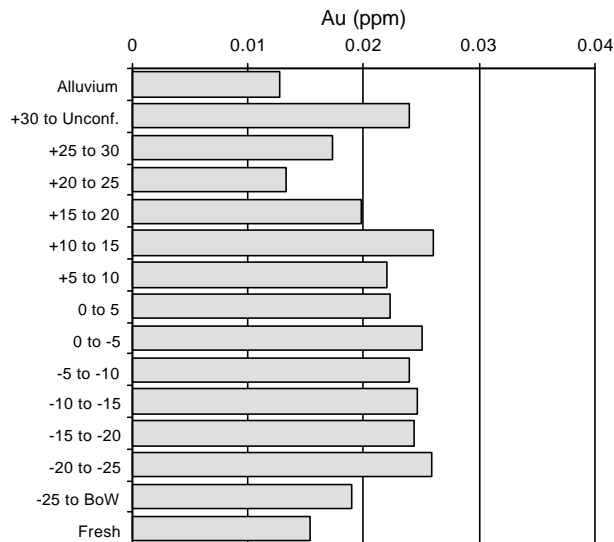


Figure 49: Geometric mean of Au grades relative to the BOCO surface (800 and 0 mN areas).

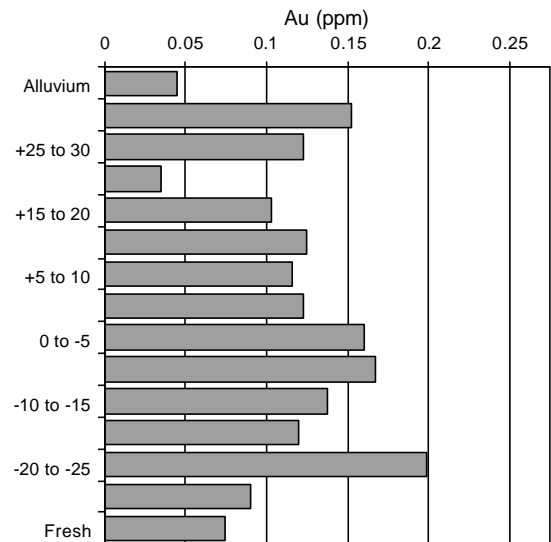


Figure 50: Arithmetic mean of Au grades relative to the BOCO surface (800 and 0 mN areas).

Table 14: Statistics of Au grades relative to the base of weathering (800 and 0 mN areas).

Depth (m)	No.	Au (ppm)			Coeff. Var.	Grade Distribution (%)		
		Geom. Mean	Arith. Mean	Std. Dev,		<0.02 ppm	0.02-0.5 ppm	≥0.5 ppm
Alluvium	4458	0.013	0.042	0.205	4.9	88.2	9.9	1.8
Oxide	2625	0.022	0.124	0.515	4.2	66.0	28.7	5.3
+30 to BOCO	260	0.023	0.120	0.349	2.9	70.0	23.5	6.5
+25 to 30	212	0.026	0.251	0.923	3.7	66.5	23.1	10.4
+20 to 25	300	0.032	0.268	0.758	2.8	62.3	21.3	16.3
+15 to 20	376	0.031	0.173	0.460	2.7	56.6	32.7	10.6
+10 to 15	369	0.026	0.117	0.290	2.5	58.0	35.0	7.0
+5 to 10	518	0.024	0.152	0.887	5.8	64.5	30.1	5.4
0 to 5	588	0.022	0.115	0.362	3.1	68.4	25.3	6.3
0 to -5	579	0.016	0.058	0.261	4.5	73.6	24.0	2.4
-5 to -10	471	0.019	0.108	0.481	4.4	70.9	25.3	3.8
-10 to -15	325	0.018	0.064	0.238	3.7	68.3	29.8	1.8
-15 to -20	297	0.020	0.129	0.527	4.1	69.7	25.3	5.1
-20 to -25	244	0.019	0.183	0.930	5.1	73.0	21.7	5.3
-25 down	1484	0.012	0.043	0.253	5.8	78.2	20.5	1.3

Geom. Mean – Geometric mean

Std. Dev. – Standard deviation

Arith. Mean – Arithmetic mean

Coeff. Var. – Coefficient of variation, calculated for arithmetic mean

The statistics for the entire Au data set in this area have been recalculated for the main weathering zones (Table 15). These results confirm the presence of Au enrichment in the transition and interface zones where the distribution of the Au grades is also more homogeneous.

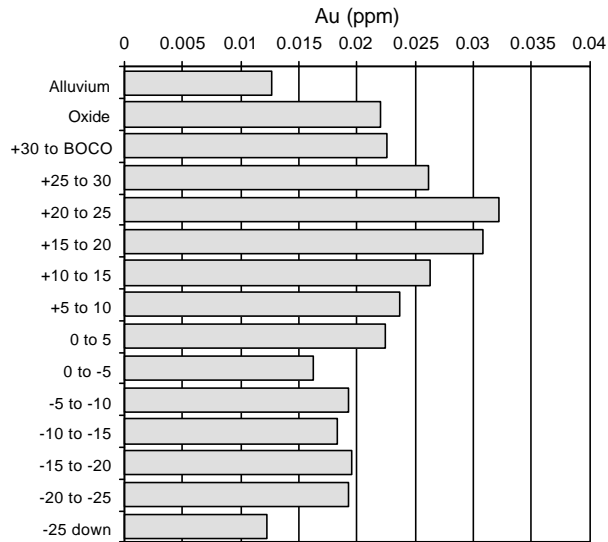


Figure 51: Geometric mean of Au grades relative to the weathering front (800 and 0 mN areas).

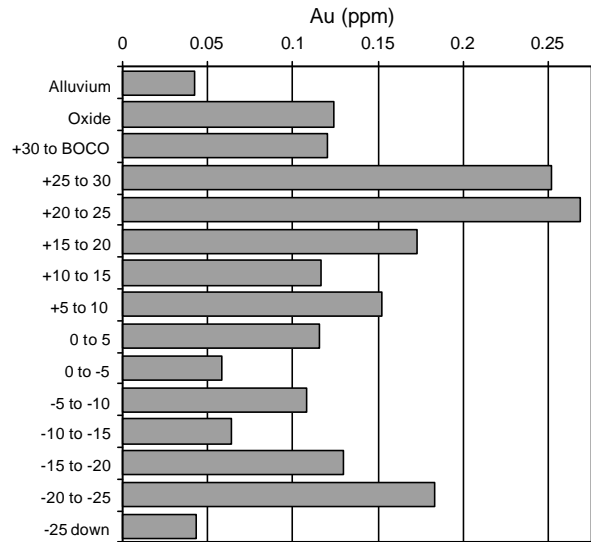


Figure 52: Arithmetic mean of Au grades relative to the weathering front (800 and 0 mN areas).

Table 15: Statistics of Au grades from whole 800 and 0 mN areas.

Zone	No.	Au means (ppm)			Coeff. Var.	Grade distribution (%)		
		Geom.	Sichel's	Arithm.		<0.02 ppm	0.02-0.5 ppm	>0.5 ppm
Alluvium	4258	0.012	0.017	0.035	5.2	90	9	1
Interface	386	0.032	0.145	0.206	2.8	58	33	9
Oxide	2439	0.021	0.059	0.117	4.3	68	27	5
Transition	2623	0.026	0.090	0.160	3.8	63	29	8
Fresh Rock	3251	0.016	0.033	0.077	5.4	74	22	4

Geom. – Geometric mean  
Arith. – Arithmetic mean

Sichel's – Sichel's mean  
Coeff. Var. – Coefficient of variation, calculated for arithmetic mean

#### 8.4 Normalization of Au to immobile elements

The mean and median values of the most immobile elements, such as Al, Zr, Hf, Th and Ti, as discussed in Section 6, are computed for each weathering zone in the 3000 and 800 mN areas (Table 16). These results were combined with the Au means presented in Table 11 and Table 15 in the following manner:

- The arithmetic, geometric and Sichel's mean Au grades in each weathering zone was divided by the corresponding mean Au grade value in the fresh rock.
- The arithmetic mean and median values of each immobile element was divided by their corresponding values in the fresh rock.
- The Au ratios obtained were divided by the immobile element ratios, considering all possible combinations. The equivalence of the weathering zones when considering Au data (GCM database) and immobile element (CRC LEME) data are given in Table 1.

These results are shown for Al, Hf and Ti in the plots of Figure 53 for the 3000 and 2400 mN areas and Figure 54 for the 800 and 0 mN areas. Zirconium results were similar to Hf, but Th gave apparently spurious results, presumably because of significant lithological variations in Th content (Section 6.8).

Several assumptions must be recognized to interpret these results usefully:

- i. Most importantly, the distribution of Au and immobile elements in the weathering zones were essentially the same as in the parent rock, which was sampled for the purpose of this investigation. This is a difficult assumption, especially in mineralized areas where lithological variations are common because of hydrothermal alteration and structural complexities.
- ii. Samples analysed are representative. This may not be a problem for Au, but the number of samples analysed for immobile elements were not always satisfactory to obtain a sound statistical representation, especially in the 800 and 0 mN areas.
- iii. Index elements were, in fact, immobile during weathering.

The calculations give a qualitative measure of the scale of Au mobility in the areas, although discrepancies related to the assumptions are evident in Figures 53 and 54. However, when the 3000 mN area is compared with the 800 mN area, some significant differences emerge:

- i. Stronger tendency for Au depletion in the 3000 mN area. Gold depletion reaches a maximum in the leached zone. The top of saprolite is enriched relative to the leached zone, implying Au addition.
- ii. Despite the lack of data for Al, Zr and Ti in the transition zone of the 800 mN area, Au enrichment there seems more obvious than in the 3000 mN area.
- iii. The saprolite of the 800 mN area is less Au depleted than in the 3000 mN area, and may even be slightly enriched.
- iv. The enrichment in the dominantly pisolitic lateritic zone of the 800 mN area is more pronounced than that in the top of saprolite of the 3000 mN area.

The data related to the alluvium are not considered due to its allochthonous nature.

*Table 16: Mean values of immobile elements in the 3000 mN and 800 mN areas.*

<b>3000 + 2400 mN areas</b>											
<b>Zone</b>	<b>No. samples</b>	<b>Means</b>					<b>Medians</b>				
		<b>Al<sub>2</sub>O<sub>3</sub> (%)</b>	<b>Ti (%)</b>	<b>Zr (ppm)</b>	<b>Hf (ppm)</b>	<b>Th (ppm)</b>	<b>Al<sub>2</sub>O<sub>3</sub> (%)</b>	<b>Ti (%)</b>	<b>Zr (ppm)</b>	<b>Hf (ppm)</b>	<b>Th (ppm)</b>
Top of saprolite	18	21.1	0.98	82	2.5	4.2	20.5	1.01	75	2.4	4.0
Leached zone	24	26.1	1.34	160	4.5	6.7	26.2	1.35	92	2.9	1.2
Lower saprolite	35 (55 for Hf, Th)	20.4	1.09	149	4.4	9.8	20.4	1.11	179	5.4	12.0
Transition	9 (40 for Hf, Th)	16.1	0.90	97	3.7	8.5	16.2	0.92	63	4.3	10.7
Fresh rock	28 (39 for Hf, Th)	13.7	0.95	71	1.9	1.1	14.1	0.98	69	1.9	0.5
<b>800 + 0 mN areas</b>											
<b>Zone</b>	<b>No. samples</b>	<b>Means</b>					<b>Medians</b>				
		<b>Al<sub>2</sub>O<sub>3</sub> (%)</b>	<b>Ti (%)</b>	<b>Zr (ppm)</b>	<b>Hf (ppm)</b>	<b>Th (ppm)</b>	<b>Al<sub>2</sub>O<sub>3</sub> (%)</b>	<b>Ti (%)</b>	<b>Zr (ppm)</b>	<b>Hf (ppm)</b>	<b>Th (ppm)</b>
Laterite	11	15.6	0.74	65	2.0	2.2	15.3	0.69	65	1.7	1.6
Saprolite	4 (31 for Hf, Th)	16.8	1.14	69	2.0	0.6	16.9	1.13	70	2.0	0.5
Transition	0 (6 for Hf, Th)				1.8	0.6				1.7	0.5
Fresh rock	28 (39 for Hf, Th)	13.7	0.95	71	1.9	1.1	14.1	0.98	69	1.9	0.5

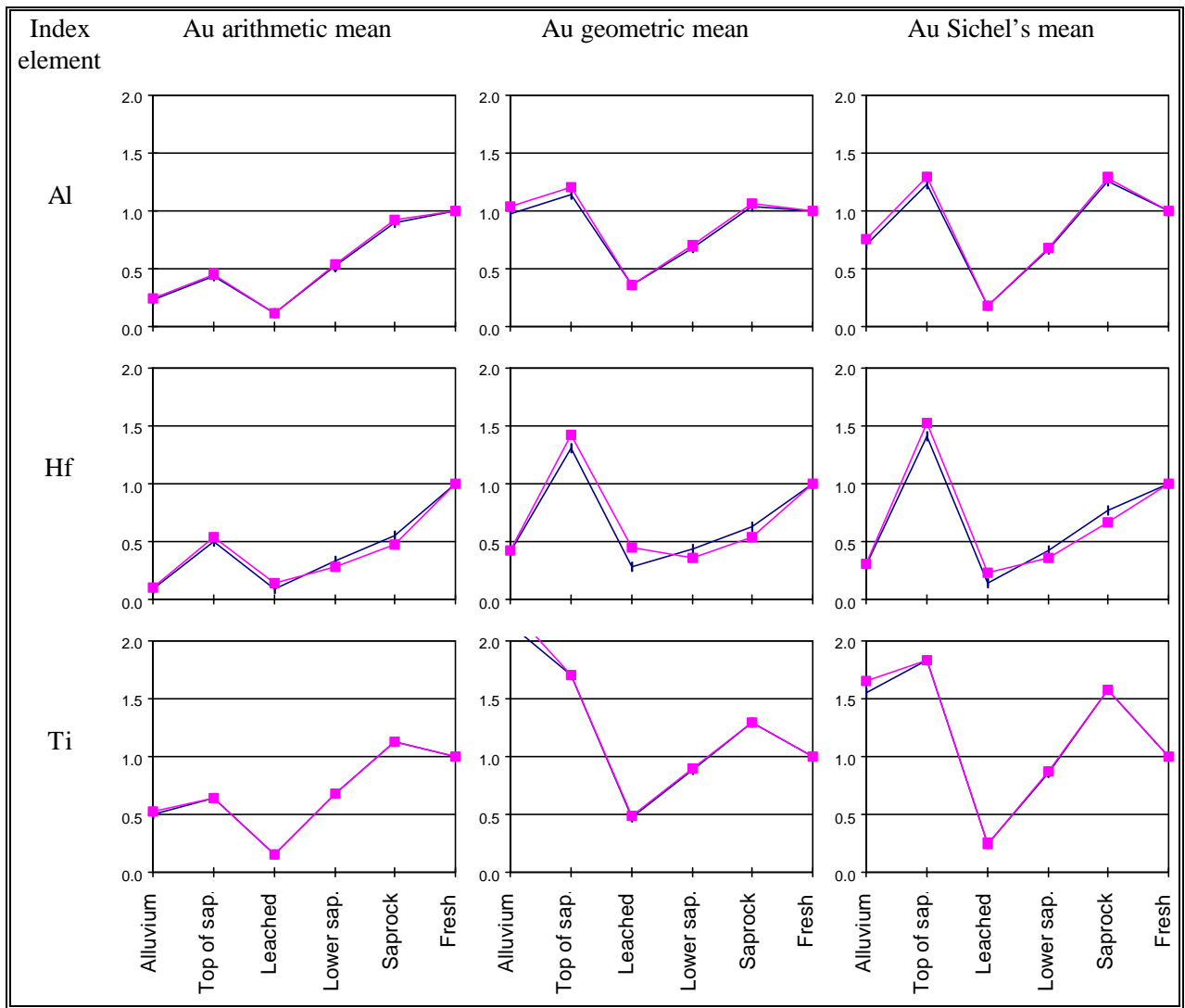


Figure 53: Normalization of Au ratios to immobile element ratios (3000 and 2400 mN areas).

Key: Squares: Au mean ratios divided by index element arithmetic mean ratio;  
 Diamonds: Au mean ratios divided by index element median ratio.

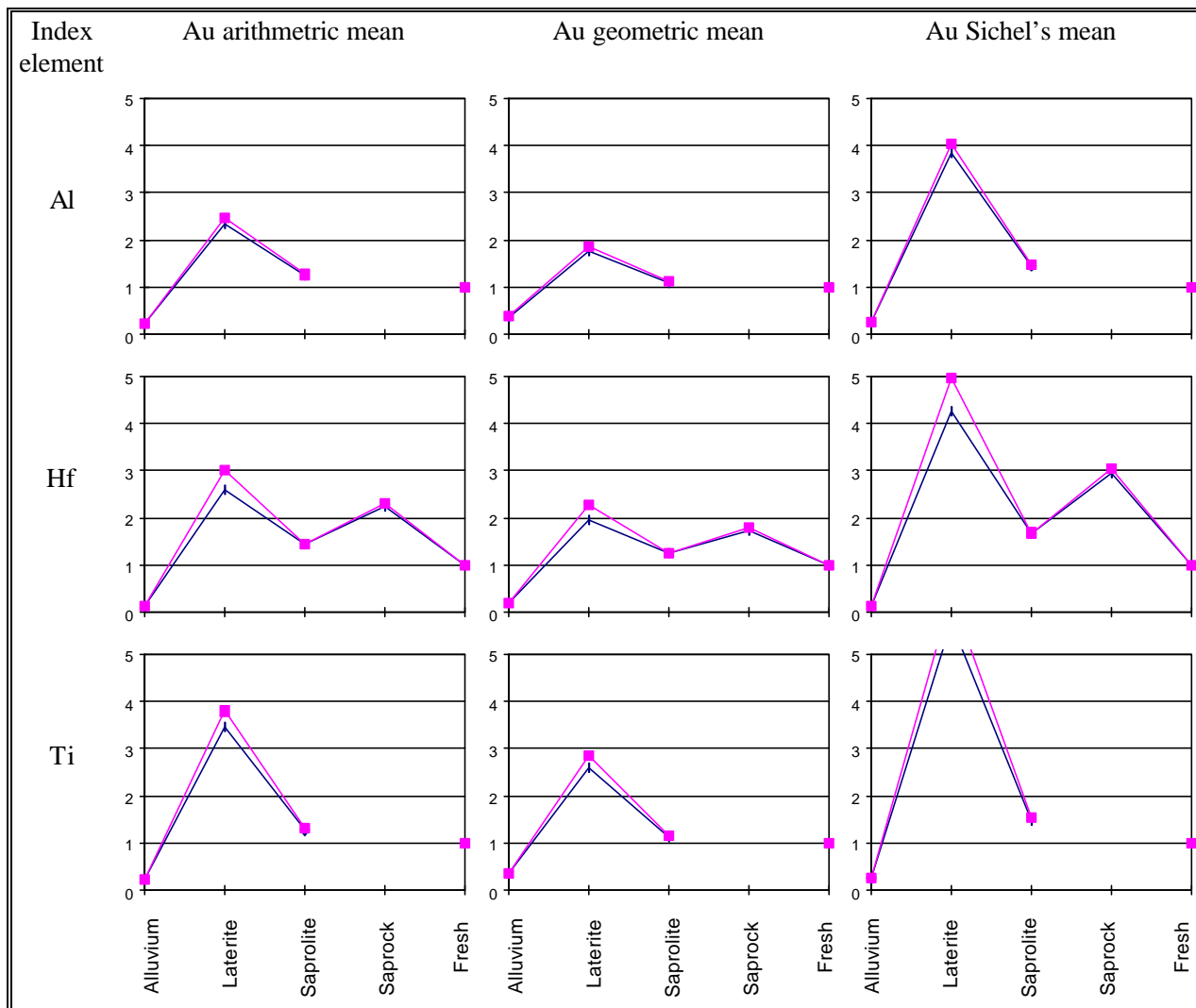


Figure 54: Normalization of Au ratios to immobile element ratios (800 and 0 mN areas).

Key: Squares: Au mean ratios divided by index element arithmetic mean ratio;  
 Diamonds: Au mean ratios divided by index element median ratio.

## 9 GOLD DISPERSION STUDIES

### 9.1 Gold selective extraction analysis

Selected samples from drill holes RC453, RC670/730 and RC218/326 were submitted for selective extraction experiments on pulverized and unpulverized subsamples. The objectives of these analyses are to indicate the proportion and degree of exposure of water-soluble Au, which is considered a very mobile source of Au, and iodide-soluble Au, which is a potentially mobile source of Au. Cyanide-soluble Au has also been determined as a measure of the total Au in the samples. Results for drill hole RC453 are given in Table 17, for drill hole RC670/730 in Table 18, and for drill hole RC218/326 in Table 19.

In the 3000 mN area, iodide-soluble gold in samples from the top of saprolite in drill hole RC453 represent more than 80% of the total Au, suggesting that it is preserved as chemical rather than particulate Au (Gray and Lintern, 1993). However, the percentage of iodide-soluble Au is significantly lower on all corresponding unpulverized samples, implying that pulverization has the effect of freeing soluble Au. At the top of saprolite, this can be explained by encapsulation of soluble Au by silicification as has been observed in siliceous horizons elsewhere in the northern Yilgarn (Gray and Lintern, 1993). Samples from drill hole RC670 also show a high proportion (27 to 72%) of iodide soluble Au at the top of saprolite. High percentages (30 to 50%) are also present in samples from the leached zone and lower saprolite, but they contain very low concentrations of cyanide-soluble Au (4 to 15 ppb). These data can be correlated to the Au distribution patterns in the 3000 mN area and suggest that the top of saprolite dominantly contains soluble Au of chemical origin, though the potential mobility may be restricted by silicification.

Table 17: Selective Au extraction of samples from drill hole RC453.

Depth (m)	Zone	Pulverised Samples					Unpulverised Samples					
		Soluble Au (ppb)			% soluble ( /cyanide )		Soluble Au (ppb)			% soluble ( /cyanide )		
		Water	Iodide	Cyanide	Water	Iodide	Water	Iodide	Cyanide	Water	Iodide	
4-5	Top of saprolite	2.0	79	92	2.1	86	1.2	28	70	1.8	40	
6-7		3.4	488	590	0.6	83	4.0	72	560	0.7	13	
8-10		1.3	17	21	6.4	81	0.8	2	25	3.1	9	
12-16	Leached		2.1	6		37		1	6		18	
51-53	Lower saprolite		6.7	13		53		4	11		41	
65-66		0.6	33	220	0.3	15	0.1	3	116	0.1	2	
68-70		24.9	456	20336	0.1	2						
71-72		0.3	3	38	0.8	7	0.2	0.4	25	0.6	2	
73-74				2.3	63		4		1	13		9
76-77		0.4	17	78	0.5	21	1.5	2	85	1.8	3	
82-84			0.9	14		7		0.5	24		3	
89-91	Saprock	2.7	142	499	0.5	28						
95-96		3.0	60	428	0.7	14	1.0	6	454	0.2	1	
97-98		50	262	13142	0.4	2	0.6	4	126	0.5	3	
99-100		19.6	298	2590	0.8	12	5.2	18	1586	0.3	1	

Table 18: Selective Au extraction of samples from drill hole RC670.

Depth (m)	Zone	Pulverised samples			Unpulverised samples		
		Iodide Au (ppb)	Cyanide Au (ppb)	Iodide Au (%)	Iodide Au (ppb)	Cyanide Au (ppb)	Iodide Au (%)
3-5	Top of saprolite	41	57	72	20	34	59
5-6		66	218	30	43	233	19
6-8		15	53	29	12	72	17
8-10		4	15	27	2	14	12
10-11	Leached zone	2	7	32	1	4	18
13-15		2	6	40	< 0.2	2	-
15-16		1	4	21	0.4	2	18
18-21		1	10	9	0.4	5	8
25-28		6	15	40	15	26	56
34-37	Lower saprolite	< 0.2	< 0.4	-	-0.2	-0.4	-
54-57		11	31	34	11	79	14
57-58		1	13	7	1	12	8
58-59		22	376	6	12	195	6

Table 19: Selective Au extraction of samples from drill hole RC218/326.

Hole	Depth (m)	Zone	Pulverised Samples					Unpulverised Samples				
			Soluble Au (ppb)			% soluble (/cyanide)		Soluble Au (ppb)			% soluble (/cyanide)	
			Water	Iodide	Cyanide	Water	Iodide	Water	Iodide	Cyanide	Water	Iodide
218	56-57	Pisolitic laterite		56	1476		4					
218	57-58		8.5	1236	4020	0.2	31	1.1	44	2400	0.1	2
218	59-60	Nodular laterite		64	393		16					
218	60-61		5.1	235	435	1.2	54	1.9	20	298	0.6	7
218	64-65		20.7	309	10949	0.2	3					
218	66-67			42.4	686		6					
218	67-68		4.0	326	603	0.7	54	0.9	10	254	0.4	4
218	68-69	Fe saprolite		20	212		10					
218	69-70		1.0	86	147	0.7	58	0.8	19	56	1.5	34
218	71-73		0.7	54	58	1.2	94	0.7	28	84	0.8	33
218	73-75				12	111		11				
326	91-95	Saprolite		2	66		3					
326	97-98		0.9	240	1176	0.1	20	0.5	23	835	0.1	3
326	99-100		2.3	250	1806	0.1	14	1.2	27	1607	0.1	2
326	101-102		0.2	26	65	0.2	40	0.1	3	62	0.2	4
326	103-104		1.3	23	60	2.2	38	0.2	3	14	1.6	23
326	105-106		0.5	44	204	0.2	22	0.2	26	494	0.0	5
326	107-108		2.9	375	1179	0.3	32	1.9	84	1268	0.2	7

In the 800 mN area, the percentage of iodide-soluble Au from drill hole RC218/326 is more variable, but generally less, than in the 3000 mN area. One pisolitic Au-rich laterite sample, with 4000 ppb of total (cyanide) Au, contains about 30% of iodide-soluble Au. Some samples of the nodular laterite and ferruginous saprolite also show some high percentage of iodide soluble Au but the distribution is more erratic than in the 3000 mN area. The pulverized samples similarly have lower concentrations of iodide-soluble Au. In this case, the soluble Au is probably encapsulated in the ferruginous fragments of the

saprolite and laterite zones, suggesting that most of the Au of chemical origin is related to the lateritization.

## 9.2 Lateral gold dispersion in the 3000 mN area

### 9.2.1 Gold distribution in the 3000 mN section

Lateral dispersion of Au has been investigated in the 3000 mN section (Figure 55). Gold dispersion is clearly most pronounced at the top of saprolite where the position of the main mineralized zone in the bedrock is also clearly defined by anomalous Au values of up to 1 ppm between 9700 and 9800 m E. The sharply contrasted W anomalies (up to 80 ppm) also effectively mark the position of the main mineralized zone in the bedrock. However, W values decrease to below detection laterally whereas the Au values remain relatively high, reaching about 100 ppb approximately 500 m to the west of the main mineralization (Figure 55). Gold values at the base of the alluvium are lower and do not indicate the position of the main mineralized zone. This is due to the allochthonous nature of the material, which does, nonetheless, contain locally reworked residual mineralized zones. Pedogenic effects near the unconformity are also likely to have contributed to this process. In the top metre of the alluvial cover, Au values are invariably below detection.

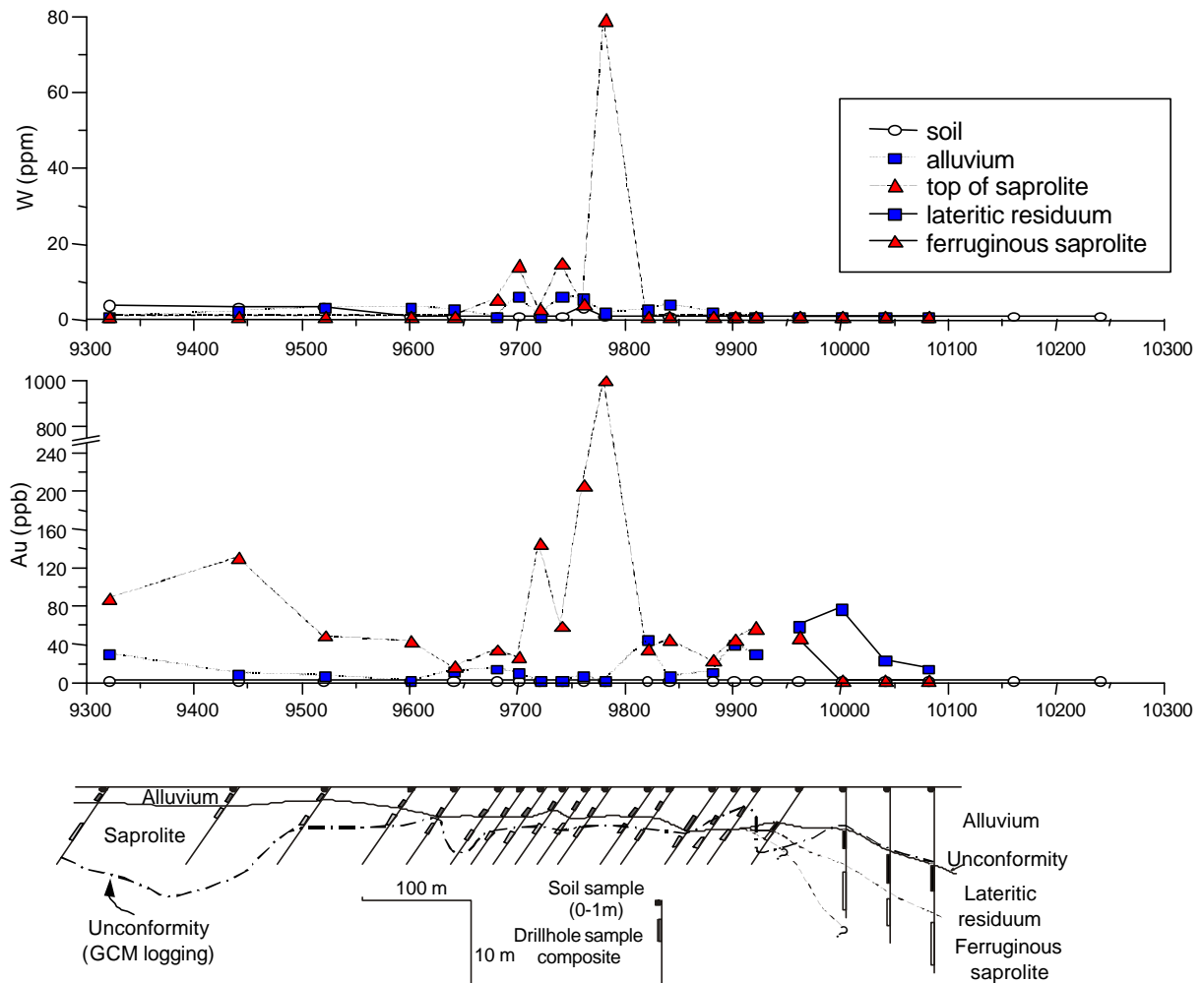


Figure 55: Distribution of Au and W in the traverse 3000 mN.

Lateritic residuum in the eastern portion of the 3000 mN section are anomalous in Au whereas the underlying ferruginous saprolite is barren and lacks W anomalies (Figure 55). The Au anomaly in the

lateritic residuum probably represents lateral dispersion similar to that described for the lateritic zone of the 800 mN area (see Section 9.3).

### 9.2.2 Grain size and selective extraction analyses

Grain size and selective extraction analyses were conducted in the 3000 mN area on three bulk samples from the top of saprolite over the main mineralized zone (drill holes RC731, 5-9m; RC453, 5-7 m; and RC457, 5m) plus one bulk sample over the dispersion halo (drill hole RC856, 5-7m). These samples were wet sieved into 5 grain size fractions and, where possible, plus another fraction containing recognizable ferruginous lithorelics. All fractions were weighted and analysed for Au, As, Sb, W, Fe and K. These results are shown in Table 20 and plotted for Au in Figure 56. Selected fractions from the RC856 and RC453 samples were submitted for selective Au extractions and the results are shown in Table 21 and in Figure 56.

Table 20: Concentrations of Au, As, Sb, W, Fe and K in size fractions from top of saprolite samples in the 3000 mN area. RC 856 is located in the halo and the others over the main mineralized zone.

Drill Hole	Depth (m)	Fraction	Weight (%)	Au (ppb)	As (ppm)	Sb (ppm)	W (ppm)	Fe (%)	K (%)
RC731	5-9	> 710 µm	43.8	214	5.0	3.0	31.3	13.6	0.2
		250-710 µm	13.9	170	4.4	1.8	18.2	8.8	0.5
		53-250 µm	14.4	151	4.5	1.8	19.9	8.3	0.4
		2-53 µm	0.1						
		< 2 µm	27.8	270	5.1	1.9	21.4	9.2	0.3
RC457	5	Lithorelics		344	2.5	1.7	5.1	10.4	0.4
		> 710 µm	49.5	250	6.7	1.2	3.0	7.4	0.5
		250-710 µm	20.8	153	6.1	0.9	3.7	6.0	0.5
		53-250 µm	11.7	140	6.2	1.0	3.8	6.5	0.5
		2-53 µm	2.1	244	5.6	1.5	4.6	10.0	0.5
< 2 µm	15.9	236	5.0	0.8	<2	5.2	0.5		
RC453	5-7	Lithorelics		176	32.4	4.9	<2	7.9	0.6
		> 710 µm	43.2	220	22.8	2.8	3.8	6.1	0.6
		250-710 µm	11.4	195	19.5	2.1	2.6	5.3	0.7
		53-250 µm	12.8	733	17.8	2.0	<2	5.3	0.6
		2-53 µm	9.1	271	23.7	3.0	4.0	6.8	0.8
< 2 µm	23.6	223	8.9	0.9	<2	3.6	0.6		
RC856	5-7	Lithorelics		93	10.8	5.3	<2	16.4	0.3
		> 710 µm	30.5	79	14.6	4.2	<2	14.1	-0.2
		250-710 µm	15.7	72	12.5	3.2	<2	12.3	0.3
		53-250 µm	17.0	100	11.7	3.1	<2	12.1	0.3
		2-53 µm	10.5	99	10.1	3.6	<2	14.3	0.3
< 2 µm	26.3	66	6.8	1.2	<2	7.4	0.2		

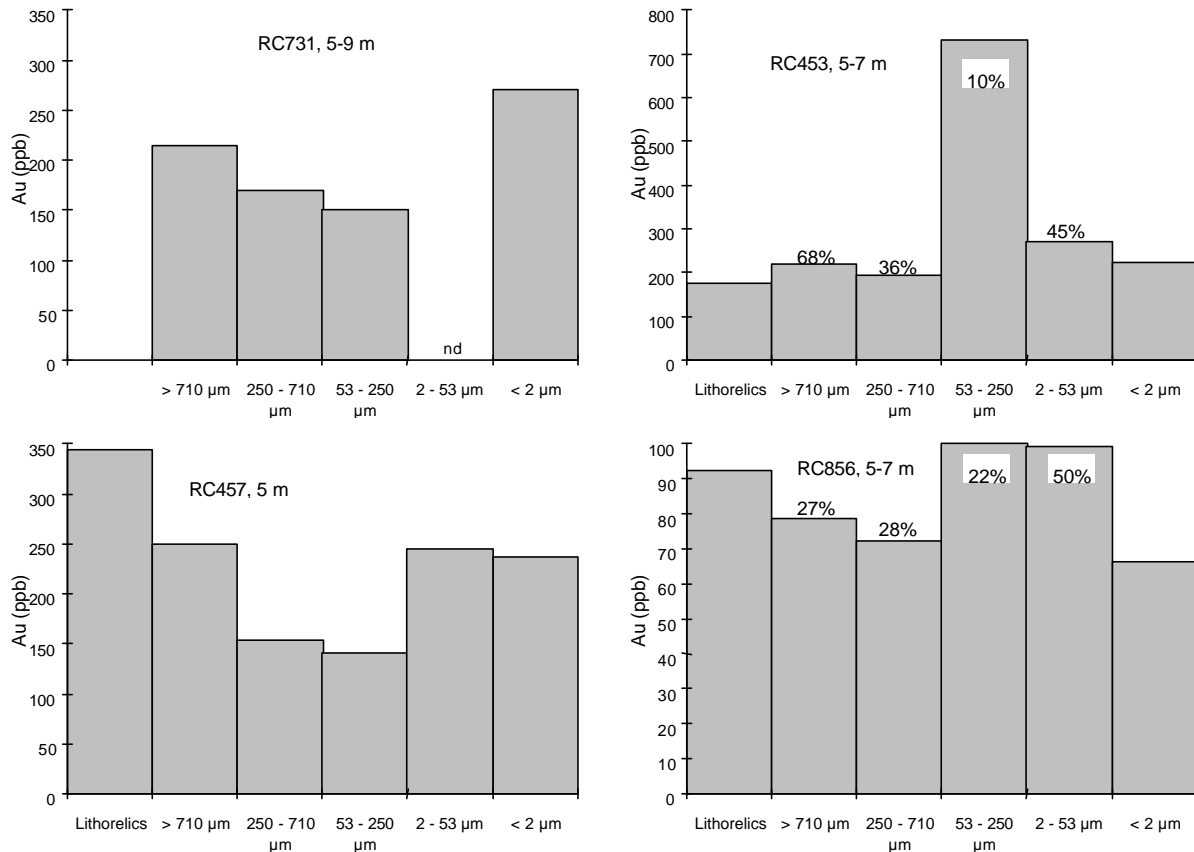


Figure 56: Gold distribution in different size fractions from drill holes in the 3000 mN area (nd - not determined). Where analysed, iodide-soluble Au (as % of cyanide-soluble Au) is shown above the Au content bar.

Gold seems to be nearly equally distributed among the fractions of samples RC453 (180-230 ppb) and RC856 (75-100 ppb) except in the 53-250  $\mu\text{m}$  fraction of sample RC453 (733 ppb). This is probably a nugget effect, since results of selective extraction show that only 11% of the Au is iodide-soluble (Table 21), implying the dominance of particulate Au in that fraction. Iodide-soluble Au in the other analysed fractions varies between 36 to 68%. A similar range of variation (22 to 50%) is observed in the dispersion halo (sample RC856). These results confirm that the enriched top of saprolite in the 3000 mN area has a significant proportion of iodide-soluble Au, due to chemical reprecipitation, and that this reprecipitation is not concentrated in any particular size fraction. The lack of any detectable W in the RC856 sample also suggests that the laterally dispersed anomaly is dominantly chemical.

Iron, too, tends to be relatively equally distributed among the finer size fractions, but concentration increases in the coarser fractions, including that containing highly ferruginous lithorelics. Antimony and As follow Fe quite closely. Potassium is also quite equally distributed among the fractions, despite the low concentrations, and reflects the presence of resistant micas.

Table 21: Selective Au extraction in grain size fractions of samples from the 3000 and 800 mN area.

Area	Drill hole	Zone depth (m)	Description	Iodide Au (ppb)	Cyanide Au (ppb)	Iodide Au / cyanide Au (%)
800 mN	218	Pisolitic (56-57)	> 710 (mag)	343	1111	31
			> 710 (non-mag)	103	695	15
			2-53 $\mu\text{m}$	336	2076	16
		Nodular (61-68)	> 710 $\mu\text{m}$	140	1512	9
	53-250 $\mu\text{m}$		27	246	11	
	326	Pisolitic (61-62)	2-53 $\mu\text{m}$	39	907	4
			> 710 (mag)	33	175	19
	> 710 (non-mag)		12	108	11	
	Nodular (64-66)	2-53 $\mu\text{m}$	7	130	6	
		> 710 $\mu\text{m}$	69	809	9	
	219	Pisolitic (65-66)	2-53 $\mu\text{m}$	14	191	7
			> 710 (mag)	22	274	8
	244	Nodular (68-70)	53-250 $\mu\text{m}$	4	644	1
			> 710 $\mu\text{m}$	64	1560	4
Pisolitic (74-76)		53-250 $\mu\text{m}$	50	3158	2	
		> 710 (mag)	27	451	6	
534	Nodular (81-83)	53-250 $\mu\text{m}$	12	62	20	
		> 710 $\mu\text{m}$	15	643	2	
	Pisolitic (86-87)	53-250 $\mu\text{m}$	7	154	5	
		> 710 (mag)	53	1026	5	
Nodular (89-90)	> 710 (non-mag)	63	276	23		
	53-250 $\mu\text{m}$	24	452	5		
3000 mN	453	Top of saprolite (5-7)	53-250 $\mu\text{m}$	2	22	11
			2-53 $\mu\text{m}$	4	77	5
			> 710 $\mu\text{m}$	124	181	68
			250-710 $\mu\text{m}$	65	181	36
	856	Top of saprolite (5-7)	53-250 $\mu\text{m}$	53	505	11
			2-53 $\mu\text{m}$	160	352	45
			> 710 $\mu\text{m}$	22	81	27
			250-710 $\mu\text{m}$	17	61	29
Nodular (81-83)	53-250 $\mu\text{m}$	19	85	22		
	2-53 $\mu\text{m}$	48	96	50		

### 9.3 Lateral gold dispersion in the 800 mN area

Lateral Au dispersion has been investigated in the Au-enriched lateritic zone of the 800 mN section using selective extraction coupled with grain size analysis. Twelve bulk samples were collected from drill holes RC218; RC326; RC219, approximately overlying the main mineralized zone and from drill holes RC244; RC245 and RC534 to the east of the main mineralized zone. In every drill hole, two samples were selected to represent the pisolitic and nodular zones (Figure 11). All samples were wet sieved into 5 size fractions, plus one additional magnetic fraction with pisoliths obtained from the pisolitic laterite. All fractions were weighed and analysed for Au, As, Sb, W, Fe and K. These results are shown in Table 22 and plotted in Figure 57 for the pisolitic laterite samples, and in Table 23 and Figure 58 for the nodular laterite samples. Selected fractions from ten of these samples were also submitted to selective Au extractions. These results are shown in Table 21, Figures 57 and 58 for pisolitic laterite and nodular laterite samples. The results obtained indicate the following:

- i. Gold concentrations in the nodular zone are lower in the samples to the east of the main mineralized zone, compared to those over the main mineralized zone. Conversely, in the pisolitic zone, the Au concentrations remain high to the east of the main mineralized zone. This situation is similar to that encountered in the eastern portion of the 3000 mN area and confirms that the Au halo in the pisolitic zone is more pronounced.
- ii. Gold concentration in the pisolitic zone is higher in the coarse fractions, which contain magnetic pisoliths. The exceptions in samples from drill holes RC218 and RC245 are due to a much higher Au concentration in all the fractions between 250 and 2  $\mu\text{m}$ , probably due to the presence of free particulate Au in that size range. The Au in the coarser fractions is locked within pisoliths.
- iii. The proportion of iodide-soluble Au is generally lower than in the 3000 mN area but relatively higher (up to 30%) in the coarser fraction of the pisolitic zone which indicates some contribution of chemical reprecipitation of Au, probably related to lateritization.

The pisolitic laterite zone presumably represents an ancient surface, which was probably locally reworked, resulting in lateritic gravel. If so, then the mechanical transport of the pisoliths is only local since yellow cutans are still preserved on most of them. Alternatively, the pisoliths possibly formed in situ. The stronger Au anomaly in the pisolitic zone to the east of the mineralization, compared to the nodular zone, suggests that the Au is transported. Clastic transport of Au could have occurred prior to or during the formation of the pisoliths or the Au could have been transported within the pisoliths.

Tungsten values are generally low. However, to the east of the main mineralized zone, in nodular and pisolitic laterite samples from drill holes RC245 and RC534, tungsten values are up to 40 ppm. These higher values in the nodular laterite, however, do not coincide with higher Au values, suggesting that the Au anomalies in this area are not residual.

The distribution of As and Sb is associated with Fe in all the size fractions and does not specifically indicate the position of the mineralized zone. Potassium is below detection, which reflects the high degree of weathering of these samples.

Table 22: Concentrations of Au, As, Sb, W, Fe and K in grain size fractions from drill hole samples of pisolitic laterite from the 800 mN traverse (see Figure 11 for drill hole location).

Drill Hole	Depth (m)	Fraction (µm)	Weight (%)	Au (ppb)	As (ppm)	Sb (ppm)	W (ppm)	Fe (%)	K (%)	
RC218	56-57	> 710 (mag)	23.9	1120	135	20	11	46.2	< 0.2	
		> 710 (non-mag)	76.1	666	93	16	5	36.7	< 0.2	
		250-710	4.7	725	105	14	7	38.2	< 0.2	
		53-250	3.0	3080	89	12	< 4	30.5	< 0.2	
		2-53	2.0	3400	85	12	< 6	29.6	< 0.2	
		< 2	16.6	342	29	3	4	10.0	< 0.2	
RC326	61-62	> 710 (mag)	39.2	382	107	18	10	46.1	< 0.2	
		> 710 (non-mag)	60.8	92	78	11	5	33.3	< 0.2	
		250-710	7.2	61	88	11	6	32.9	< 0.2	
		53-250	7.2	55	75	9	< 6	26.7	< 0.2	
		2-53	5.0	108	64	8	< 6	22.1	< 0.2	
		< 2	30.2	24	29	3	3	9.5	< 0.2	
RC219	65-66	> 710 (mag)	47.0	137	99	18	8	47.0	< 0.2	
		> 710 (non-mag)	53.0	33	77	11	7	33.7	< 0.2	
		250-710	9.0	93	68	10	6	29.0	< 0.2	
		53-250	8.9	19	55	7	7	22.1	< 0.2	
		2-53								
		< 2	41.7	29	21	3	5	8.9	< 0.2	
RC244	74-76	> 710 (mag)	21.0	386	80	10	13	39.5	< 0.2	
		> 710 (non-mag)	79.0	109	65	7	10	29.4	< 0.2	
		250-710	6.9	159	59	6	8	24.8	< 0.2	
		53-250	6.8	68	41	4	8	17.5	0.3	
		2- 53	0.1							
		< 2	59.2	51	8	2	6	5.8	< 0.2	
RC245	82	> 710 (mag)	27.6	115	121	14	23	48.5	< 0.2	
		> 710 (non-mag)	72.4	1080	100	12	26	33.8	< 0.2	
		250-710	3.1	310	86	10	17	27.5	< 0.2	
		53-250	4.2	5480	69	8	13	20.7	< 0.2	
		2-53	0.9	24400	68	9	18	19.4	< 0.2	
		< 2	71.3	221	24	4	9	9.9	< 0.2	
RC534	86-87	> 710 (mag)	15.7	1630	97	13	23	49.2	< 0.2	
		> 710 (non-mag)	84.3	235	87	9	21	35.5	< 0.2	
		250-710	3.1	122	67	7	18	29.7	< 0.2	
		53-250	3.9	335	43	5	12	21.3	< 0.2	
		2-53	0.1							
		< 2	71.5	160	11	3	11	7.5	0.3	

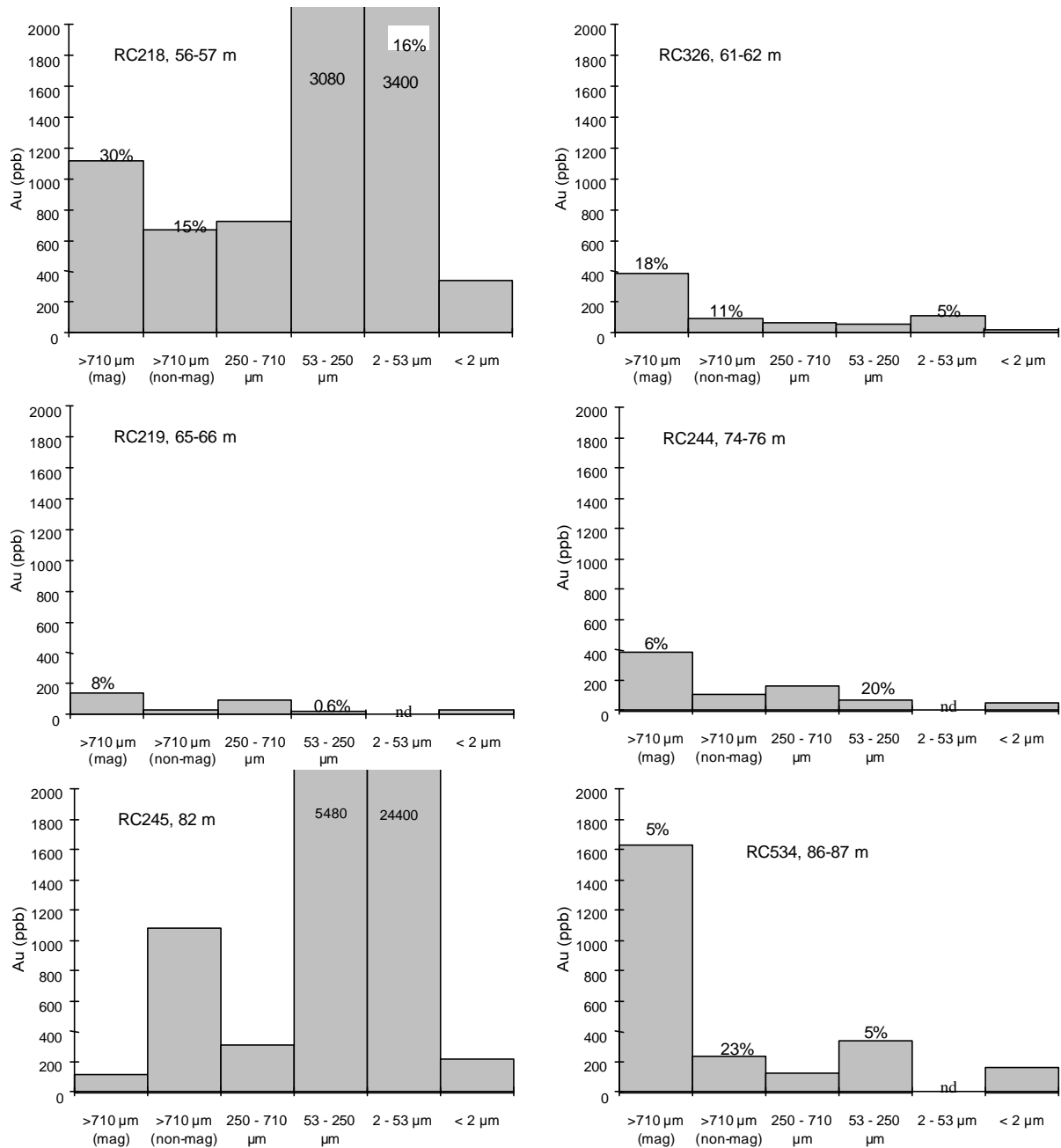


Figure 57: Gold distribution in size fractions of pisolitic laterite samples from the 800 mN traverse (nd - not determined). Where analysed, iodide-soluble Au (as % of cyanide-soluble Au) is shown above the Au content bar.

Table 23: Concentrations of Au, As, Sb, W, Fe and K in grain size fractions from drill hole samples of nodular laterite from the 800 mN traverse (see Figure 11 for drill hole location).

Drill Hole	Depth (m)	Fraction (µm)	Weight (%)	Au (ppb)	As (ppm)	Sb (ppm)	W (ppm)	Fe (%)	K (%)
RC218	61-68	> 710	24.5	904	35	4	5	34	< 0.2
		250-710	7.8	582	51	4	5	30	< 0.2
		53-250	13.4	399	41	3	< 6	19	< 0.5
		2-53	0.8	977	32	3	< 6	11	< 1
		< 2	53.4	202	19	2	5	9	< 0.2
RC326	64-66	> 710	47.0	756	53	4	5	30	< 0.2
		250-710	4.0	256	51	3	4	27	< 0.2
		53-250	5.8	132	27	1	< 6	14	< 1
		2-53	4.4	188	17	2	< 2	8	< 0.2
		< 2	38.9	71	22	1	4	11	< 0.2
RC219	68-70	> 710	25.9	1910	17	5	5	24	< 0.2
		250-710	5.7	528	18	3	< 2	24	< 0.2
		53-250	5.7	1990	14	3	< 2	18	< 0.2
		2-53							
		< 2	60.5	67	4	2	< 2	8	< 0.2
RC244	81-83	> 710	16.6	674	58	7	6	24	< 0.2
		250-710	4.7	234	47	5	5	20	< 0.2
		53-250	6.7	328	40	5	5	17	< 0.2
		2-53	0.2						
		< 2	71.8	30	13	3	5	6	< 0.2
RC245	85-90	> 710	20.0	23	87	13	39	33	< 0.2
		250-710	7.7	43	84	10	34	25	< 0.2
		53-250	11.9	17	75	9	25	22	0.2
		2-53	0.5	50	63	8	23	18	< 0.2
		< 2	60.0	16	40	4	14	10	0.2
RC534	89-90	> 710	8.3	< 5	17	3	12	24	< 0.2
		250-710	2.6	10	20	3	12	17	< 0.2
		53-250	5.5	50	15	3	11	14	< 0.2
		2-53	4.1	55	9	3	8	8	< 0.2
		< 2	79.4	11	8	2	7	6	< 0.2

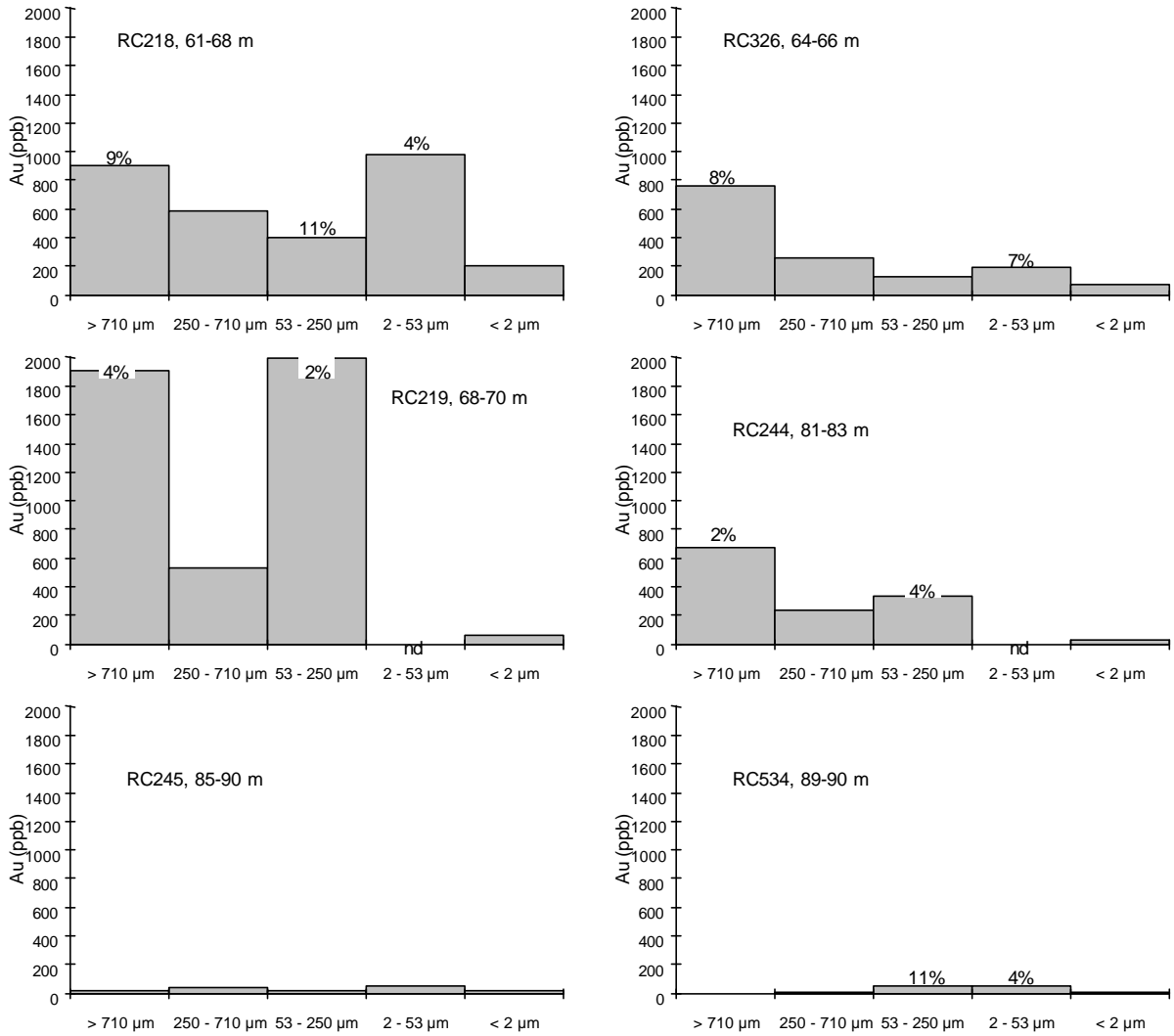


Figure 58: Gold distribution in size fractions of nodular laterite samples from the 800 mN traverse (nd - not determined). Where analysed, iodide-soluble Au (as % of cyanide-soluble Au) is shown above the Au content bar.

## 10 CHARACTERISTICS OF PARTICULATE GOLD

### 10.1 Mineral composition of heavy concentrates

Fourteen bulk samples from the regolith plus two pulp samples from primary mineralization were submitted to heavy mineral and gold grains separation for detailed mineralogical analysis (see Section 2.5). The mineralogy of the heavy concentrates is summarized in Table 24.

Table 24: Mineral composition of heavy concentrates from bulk samples, Mt Joel

Sample	Zone	Abundant	Moderate	Minor	Trace
RC218/65	L	FeOx		Bast, Bar	Zrn
RC731/5-9	TS	FeOx		Leuc	Bar
RC216/65	FS	FeOx		Bar, Zrn, Leuc	Garn?, Py, Mal?
RC488/25	S	Mgt	FeOx	Bar, Zrn	Leuc
RC454/41	S	FeOx, Mgt		Zrn	MnOx, Py
RC453/69-70	LS	FeOx		Leuc, Zrn	
RC217/117	LS	FeOx, Mgt	Bar, Leuc		Py, Mica
RC670/85-86	LS	Leuc, FeOx	Mgt	Zrn	Py
RC216/103	LS	FeOx	Bar, Mgt	Rut, Leuc, Zrn,	Py
RC670/96-97	SR	Py	FeOx, Mgt	Leuc	Zrn, Tour
RC549/92-93	SR	Mgt, FeOx	Py	Zrn, Mica	Tour, Rut
RC730/97-101	SR	Py, Mgt	FeOx	Mica, Bar, Zrn,	Leuc, MnOx, Rut
RC453/90-91	SR	FeOx, Mgt	Hol	Zrn,	Mica, Bar, Rut, Garn?
RC455/115-119	F	Py		Bar	Zrn, Ilm
GD 272195	F	Py		Px, Mgt	
GD 272215	F	Py		Px, Mgt	Bar

Zones: L - nodular laterite; TS - top of saprolite; FS - ferruginous saprolite; S - saprolite; LS - lower saprolite; SR - saprock; F - fresh rock

Minerals: Bar - barite; Bast - bastnesite; FeOx - iron oxides; Garn - garnet; Hol - hollandite; Leuc - leucoxene; Mal - malachite; Mgt - magnetite; MnOx - manganese oxides; Px - pyroxene; Py - pyrite; Rut - rutile; Tour - tourmaline; Zrn - zircon; Ilm - ilmenite.

In the primary mineralization, pyrite is the dominant heavy mineral, occurring as pristine cubic crystals and anhedral grains up to 3 mm. Barite, magnetite and pyroxenes are present in lesser amounts. In the lower saprolite, the pyrite abundance declines and the principal minerals are magnetite, Fe oxides with minor amounts of Mn oxides, zircon and barite. Manganese oxides in the sample RC453/90-91 contain some Ba and K, suggesting hollandite or possibly romanechite. In the middle and the upper saprolite, Fe oxides and magnetite prevail, with pyrite only occurring in trace amounts. Iron oxides form pseudomorphs after pyrite crystals and also occur as botryoidal colloform aggregates. In the lateritic residuum (RC218/65) some unusual small white spherules were observed. Cerium and La, with traces of Al and Si, were detected by energy dispersion X-ray system (EDXS). This mineral was identified by XRD as Ce, La carbonate - bastnesite.

## 10.2 Characteristics of gold grains

### 10.2.1 Size

The length of Au grains is used as their size characteristic. The grains were sorted into 12 categories as shown for each sample in Tables 25 and 26, and as histograms in Figures 59 to 63.

Table 25: Size distribution of gold grains collected from bulk samples from Mt Joel.

Sample	Zone	Au (ppm)	No. grains	Size (µm)											
				<10	10-20	20-30	30-40	40-50	<50	50-100	100-150	150-200	200-250	250-300	>300
RC218/65	L	6.63	331	3	56	78	59	45	241	68	20	1	1	0	0
RC731/5-9	TS	0.22	270	1	30	66	69	58	224	37	6	3	0	0	0
RC216/65	FS	3.13	134	1	4	7	12	19	43	64	16	8	2	1	0
RC488/25	S	1.83	55	0	17	14	14	2	47	8	0	0	0	0	0
RC454/41	S	0.84	76	7	15	25	10	3	60	16	0	0	0	0	0
RC453/69-70	LS	16.93	385	22	66	81	48	34	251	53	23	8	6	11	33
RC217/117	LS	1.23	104	0	2	22	29	18	71	27	5	1	0	0	0
RC670/85-86	LS	2.27	288	1	18	72	69	48	208	78	2	0	0	0	0
RC216/103	LS	4.16	305	2	22	56	71	50	199	75	28	2	0	0	0
RC670/96-97	SR	2.14	286	20	92	84	43	30	269	15	1	0	1	0	0
RC549/92-93	SR	2.39	197	5	14	43	53	27	142	49	4	2	0	0	0
RC730/97-101	SR	1.66	261	3	42	85	56	35	221	32	4	2	2	0	0
RC453/90-91	SR	1.54	255	1	15	20	43	57	136	98	14	3	3	0	1
RC455/115-119	F	7.03	312	1	20	58	42	51	172	75	31	19	5	6	4
GD 272195	F	4.43	382	7	27	70	50	52	206	147	18	5	5	1	0
GD 272215	F	5.1	264	2	4	22	34	29	91	99	41	19	8	3	3

Zones: L - nodular laterite; TS - top of saprolite; FS - ferruginous saprolite; S - saprolite; LS - lower saprolite; SR - saprock; F - fresh rock

Table 26: Size distribution (% of total) of gold grains collected from bulk samples from Mt Joel.

Sample	Zone	Au (ppm)	Size ( $\mu\text{m}$ )											
			< 10	10-20	20-30	30-40	40-50	< 50	50-100	100-150	150-200	200-250	250-300	> 300
RC218/65	L	6.63	0.9	16.9	23.6	17.8	13.6	72.8	20.5	6	0.3	0.3	0	0
RC731/5-9	TS	0.22	0.4	11.1	24.4	25.6	21.5	83	13.7	2.2	1.1	0	0	0
RC216/65	FS	3.13	0.7	3	5.2	9	14.2	32.1	47.8	11.9	6	1.5	0.7	0
RC488/25	S	1.83	0	30.9	25.5	25.5	3.6	85.5	14.5	0	0	0	0	0
RC454/41	S	0.84	9.2	19.7	32.9	13.2	4	79	21	0	0	0	0	0
RC453/69-70	LS	16.93	5.7	17.2	21	12.5	8.8	65.2	13.8	6	2.1	1.6	2.9	8.6
RC217/117	LS	1.23	0	1.9	21.2	27.9	17.3	68.2	26	4.8	1	0	0	0
RC670/85-86	LS	2.27	0.3	6.2	25	24	16.7	72.2	27.1	0.7	0	0	0	0
RC216/103	LS	4.16	0.6	7.2	18.4	22.6	16.4	65.2	24.6	9.2	0.7	0	0	0.3
RC670/96-97	SR	2.14	7	32.1	29.4	15	10.5	94	5.2	0.4	0	0.4	0	0
RC730/97-101	SR	1.66	1.1	16.1	32.6	21.5	13.4	84.7	12.3	1.5	0.8	0.8	0	0
RC549/92-93	SR	2.39	2.6	7.1	21.8	26.9	13.7	72.1	24.9	2	1	0	0	0
RC453/90-91	SR	1.54	0.4	5.9	7.8	16.9	22.3	53.3	38.4	5.5	1.2	1.2	0	0.4
RC455/115-119	F	7.03	0.3	6.4	18.6	13.5	16.4	55.2	24.2	9.8	6.3	1.4	1.8	1.3
GD 272215	F	5.1	0.8	1.5	8.3	12.9	11	34.5	37.5	15.5	7.2	3	1.1	1.1
GD 272195	F	4.43	1.8	7.1	18.3	13.1	13.6	53.9	38.5	4.7	1.3	1.3	0.3	0

Zones: L - nodular laterite; TS - top of saprolite; FS - ferruginous saprolite; S - saprolite;  
LS - lower saprolite; SR - saprock; F - fresh rock

### 10.2.2 Morphology.

Six different morphologies of Au grains were recognized:

- i. Crystals: euhedral-subhedral combinations of cubes and octahedra, pseudo-hexagonal and trigonal tabular, prismatic and elongate crystals (Photos 13-18, 28-34).
- ii. Round: sub-spherical particles (Photos 8, 35).
- iii. Equant: anhedral-subhedral equidimensional particles (Photo 7).
- iv. Irregular: anhedral, xenomorphic, commonly very complex grains (Photos 2, 4).
- v. Flat: anhedral sheets, plates and scales (Photos 5, 6).
- vi. Elongate: anhedral grains, commonly with very rough hackly surfaces (Photos 11, 12).

The morphology of the different grain types is summarized in Table 27.

Table 27: Shape distribution (in % of total) of gold grains collected from bulk samples from Mt Joel.

Sample	Zone	Octa- hedra	Cube	Tabular crystal	Prismati c crystal	Crystal aggregate	Total crystals	Round	Equant	Irreg- ular	Flat	Elon- gate
RC218/65	L	4.5	1.5	7.6	12.4	7.6	33.5	14.2	19.6	30.5	0.3	1.8
RC731/5-9	TS	1.5	0.4	8.5	3	11.8	25.2	23.3	18.9	29.6	1.5	1.5
RC216/65	FS	5.2	0.7	3	4.5	4.5	17.9	1.5	10.5	68.7	0.7	0.7
RC488/25	S	3.6	0	29.1	27.3	25.5	85.5	5.4	7.3	0	1.8	0
RC454/41	S	7.9	1.3	19.7	19.7	6.6	55.3	13.2	11.8	17.1	1.3	1.3
RC453/69-70	LS	2.1	0.3	4.2	6	5.7	18.2	16.1	26.2	37.9	0	1.6
RC217/117	LS	1	0	6.7	5.9	5.9	20.2	10.6	22.1	47.1	0	1
RC670/85-86	LS	0.7	0.3	3.5	3.5	7.3	15.3	7.3	35.4	34.7	4.9	2.4
RC216/103	LS	20	0.7	11.5	9.8	6.6	48.5	8.5	7.2	34.4	0.3	1
RC670/96-97	SR	4.2	0.7	14	12.2	4.6	35.7	13.6	24.1	16.1	8.7	1.8
RC549/92-93	SR	4.6	0	10.1	7.1	6.6	28.4	9.6	20.3	33.5	6.1	2
RC730/97-101	SR	3.4	0	5.4	5.4	6.5	20.7	18	21.5	38.7	0.4	0.8
RC453/90-91	SR	3.1	0.4	0.8	3.1	1.6	9	19.6	26.3	38.4	0	6.7
RC455/115- 119	F	0.2	1.6	0.2	1	0.6	3	7.7	18	66.9	0.2	3.7
GD 272195	F	0.3	0.8	0.3	1.1	0	2.4	3.1	17.5	72.8	0.8	3.4
GD 272215	F	1.1	0	0	0.4	0	1.5	0.4	16.9	72.4	0	10

Zones: L - nodular laterite; TS - top of saprolite; FS - ferruginous saprolite; S - saprolite;  
LS - lower saprolite; SR - saprock; F - fresh rock

### 10.2.3 Composition.

The composition of Au particles was firstly established by SEM and an energy dispersion X-ray system (EDXS) but due to surface effect of the unpolished grain surfaces, the data obtained are, at best, semi-quantitative. The majority of Au grains contained no Ag or other elements at the detection limit of the EDXS, estimated between 0.1 and 1%. However selected Au grains were analysed quantitatively by electron microprobe (see Section 2.5). The data obtained show, Al, As, Cl, I, Te and Zn concentrations below detection limits, and an analysis for Br had some analytical problems. The Au compositions are shown in Tables 28 to 30. The data in the tables of results have not been corrected for matrix effects and there is some analytical uncertainty, possibly as high as 20%.

### 10.3 Gold grains in the primary mineralization

Gold grains in the primary mineralization are small, with 72 to 92% being less than 100  $\mu\text{m}$  in diameter, and only 0.3-3.1% exceeding 250  $\mu\text{m}$  (Table 26, Figure 59). Gold particles less than 50  $\mu\text{m}$  prevail.

The shapes of the Au grains in three bulk samples from the primary mineralization are very similar: most grains (67-73%) are irregular, xenomorphic, or with unclear crystal faces. There are fewer equant and elongate grains (17-18% and 3.4-10%), and round, flat particles and crystal morphologies are rarely observed. The surfaces of the primary grains are very rough, with numerous pits, cavities, fractures, scratches and imprints from adjacent minerals. Some of the scratches are due to mechanical damage during drilling and sample preparation.

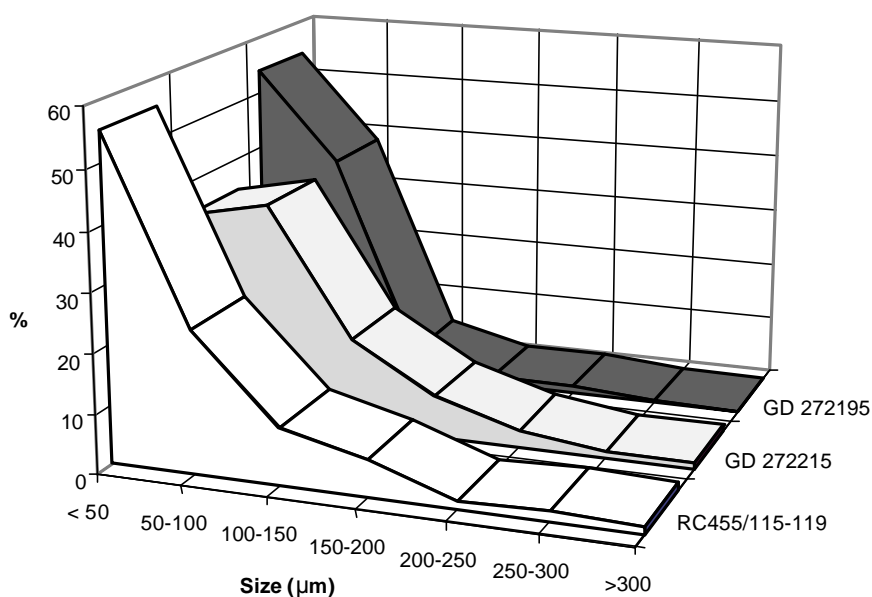


Figure 59: Size distribution of gold grains in the primary mineralization (%).

The principal minerals associated with Au in primary mineralization are pyrite, with lesser quartz and muscovite. Pyrite forms intergrowths with Au, preferentially as cubes or cubo-octahedral crystals, at the surface of Au grains (Photo 1, 2, 4), with some as more complex aggregates (Photo 3). Anhedral quartz grains were observed in the cavities at the surface of irregular Au particles and also as small inclusions in Au grains. Some grains are complex intergrowths of flakes of muscovite and small Au plates (Photo 5, 6).

Primary Au has relatively low Ag contents, ranging from 1.5 to 5.0% with average 2.7%. Also, Au contains detectable amounts of Si (280-630 ppm), S (200-380 ppm), Cu (<40-300 ppm) and Fe (70-250 ppm). Chlorine and I abundances are below detection limits (Table 28).

Table 28: Electron microprobe analyses of Au from the primary mineralization (ppm).

Element	Mean	Std. Dev.	Min	Max
Ag	27253	89.7	15129	50158
Cu	182	13.5	<40	303
Fe	135	10.9	66	254
Si	415	5.0	283	636
S	312	11.4	202	378

Std. Dev. - Standard deviation, based on counting statistics

#### 10.4 Gold grains in the saprock

The Au grains in the saprock are smaller than in the primary mineralization, with 92 to 99% of the grains less than 100 µm (Table 26, Figure 60). In some samples, only fine-grained (< 50 µm) Au was observed (e.g., RC670/96-97). The shape distributions (Table 27) are very different to that in the primary mineralization: the proportion of irregular particles reduces from 67-73% to 16-39%, and the proportion of crystals, equant and round grains increases to 73%.

All Au crystals in the saprock are fine-grained (< 50 µm). The most common crystal forms are pseudo-hexagonal and trigonal thick tabular and prismatic crystals, which exhibit a range of distorted habits with combinations of cubic and octahedral faces. Less commonly, cubes, octahedra and elongate crystals occur. Some Au crystals form clusters, joined at their edges. The Au crystals are mainly

pristine and uncorroded, having smooth surfaces and sharp edges; some have xenomorphic imprints from adjacent minerals. Patchy films of Fe oxides or clay minerals are observed at the surface of some crystals. Gold crystals contain no Ag at the detection limit of the EDX.

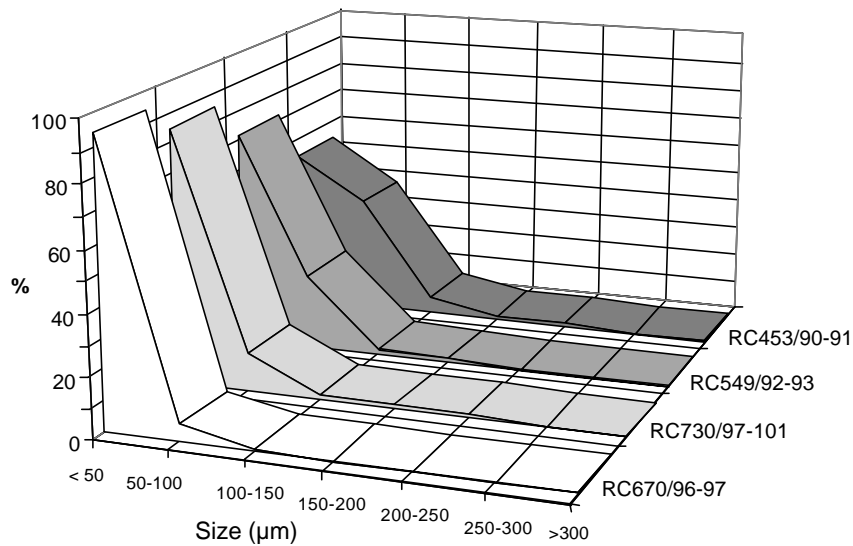


Figure 60: Size distribution of gold grains in the saprock (%).

The sharp difference in morphology and composition of Au crystals from primary grains suggests their supergene origin. Probably some of the pure round and equant grains are also secondary, but this is difficult to prove.

### 10.5 Gold grains in the lower saprolite

The size of Au grains is still small in the lower saprolite, but slightly increased compared to the saprock: the mean proportion of the grains  $> 50 \mu\text{m}$  increasing from 24 to 32% (Table 26). One sample (RC453/69-70) has a high abundance of coarse gold: 13% of Au grains are from 200 to 600  $\mu\text{m}$  in diameter (Table 26, Figure 61).

The proportion of Au crystals varies within the wide limits in this zone, ranging from 15 to 49%. Gold crystals are preferentially euhedral (Photos 13 to 15), less commonly subhedral with inclusions of quartz grains or aggregates of Fe oxides indicating growth in confined locations (Photos 16 to 18, 21 to 23). Pristine crystals prevail, with few etched crystals observed; corrosion is probably due to leaching of adjacent grains to Au (Photos 19 to 20). In contrast, irregular Au grains are mainly corroded (Photos 24 to 25). Many of the grains have porous texture with numerous “channels” near the surface and several have thin, patchy high fineness rims, from which Ag has been leached (Photo 26). Coarse irregular grains from the sample RC453/69-70 contain numerous small quartz grains as inclusions, suggesting a primary origin.

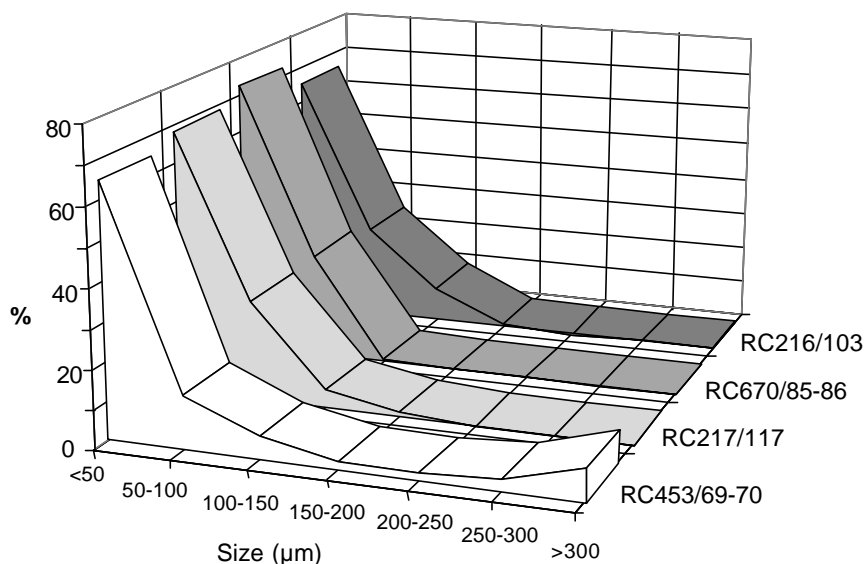


Figure 61: Size distribution of gold grains in the lower saprolite (%).

Gold crystals are very distinct in composition from irregular grains. The latter contain detectable amounts of Ag and are presumably residual (Table 29). The crystals and some of equant grains are of high fineness, all analyses show Ag values below detection limit which ranges from 40 to 90 ppm (Table 30). The supergene gold crystals contain Fe (<16-7700 ppm), Si (130-1240 ppm) and S (<16-370 ppm), with low Cu abundances. Chlorine and I values are below detection limits. SEM detected some traces of Cl at the surface of Au crystals, but this may be an artefact, due to handling or other contamination.

Table 29: Electron microprobe analyses of the residual Au from the regolith (ppm).

Element	Zone	No.	Mean	Std. Dev.	Min	Max
Ag	TS	13	25949	87	12699	47765
	S	5	32486	48	226	59158
	LS	1	16742	57		
Cu	TS	13	167	14	49	460
	S	5	82	7	21	192
	LS	6	296	14		
Fe	TS	13	92	11	<16	202
	S	5	482	5	<16	2133
	LS	6	214	11		
Si	TS	13	632	5	241	3776
	S	5	210	3	196	223
	LS	6	450	5		
S	TS	13	216	11	11	290
	S	5	111	5	<15	205
	LS	1	249	11		

Zones: TS - top of saprolite; S - saprolite; LS - lower saprolite

Std. Dev. Standard Deviation, based on counting statistics

Table 30: Electron microprobe analyses of the supergene Au from the regolith (ppm).

Element	Zone	No.	Mean	Std. Dev.	Min	Max
Ag	L	8	<90	30		
	TS	1	<90	30		
	S	6	<45	15		

	LS	24	<90	30		
Cu	L	8	<40	14		
	TS	1	<40	13		
	S	6	25	7	<20	98
	LS	24	22	13	<20	72
Fe	L	8	153	11	82	394
	TS	1	134	11		
	S	6	7140	5	22	38117
	LS	24	813	11	<16	7718
Si	L	8	463	5	411	509
	TS	1	488	5		
	S	6	3216	3	166	15502
	LS	24	519	5	133	1237
S	L	8	313	12	273	399
	TS	1	333	11		
	S	6	83	5	70	170
	LS	24	259	11	<16	374

Zones: L - nodular laterite; TS - top of saprolite; S - saprolite; LS - lower saprolite

Std. Dev. - Standard Deviation, based on counting statistics

### 10.6 Gold grains in the saprolite

The saprolite just below the leached zone has the smallest gold grains, all being less than 100  $\mu\text{m}$ , with 79 to 86% less than 50  $\mu\text{m}$  (Table 26, Figure 62). Gold recoveries during separation were much poorer than expected from the analytical grade, probably due to the small size of the grains.

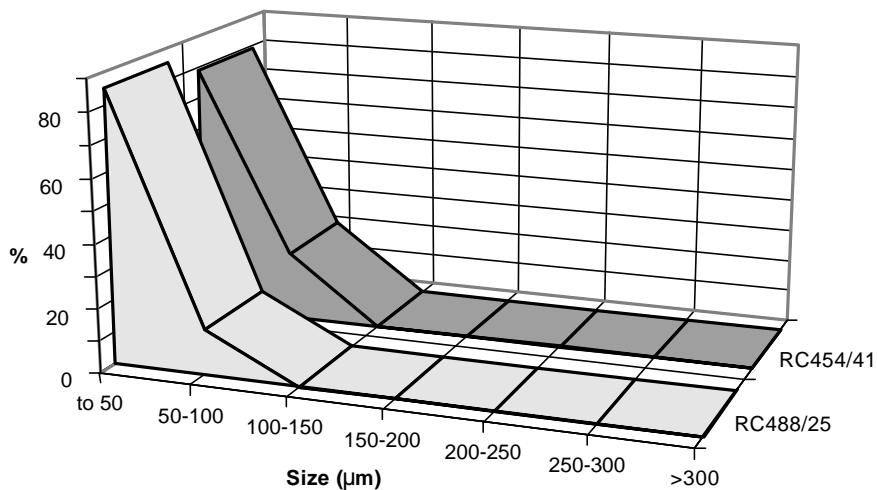


Figure 62: Size distribution of gold grains in the upper saprolite (%).

Secondary crystals prevail (55 to 86%) in the saprolite, mainly as thick, hexagonal, tabular and prismatic crystals. The bulk sample RC488/25 mainly contains crystals, with no irregular grains. Such size and shape distribution patterns of the Au grains indicate a supergene origin of most of the Au at this level. The compositions are similar to Au of the lower saprolite. Irregular Au grains mainly retain high Ag, Cu and S concentrations, some with depletion in several samples (Table 29).

**10.7 Gold grains in the top of saprolite, ferruginous saprolite and nodular laterite**

These three zones represent the gold anomalies at the top of the residual weathering profile, but they are different regolith units, so the Au grains have different characteristics. The siliceous saprolite and the nodular laterite mainly contain fine-grained Au less than 50 µm, whereas in the ferruginous saprolite sample RC216/65 68% of Au grains are greater than 50 µm (Table 26, Figure 63).

Gold is represented by moderately corroded, residual grains and secondary pristine crystals in various ratios (Photo 27). Corrosion of supergene Au crystals at the top of the profile is minor, with the majority remaining pristine in the ferruginous saprolite and nodular laterite (Photos 28-33). Only one etched crystal was observed in the ferruginous saprolite (Photo 36). One high-fineness round grain from the nodular laterite has an inner core and an outer coating, suggesting multi-staged growth (Photo 35). The compositions of Au are similar to that of the saprolite.

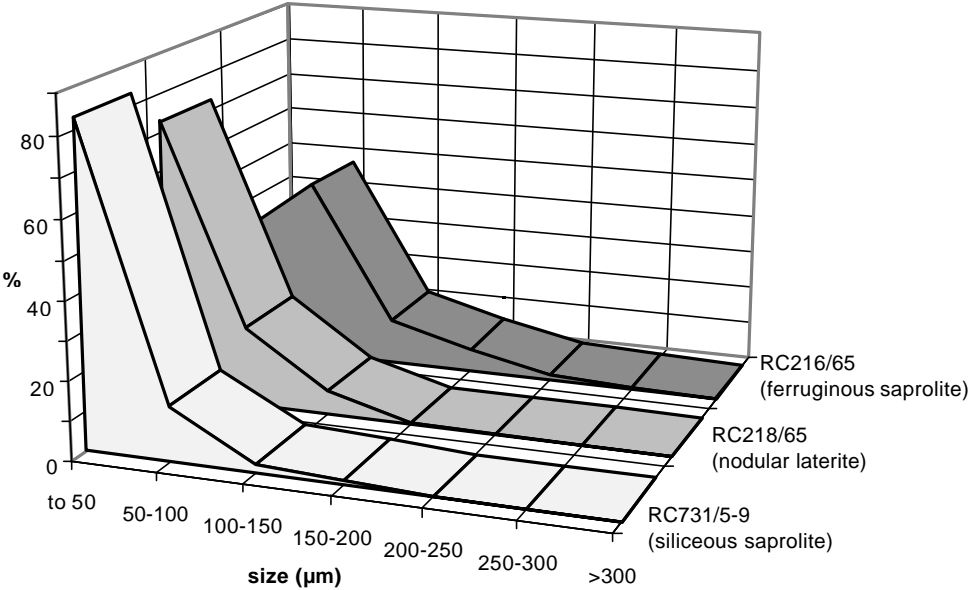


Figure 63: Size distribution of gold grains in the siliceous saprolite, ferruginous saprolite and nodular laterite (%).

**10.8 Gold selective extractions in the bulk samples**

Selective extractions of Au were performed on the bulk samples in a similar manner to that for the drill hole samples (Section 9.1) in order to obtain data on Au solubility and to compare the chemical and mineralogical data for Au. The results of Au solubility by water, iodide and cyanide reagents are summarized in Table 31.

Dissolution of Au by various reagents is difficult to interpret because of the difference in absolute Au concentrations in the samples studied. The results demonstrate rather low Au solubility in water and iodide solutions. Only three samples, from different levels of the profile, have significant proportions of iodide-soluble Au. The chemical and mineralogical data were investigated by factor analysis to determine

any relationships between the observations. The factors were extracted from the correlation matrix using computed communalities (the diagonal of the correlation matrix). The factors were reduced using the Kaiser criterion (eigenvalues >1), and the factor solution was rotated using standard computational method-the varimax rotation, to yield a factor structure that is simplest to interpret. Three 3 data sets were analyzed versus each other as follows:

- i. Size distribution of Au grains.
- ii. Shape distribution of Au grains.
- iii. The results of selective extractions.

*Table 31: Selective Au extraction of Mt Joel bulk samples.*

Drill hole	Depth (m)	Zone	Total water Au (ppb)	Total iodide Au (ppb)	Total CN Au (ppb)	Water Au (% of CN)	Iodide Au (% of CN)
218	65	L	20.7	308	10949	0.19	2.8
731	5-9	TS	3.3	77	217	1.51	35
216	65	FS	0.66	18	230	0.29	7.7
453	69-70	LS	24.9	456	20336	0.12	2.2
216	103	LS	1.1	9	1073	0.10	0.8
217	117	LS	2.2	25	363	0.62	6.9
670	85-86	LS	6.1	74	3046	0.22	2.4
453	90-91	LS	2.7	142	499	0.54	28
549	92-93	SR	6.9	652	1304	0.53	50
670	96-97	SR	1.1	58	2602	0.04	2.2
730	97-101	SR	3.5	71	1115	0.31	6.4
455	115-119	F	11.8	142	8742	0.14	1.6

Zones: L - nodular laterite; TS - top of saprolite; FS - ferruginous saprolite;  
LS - lower saprolite; SR - saprock; F - fresh rock

#### **10.8.1 Size distribution of Au grains versus shape distribution of Au grains.**

Three significant factors were retained with eigenvalues >1 (Figure 64, Table 32). Factor loadings, which can be interpreted as correlations between the respective variables and factors (Table 33, Figure 65), demonstrate two significant clusters, composed of:

- i. small (< 10 and 10-30  $\mu\text{m}$ ) Au grains;
- ii. coarse (>100  $\mu\text{m}$ ) and irregular Au grains.

These results are in good agreement with mineralogical data observed: abundances of < 10 and 10-30  $\mu\text{m}$  gold grains are well correlated; coarse gold grains are mainly irregular in shape.

*Table 32: Significant eigenvalues - size distribution versus shape distribution of Au grains*

Value	Eigenvalue	% Total variance	Cumulative eigenvalue	Cumulative %
1	3.090	28.09	3.090	28.09
2	2.837	25.79	5.927	53.88
3	1.237	11.25	7.165	65.13

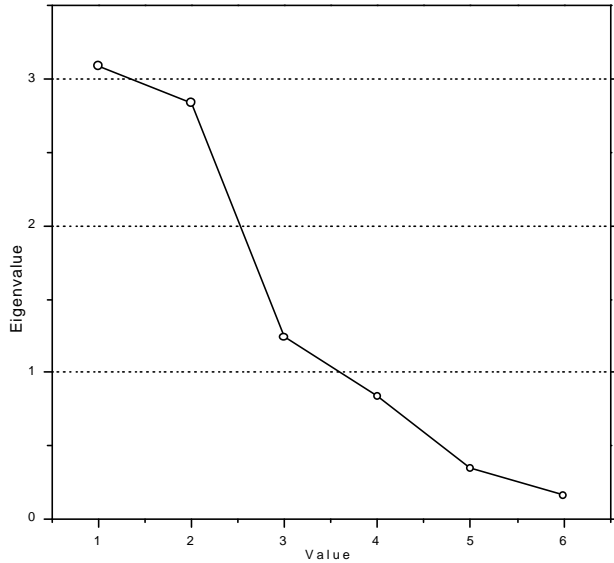


Figure 64: Plot of eigenvalues for size vs shape distribution.

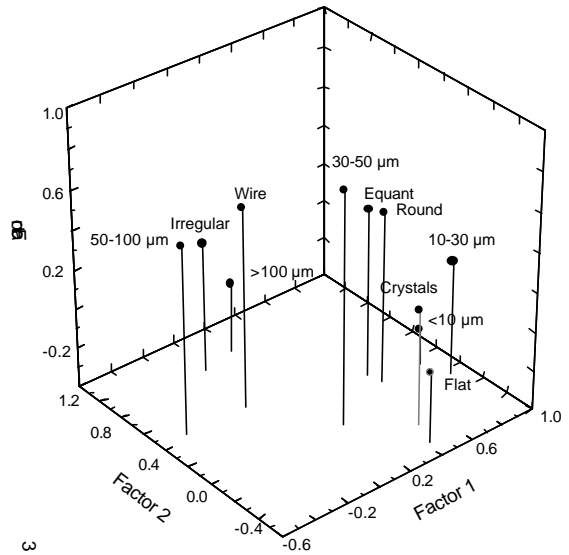


Figure 65: 3D plot of factor loadings for size vs shape distribution.

Table 33: Factor loadings - size distribution versus shape distribution of Au grains (significant values in bold type).

Variable	Factor 1	Factor 2	Factor 3
<10 μm	<b>0.843</b>	0.140	-0.226
10-30 μm	<b>0.900</b>	-0.042	0.179
30-50 μm	0.194	-0.043	<b>0.781</b>
50-100 μm	-0.446	0.438	0.552
>100 μm	0.179	<b>0.918</b>	-0.045
Crystals	0.481	-0.302	0.183
Rounded	0.589	0.136	0.469
Equant	0.572	0.242	0.451
Irregular	-0.031	<b>0.860</b>	0.258
Flattened	0.427	-0.473	-0.040
Wire	-0.077	0.440	0.609
Explained variation	2.885	2.383	1.897
Proportion of total	0.262	0.217	0.172

### 10.8.2 Size distribution of Au grains versus the results of selective extractions.

The results are summarized in Figures 66 and 67, Tables 34 and 35. There are significant correlations between the proportion of coarse (> 100 μm) Au grains, cyanide- and water-soluble Au. Correlations between the first two parameters are obvious, and absolute water-soluble Au concentrations correspond with total Au concentrations in the sample. The second factor includes the percentages of water and iodide soluble Au, which reflects links between relative amounts of water and iodide soluble Au. The third factor is composed of the proportions of small (< 10 and 10-30 μm) Au grains.

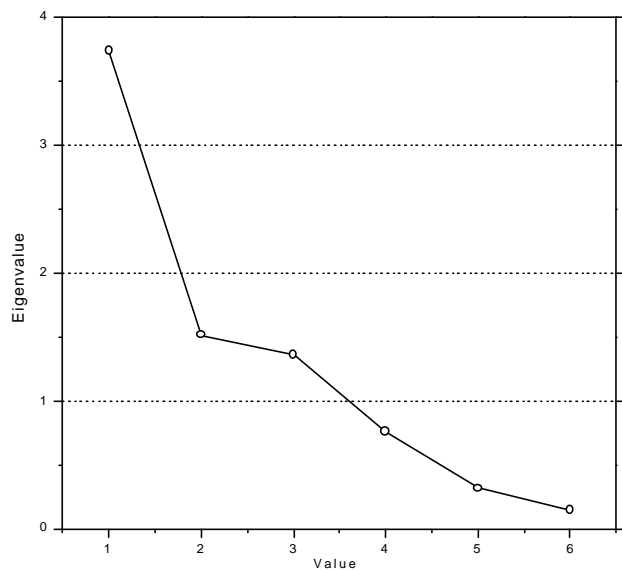


Figure 66: Plot of eigenvalues for size distribution vs. selective extraction.

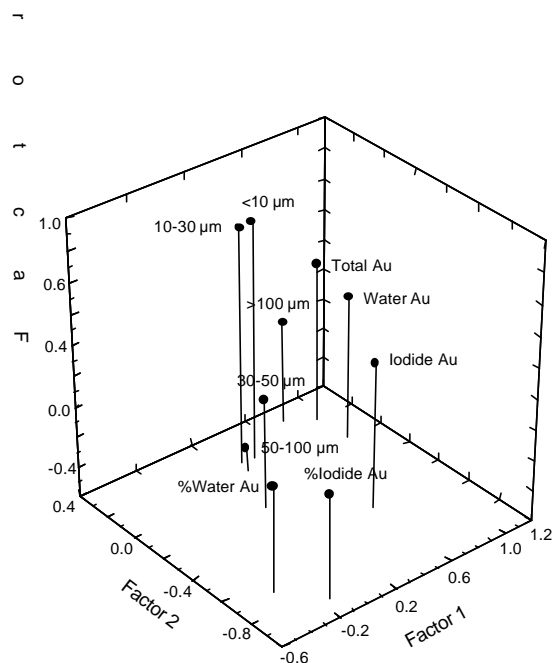


Figure 67: 3D plot of factor loadings for size distribution vs. selective extraction.

Table 34: Significant eigenvalues - size distribution of Au grains vs selective extraction results

Value	Eigenvalue	%Total variance	Cumulative eigenvalue	Cumulative %
1	3.736	37.36	3.736	37.36
2	1.515	15.15	5.251	52.51
3	1.361	13.61	6.612	66.12

Table 35: Factor loadings - size distribution of Au grains vs selective extraction results (significant values in bold type).

Variable	Factor 1	Factor 2	Factor 3
<10 μm	0.403	0.142	<b>0.748</b>
10-30 μm	0.321	0.151	<b>0.745</b>
30-50 μm	0.140	-0.185	-0.089
50-100 μm	0.291	0.084	-0.646
>100 μm	<b>0.779</b>	0.291	-0.138
Water Au	<b>0.950</b>	-0.001	0.145
Iodide Au	0.601	-0.490	0.158
Total Au	<b>0.937</b>	0.202	0.245
%Water Au	-0.323	<b>-0.686</b>	-0.112
%Iodide Au	-0.133	<b>-0.871</b>	-0.122
Explained variation	3.240	1.679	1.693
Proportion of total	0.324	0.168	0.169

### 10.8.3 Shape distribution of Au grains versus the results of selective extractions.

The results are summarized in Figures 68 and 69, Tables 36 and 37. The proportion of equant Au grains surprisingly correlates with cyanide- and water-soluble Au concentrations. Data indicate rather slight solubility of equant Au grains by the iodide reagent. The second cluster includes the percentages of water- and iodide-soluble Au.

The data obtained demonstrate slight solubility of coarse Au, but do not indicate increasing solubility with reduction of grain size or any connections between Au solubility and the proportion of supergene Au grains. It is probable that either a significant proportion of soluble Au occurs as “invisible” colloid-size particles, for which there is no any mineralogical information, or some of the Au grains are protected by insoluble coatings, such as clay minerals, silica or fine-grained Fe oxides.

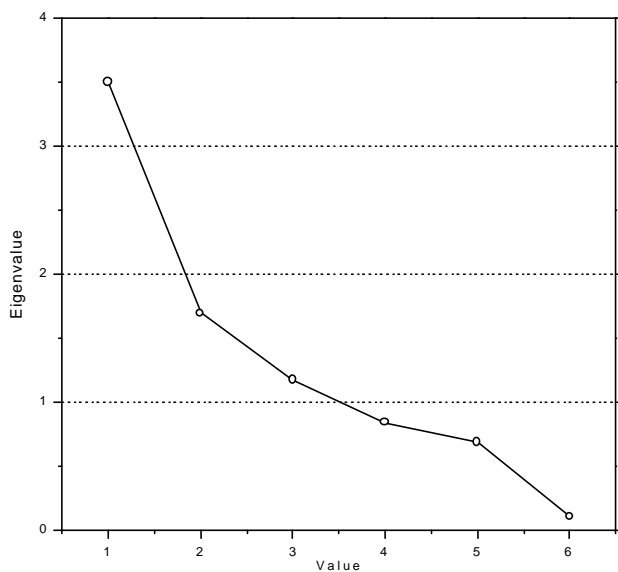


Figure 68: Plot of eigenvalues for shape distribution vs selective extraction.

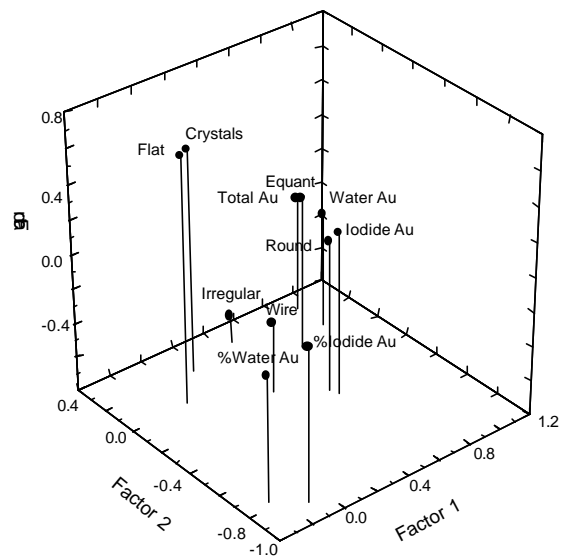


Figure 69: 3D plot of factor loadings for shape distribution vs selective extraction.

Table 36: Significant eigenvalues - shape distribution of Au grains vs selective extraction results

Value	Eigenvalue	%Total variance	Cumulative eigenvalue	Cumulative %
1	3.499	31.81	3.499	31.81
2	1.694	15.40	5.193	47.21
3	1.173	10.67	6.366	57.88

Table 37: Factor loadings - shape distribution of Au grains vs selective extraction results (significant values in bold type).

Variable	Factor 1	Factor 2	Factor 3
Crystals	0.153	0.197	0.490
Round	0.574	-0.303	0.071
Equant	<b>0.710</b>	0.025	0.092
Irregular	0.458	0.257	-0.636
Flat	-0.046	0.015	0.621
Wire	0.352	-0.157	-0.394
Water Au	<b>0.933</b>	0.109	-0.138
Iodide Au	0.586	-0.354	0.142
Total Au	<b>0.919</b>	0.280	-0.133
%Water Au	-0.250	<b>-0.762</b>	-0.074
%Iodide Au	-0.104	<b>-0.870</b>	0.082
Explained variation	3.324	1.775	1.268
Proportion of total	0.302	0.161	0.115

### 10.9 Interpretation

As a result of the study, two genetic types of Au can be distinguished in the weathered materials at Mt Joel: primary residual; and supergene.

The principal features of primary Au at Mt Joel are anhedral, xenomorphic forms having corroded surfaces with low, but detectable, Ag contents of approximately 1-3%. Supergene Au occurs as pristine crystals and round grains of high fineness.

Supergene Au grains are present in all parts of the regolith that are enriched in Au. The highest proportion of supergene Au crystals (55-86% of total) was observed in the saprolite, just beneath the Au depleted zone (Figure 70). Poor mechanical recovery of Au grains from this horizon implies that the Au is very fine grained. These data, compared with that on Au distribution, suggest the Au may have been derived from the overlying leached zone. Supergene Au grains are also common in the lower part of the regolith, in the lower saprolite and the saprock. This secondary enrichment is very patchy and irregular: the proportion of the secondary crystals varies from 9 to 49%. The residual Au grains are larger than the secondary Au, so the contribution of the supergene Au in weight percent is less and does not exceed 26%. Secondary Au crystals also occur within the upper Au anomaly just beneath a transported overburden, ranging from 18 to 34% of total.

The characteristics of the Au grains observed in the regolith at Mt Joel are more or less typical of Western Australian deposits. Their common features are that (a) almost all primary Au in the regolith is corroded, and (b) secondary Au is present in all parts of the profile other than the near-surface depleted zone (Butt et al., 1991). The prismatic and tabular cubo-octahedral supergene Au crystals, which are characteristic for Mt Joel, are observed in many of the Western Australian deposits. A specific feature of the secondary Au crystals at Mt Joel is their very slight corrosion through the profile: the euhedral crystals are preferentially pristine and the majority of the subhedral and pitted crystals appear to be the result of the crystals growing in confined locations.

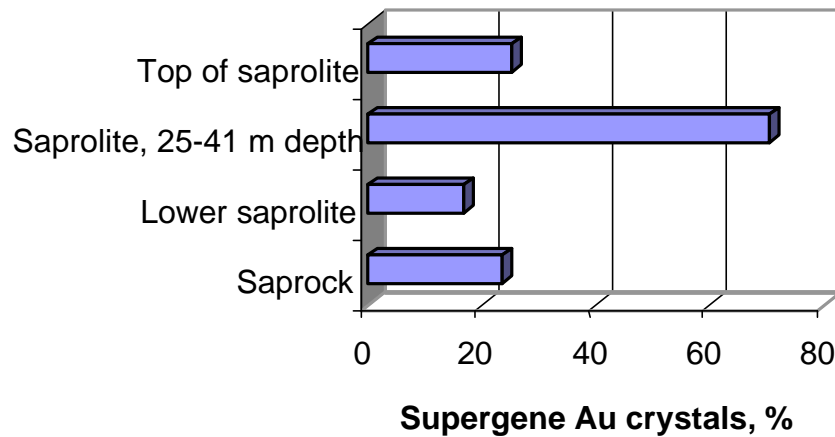


*Figure 70: Percentage of the supergene Au crystals in the regolith, 3000mN area.*

Secondary Au demonstrates surprising similarity of grain morphology and composition through the profile, consistent with a single form of supergene transport at all depths from the ferruginous saprolite to the base of the saprock. This is a commonly observed feature for supergene Au in the Yilgarn Craton (Butt, 1989; Lawrance, 1991). In many deposits in other regions of the world newly formed Au at the top of the regolith is commonly represented by high fineness crystals, with minor hackly and dendritic forms. In contrast, supergene Au at the bottom of the profile is usually irregular in shape and of low fineness, and may even show a substantial enrichment in Ag in comparison to primary Au. Such Au is commonly associated with secondary S and Se minerals (Boyle, 1979; Webster and Mann, 1984; Stoffregan, 1986; Sergeev et al., 1994, 1996). The characteristics of supergene Au in the Yilgarn Craton may be explained by the hypothesis of Butt (1987) that supergene Au redistribution in this region is due to its multi-stage mobilization and reprecipitation downwards in the profile during lowering of the groundwater levels under increasing arid conditions.

## 11 DISCUSSION AND CONCLUSIONS

### 11.1 Regolith evolution

The 3000 and 800 mN areas represent two distinct regolith environments. The 3000 mN area represents a palaeohigh (with some degree of erosion) and the 800 mN area a palaeochannel with complete in situ regolith profile, buried by more than 80 m of channel sediments (Figure 71). Both areas are further covered by up to 10 m of sediments, presumably alluvial. The weathering profile is generally deepest around the areas of mineralisation, in particular the strong mineralisation in the 3000 mN area.

At least some areas of the residual weathering profile were lateritized prior to burial. Much of the lateritic Fe in the lowlands probably derived from upslope areas, consistent with the fact that immobile elements in the lateritic zone of the 800 mN area are not residually enriched but, rather, are diluted by the addition of Fe. At the 800 mN area and the eastern portions of the 3000 mN section, lateritic residuum occurs with an upper pisolitic layer. It is likely that mechanical transport of lateritic material from upslope took place during burial of the lateritic residuum (Figure 71). This resulted in the accumulation of lateritic gravels, rich in pisoliths, at the top of lateritic residuum in the lowland areas. Such transport, however, was not enough to erode the cutans from the pisoliths, suggesting dominantly colluvial deposition. The occurrence of lateritic residuum in a similar landscape situation has also been identified in the nearby Bronzewing area (Varga et al., 1997) and in the Harmony area (Robertson et al., 1996b).

The leached zone lies more or less parallel with modern topography, indicating that leaching in the saprolite occurred after the burial of the palaeosurface (Figure 71). The leaching resulted in the removal of up to 50% of Au. Silicification and carbonatization are more recent phenomena. They appear to be related to aridity and have also affected the alluvial cover.

### 11.2 Gold distribution

Contrasting patterns of Au distribution were observed between the 3000 and 800 mN areas. In the 3000 mN area, a general Au depletion is observed, especially from the Leached Zone. Enrichment takes place only at the top of the saprolite, where Au distribution is more homogeneous and the amount of soluble Au is greatest. Gold redistribution has also taken place in the transition zone but did not result in significant enrichment. In the 800 mN area, general enrichment is observed, especially in the lateritic residuum and, possibly, the transition zone.

The stronger anomaly and dispersion in the lateritic residuum compared to the top of saprolite is illustrated in Figures 72 and 73 which use data from the 2400 mN area and 0 mN areas. The Au anomaly in the top of saprolite is no longer visible when the cut-off is increased from 0.05 ppm to 0.1 ppm. When the same cut-off is applied to the lateritic residuum, the dispersion patterns remains visible.

The nature of Au enrichment at the top of saprolite is predominantly chemical, given the high percentage of iodide-soluble Au. Such enrichment has probably resulted from continuous downwards migration of Au during the lowering of the landsurface and was preserved from leaching which occurred mostly in the subsurface, under the influence of water table fluctuation. Particulate Au with supergene features such as crystalline shapes and high fineness are also present, possibly indicating a cumulative effect of Au precipitation over time. This enrichment, however, took place right over

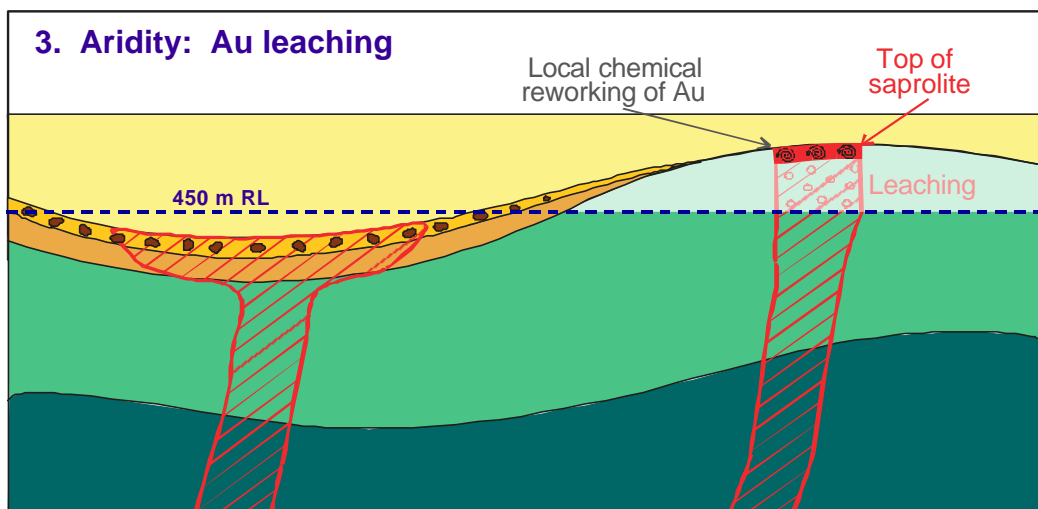
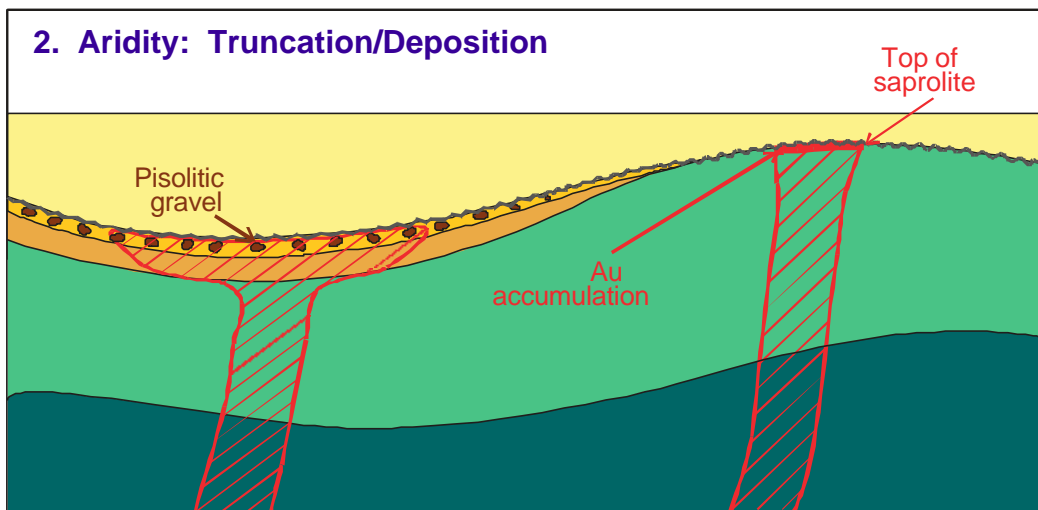
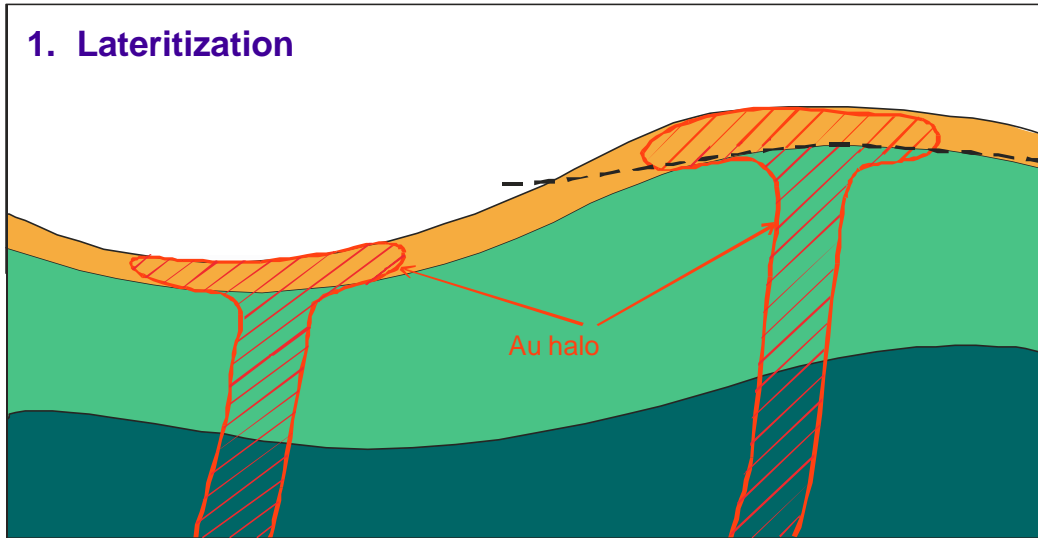


Figure 71: Diagrammatic model for proposed regolith evolution at Mt Joel (see text for details).

primary mineralized zones, resulting in homogenization of the Au grades but not significant lateral dispersion.

Gold enrichment and dispersion in the lateritic residuum derives from chemical and residual processes related to lateritization (Butt, 1989). Chemical enrichment is preserved in the pisolitic fractions and in the form of crystalline Au particles. The percentage of this Au that is soluble is lower than in the 3000 mN area, possibly due to aging. Lateral dispersion is most pronounced in the pisolitic layer, presumably due to mechanical transport of Au-bearing lateritic material before and during burial by the channel sediments. Such dispersion tends to follow the direction of the palaeoslope. This situation is also apparent in the eastern portion of the 3000 mN section.

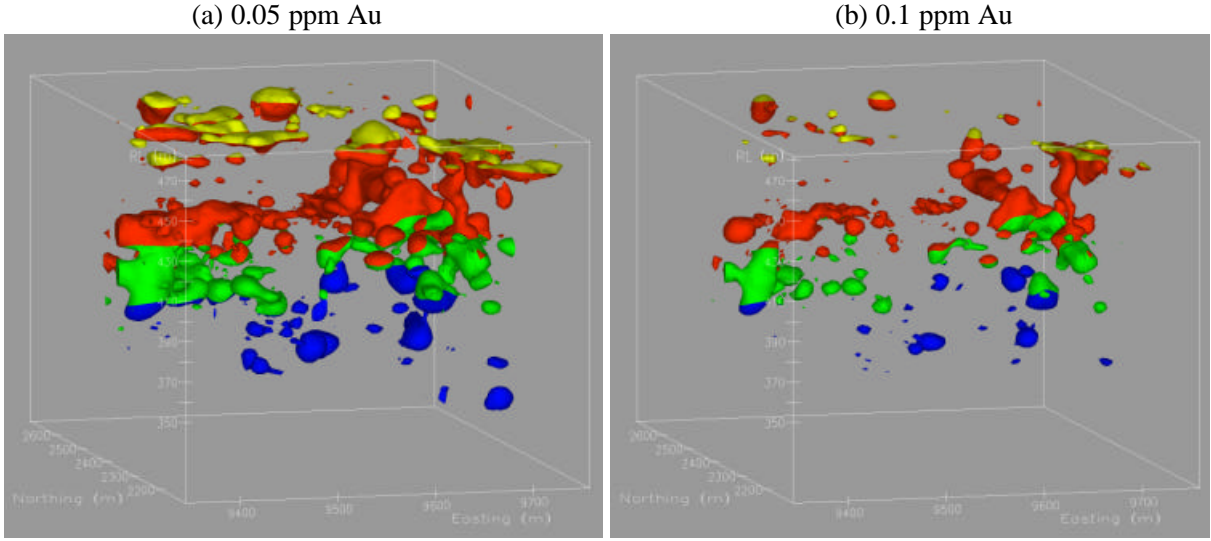


Figure 72: 3D plot showing the weathering zones (blue: fresh; green: transition; red: oxide; yellow: alluvium) and Au distribution for the 2400 mN area, using a cut-off of (a) 0.05 ppm and (b) 0.1 ppm.

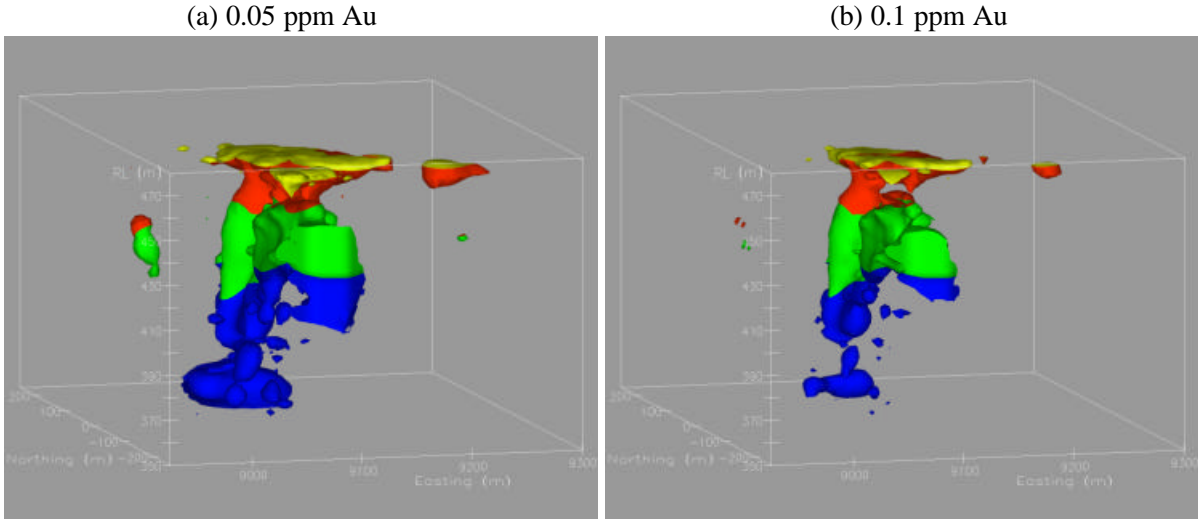


Figure 73: 3D plot showing the weathering zones (blue: fresh; green: transition; red: oxide; yellow: alluvium) and Au distribution for the 0 mN area, using a cut-off of (a) 0.05 ppm and (b) 0.1 ppm.

### **11.3 Gold dissolution and role of the present groundwater:**

The Au leached zone in the 3000 mN area is an outstanding feature, which is not present in the 800 mN area. The fate of the leached Au is unresolved. Some may be reprecipitated lower in the profile, as suggested by the presence of supergene Au with low fineness in several levels of the saprolite. Such reprecipitation may have contributed to the slight enrichment and homogenization of Au in the transition zone. However, the bulk of supergene Au in this zone is more likely the result of local dissolution and reprecipitation since the net effect is one of an upwardly increasing leaching.

Present day groundwater conditions are not conducive to Au mobilization, consistent with lack of dissolution features on supergene Au particles. Most of the Au mobilization was probably related to past regimes, when groundwater conditions may have been more saline. Secondary Au grains have similar morphologies and chemical compositions throughout the profile, suggesting similarities in the mechanisms of Au mobilization at all depths, probably dominated by chloride complexes.

Gold mobilization under present conditions at Mount Joel is possible only in the deeper groundwater system. This shows more heterogeneous hydrogeochemical properties, such as pH and salinity, which may be locally weakly conducive to present day Au remobilization, as Au chloride, in the transition zone. Whether or not this could explain the enrichment of Au in the transition zone of the 800 mN area by deep groundwater transport is more difficult to show.

### **11.4 Exploration significance**

The concentration of trace metals related to mineralization is generally low throughout the regolith, reflecting their low abundances in primary mineralization. Although As and Sb tend to be enriched in the ferruginous zone, especially in the lateritic residuum, no information has been obtained on their concentration in background areas far enough from the main mineralization to assess their dispersion patterns. However, considering the data obtained from the 3000 mN traverse, As and Sb do not indicate the presence of mineralization as clearly as W in the top of saprolite, although with a very limited lateral extension.

Anomalies of Au and associated trace elements in the alluvial cover have not been observed. The Au anomalies at the base of the alluvium are most probably detrital. This indicates there is no upward diffusion of these elements, which is in agreement with hydrogeochemical data. It is therefore necessary to target exploration sampling at the residuum and for that, a sound understanding of the regolith stratigraphy is essential. Results from the PIMA investigation were encouraging in discriminating residual from alluvial regolith materials.

The best residual weathering zone for sampling lies just below the palaeosurface where Au concentration and dispersion are most pronounced. This includes areas truncated to the saprolite level or dominated by lateritic residuum. Because the nature of Au concentration in these materials is different, resulting in different Au distribution patterns, different background values and different size of dispersion halos, these data should be separated and interpreted accordingly.

Gold anomalies and dispersion in the top of saprolite are probably younger and result mostly in a general homogenization of grade and only limited lateral dispersion from their primary sources. However, the full extent of the dispersion halo was not assessed at the ppb level. Despite the close sample spacing apparently necessary for this type of material, its position in the palaeotopography, namely closer to surface, is a logistical advantage.

Gold anomalies and dispersion in lateritic residuum are stronger and result from a longer weathering history since lateritization when chemical enrichment took place. This was later enhanced by mechanical dispersion during burial by alluvium. However, the full extent of the dispersion halo was not assessed at the ppb level. Although it apparently compares favourably in relation to the dispersion in the top of saprolite, the dispersion pattern is likely to follow the palaeotopography due to its strong mechanical component.

## **ACKNOWLEDGMENTS**

We would like to thank Great Central Mines Ltd for kindly providing access to the Mount Joel site and to their exploration database. Personnel from the Yandal exploration group are greatly acknowledged for their support during fieldwork and later analyses. Mr Brian Davis is thanked for producing a 3D block model of the gold grade distribution. Dr Neil Phillips and Dr Jim Wright are also acknowledged for in-house discussions. We also received laboratory support from Dale Longman, Sheryl Keppler, Paula Voyvodic and Michael Hart at CSIRO, Perth and from Lesley Dotter at CSIRO, Sydney. Dr Charles Dornan from UWA is thanked for his help in organizing the gravity separation of heavy minerals. We also thank Dr Tom Cudahy and Dr Erick Ramanaidou for their support of the PIMA analyses. Dr Charles Butt, Dr Ian Robertson, Mr John Wildman, Dr Ravi Anand and Ms Allison Britt provided invaluable advice during the course of this work and preparation of this report. CRC LEME is established and supported under the Australian Government's Cooperative Research Centres Program.

## REFERENCES

- Boyle, R.W., 1979. The geochemistry of gold and its deposits. Geological Survey of Canada Bulletin 280, 584pp.
- Brindley, G.W. and Brown, G., 1980. Crystal structure of clay minerals and their x-ray identification. Mineralogical Society Monograph 5.
- Bristow, A.P.J., Gray, D.J. and Butt, C.R.M., 1996. Geochemical and spatial characteristics of regolith and groundwater around the Golden Delicious prospect, Western Australia. CSIRO Division of Exploration and Mining Restricted Report 280R, 175pp.
- Butt, C.R.M., 1987. The dispersion of gold in the weathered zone, Yilgarn Block, Western Australia. Meaningful sampling in gold exploration. Australian Institute of Geoscientists Bulletin 7, p27-53.
- Butt, C.R.M., 1989. Genesis of supergene gold deposits in the lateritic regolith of the Yilgarn Block, Western Australia. In: R.R. Keays, W.R.H. Ramsay and D.I. Groves (Editors). The geology of gold deposits: the perspective in 1988. Economic Geology Monograph No.6, p460-470.
- Butt, C.R.M., Gray, D.J., Lintern, M.J. and Robertson, I.D.M., 1993. Gold and associated elements in the regolith - dispersion processes and implications for exploration. Final Report, Project P241A. CSIRO Division of Exploration Geoscience Restricted Report 396R, 64pp.
- Butt, C.R.M., Gray, D.J., Lintern, M.J., Robertson, I.D.M., Taylor, G.F. and Scott, K.M., 1991. Gold and associated elements in the regolith - dispersion processes and implications for exploration. CSIRO Division of Exploration Geoscience Restricted Report 167R, 114pp.
- Butt, C.R.M., Gray, D.J., Robertson, I.D.M., Lintern, M.J., Anand, R.R., Britt, A.F., Bristow, A.P.J., Munday, T.J., Phang, C., Smith, R.E. and Wildman, J.E., 1997. AMIRA P409 – Geochemical exploration in areas of transported overburden, Yilgarn Craton and environs, WA, final report. CSIRO Division of Exploration and Mining Restricted Report 333R, 164pp.
- Butt, C.R.M., Horwitz, R.C. and Mann, A.W., 1977. Uranium occurrences in calcrete and associated sediments in Western Australia. CSIRO Division of Mineralogy Report FP16, 67pp.
- Cavaney, R.J., 1984. Lake Maitland uranium deposit. In: Surficial uranium deposits. International Atomic Energy Agency, Vienna, 252pp.
- Douglas, G.B., Gray, D.J. and Butt, C.R.M., 1993. Geochemistry, mineralogy and hydrogeochemistry of the Ambassador multi-element lignite deposit, Western Australia. (CSIRO Weathering Processes Group). CSIRO Division of Exploration Geoscience Restricted Report 337R.
- Drever, J.I., 1982. The geochemistry of natural waters. Prentice-Hall, Inc, Englewood Cliffs, NJ, USA, 388pp.
- Gray, D.J., 1990. Hydrogeochemistry of the Panglo gold deposit. CSIRO Division of Exploration Geoscience Restricted Report 125R, 74pp.
- Gray, D.J., 1991. Hydrogeochemistry in the Mount Gibson gold district. (CSIRO/AMIRA P240: Laterite Geochemistry). CSIRO Division of Exploration Geoscience Restricted Report 120R, 80pp.
- Gray, D.J., 1992a. Hydrogeochemistry of sulphide weathering at Boags Pit, Bottle Creek, Western Australia. (CSIRO/AMIRA P241A: Weathering Processes). CSIRO Division of Exploration Geoscience Restricted Report 237R, 13pp.
- Gray, D.J., 1992b. Geochemical and hydrogeochemical investigations of alluvium at Mulgarrie, Western Australia. (CSIRO/AMIRA P241A: Weathering Processes). CSIRO Division of Exploration Geoscience Restricted Report 339R, 66pp.

- Gray, D.J., 1993a. Investigation of the hydrogeochemical dispersion of gold and other elements from mineralized zones at the Granny Smith gold deposit, Western Australia. (CSIRO Weathering Processes Group). CSIRO Division of Exploration Geoscience Restricted Report 383R, Volumes I and II, 93pp.
- Gray, D.J., 1993b. Investigation of the hydrogeochemical dispersion of gold and other elements in the Wollubar palaeodrainage, Western Australia. (CSIRO/AMIRA P241A: Weathering Processes Group). CSIRO Division of Exploration Geoscience Restricted Report 387R, Volumes I and II, 133pp.
- Gray, D.J., 1994. Investigation of the hydrogeochemical dispersion of gold and other elements at Lawlers, Western Australia. (CSIRO/AMIRA P409: Weathering Processes Group). CSIRO Division of Exploration and Mining Restricted Report 26R, Volumes I and II, 151 pp.
- Gray, D.J., 1995. Hydrogeochemical dispersion of gold and other elements at Baxter, Western Australia. (CSIRO/AMIRA P409: Weathering Processes Group). CSIRO Division of Exploration and Mining Restricted Report 169R, 85pp.
- Gray, D.J., 1996. Hydrogeochemistry in the Yilgarn Craton. (CSIRO/AMIRA P409: Weathering Processes Group). CSIRO Division of Exploration and Mining Restricted Report 312R, 75pp.
- Gray, D.J. and Cudahy, T.J., 1996. Pilot spectral study of the Mount Percy gold deposit, Western Australia. CSIRO Exploration and Mining Report 175R, 69pp.
- Gray, D.J. and Lintern, M.J., 1993. Further aspects of the chemistry of gold in some Western Australian soils. (CSIRO/AMIRA P241: Weathering Processes). CSIRO Division of Exploration Geoscience Restricted Report 391R, 50pp.
- Lawrance, L.M., 1991. Distribution of gold and ore-associated elements within lateritic weathering profiles of the Yilgarn Block, Western Australia. PhD Thesis, University of Western Australia.
- Lintern, M.J. and Gray, D.J., 1995a. Progress statement for the Kalgoorlie study area - Steinway prospect, Western Australia. (CSIRO/AMIRA P409: Weathering Processes Group). CSIRO Division of Exploration and Mining Restricted Report 95R, 121pp.
- Lintern, M.J. and Gray, D.J., 1995b. Progress statement for the Kalgoorlie study area - Argo deposit, Western Australia. (CSIRO/AMIRA P409: Weathering Processes Group). CSIRO Division of Exploration and Mining Restricted Report 96R, 153pp.
- Mann, A.W. and Horwitz, R.C., 1979. Groundwater calcrete deposits in Australia: some observations from Western Australia. *Journal of Geological Society of Australia*, 26:293-303.
- Murphy, J. and Riley, J.P., 1962. A modified single solution method for the determination of phosphate in natural waters. *Analytica Chimica Acta*, 27:31-36.
- Parkhurst, D.L., Thorstenson, D.C. and Plummer, L.N., 1980. PHREEQE, a computer program for geochemical calculations. *US Geological Survey Water Resources Investigations* 80-96, 210p.
- Phillips, G.N., Vearncombe, J. R. and Eshuys, E., 1998. Yandal greenstone belt, Western Australia: 12 million ounces of gold in the 1990s. *Mineralium Deposita*, 33:310-316.
- Plummer, L.N. and Parkhurst, D.L., 1990. Application of the pitzer equations to the PHREEQE geochemical model. In Melchior, D.C. and Bassett, R.L. (Editors). *Chemical modeling of aqueous systems II*. American Chemical Society Symposium Series 416, Washington DC, American Chemical Society, p128-137.
- Pontual, S. and Merry, N., 1996. An exploratory strategy to aid the differentiation of residual from transported kaolinities using field-based spectral analysis. *Restricted Report*, AusSpec International, Melbourne, 112pp.
- Robertson, I.D.M., Dyson, M., Hudson, E.G., Crabb, J.F., Willing, M.J. and Hart, M.K.W., 1996a. A case-hardened, low contamination ring mill for multi-element geochemistry. *Journal of Geochemical Exploration*, 57:153-158.

- Robertson, I.D.M., Phang, C. and Munday, T. J., 1996b. The regolith geology and geochemistry of the area around the Harmony gold deposit, (Baxter mining centre), Peak Hill, Western Australia. (CSIRO/AMIRA P409: Geochemical exploration in areas of transported overburden, Yilgarn Craton and environs, WA). CSIRO Division of Mining and Exploration Restricted Report 194R.
- Sergeev, N.B., Zaikov, V.V. and Laputina, I.P., 1994. Gold and silver in the supergene zone of the Gai deposit, the Southern Urals. *Geology of Ore Deposits*, 36:169-183.
- Sergeev, N.B., Bugelskii, Yu.Yu. and Kuznetsova, O.Yu., 1996. Distribution of gold in the oxidation zone of the Ural massive sulfide deposits: influence of the primary ore compositions and climate. *Geology of Ore Deposits*, 38:321-332.
- Sichel, H.S., 1966. The estimation of means and associated confidence limits for small samples from lognormal populations. In: *Symposium of Mathematical Statistics and Computer applications in Ore Evaluation..* South African Int. Min. Metall., Johannesburg, p106-122.
- Stoffregen, R., 1986. Observations on the behaviour of gold during supergene oxidation at Summitville, Colorado, USA, and implications for electrum stability in the weathering environment. *Applied Geochemistry*, 1:549-558.
- Varga, Z.S., Anand, R.R. and Wildman, J.E., 1997. Regolith-landscape and geochemical dispersion about the Bronzewing gold deposit, WA. (CSIRO/AMIRA P409: Geochemical exploration in areas of transported overburden, Yilgarn Craton and environs, WA). CSIRO Division of Mining and Exploration Restricted Report 308R, 59pp.
- Weast, R.C., 1983. *CRC Handbook of Chemistry and Physics*, 63rd Edition. CRC Press Inc, Boca Raton, Florida.
- Webster, J.G. and Mann, A.W., 1984. The influence of climate, geomorphology and primary geology on the supergene migration of gold and silver. *Journal of Geochemical Exploration*, 22:21-42.
- Zall, D.M., Fisher, D. and Garner, M.D., 1956. Photometric determination of chlorides in water. *Analytical Chemistry*, 28:1665.